

ERII DOC. NO. 800-0045
NASA-Ames Grant NSG-2032

LUNAR PHYSICAL PROPERTIES FROM
ANALYSIS OF MAGNETOMETER DATA

FINAL REPORT

31 August 1979

Copy #2

Eyring Research Institute



Eyring Research Institute Inc.

(NASA-CR-162288) LUNAR PHYSICAL PROPERTIES
FROM ANALYSIS OF MAGNETOMETER DATA Final
Report, 1 Nov. 1975 - 31 Aug. 1979 (Eyring
Research Inst., Provo, Utah.) 173 p
HC A08/MF A01

N79-32144

Unclas

CSCL 03B G3/91 35765



FINAL REPORT

LUNAR PHYSICAL PROPERTIES FROM ANALYSIS
OF MAGNETOMETER DATA

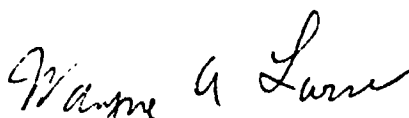
NASA-Ames Grant NSG-2082

31 August 1979

Covering the Period
1 November 1975 to 31 August 1979

Principal Investigator:
William D. Daily

Approved by:



Dr. Wayne A. Larsen
Director, Advanced Systems Research Division

Submitted to:

NASA Technical Officer: Dr. Palmer Dyal
NASA-Ames Research Center
Moffett Field, CA
94035

Submitted by:

EYRING RESEARCH INSTITUTE, INC.
1455 West 820 North
Provo, Utah 84601

TABLE OF CONTENTS

<u>Section</u>	<u>Page</u>
1.0 INTRODUCTION	1-1
2.0 LUNAR ELECTRICAL CONDUCTIVITY	2-1
2.1 Bulk Conductivity	2-1
2.2 Crustal Conductivity	2-3
2.3 Local Anomalous Conductivity	2-5
3.0 LUNAR MAGNETIC PERMEABILITY	3-1
3.1 Bulk Permeability Measurements	3-1
3.2 Iron Abundance Estimates	3-3
3.3 Core Size Limits	3-4
4.0 LUNAR IONOSPHERE AND ATMOSPHERE	4-1
5.0 LUNAR CRUSTAL MAGNETIC REMANENCE	5-1
5.1 Scale Size Measurements	5-1
5.2 Constraints on Crustal Remanence Origin	5-2
6.0 PUBLICATIONS AND ABSTRACTS	6-1
REFERENCES	R-1
APPENDIXES	
Appendix A On the Phase Relationship Between the Energetic Particle Flux Modulation and Current Disc Penetrations in the Jovian Magnetosphere: Pioneer 10 Inbound	A-1
Appendix B Theories for the Origin of Lunar Magnetism	B-1
Appendix C Electrical Conductivity Anomalies Associated with Circular Lunar Maria . . .	C-1
Appendix D Electromagnetic Properties of the Moon . . .	D-1
Appendix E Mare Serenitatis Conductivity Anomaly Detected by Apollo 16 and Lunokhod 2 Magnetometers	E-1
Appendix F Lunar Properties from Magnetometer Data: Effects of Data Errors	F-1

1.0 INTRODUCTION

Research during the period of this grant (1 November 1975 to 31 August 1979) had the primary objective of studying the electromagnetic properties of the lunar interior. Progress and final results of this research are presented in this document.

2.0 LUNAR ELECTRICAL CONDUCTIVITY

2.1 BULK CONDUCTIVITY

Electrical conductivity of the moon has been calculated from global eddy current response to changes in the magnetic field external to the moon. When the moon is subjected to a change in the external field, an eddy current field is induced in the moon which opposes the change. The induced field responds with a time dependence which is a function of the electrical conductivity distribution in the lunar interior. Simultaneous measurements of the transient driving field by an Explorer 35 magnetometer and the lunar response field by an Apollo surface magnetometer allow calculation of the lunar conductivity. Since the electrical conductivity of geologic materials is a strong function of their temperature, a thermal profile can be calculated from the conductivity profile for a given compositional model of the lunar interior.

When the moon is in the solar wind, lunar eddy current fields form an induced lunar magnetosphere which is distorted in a complex manner due to flow of solar wind plasma past the moon. The eddy current field is compressed on the dayside of the moon and is swept downstream and confined to a cavity on the lunar nightside. Because of the complex boundary conditions necessary to model these processes, early analysis included a time dependent theory for transient response of a sphere in a vacuum to model lunar response as measured on the lunar nightside and the lunar response measured in the geomagnetic tail where plasma confinement effects are minimized.

Recent analysis was of data selected from measurements obtained in the lobes of the geomagnetic tail, during times when there is no indication of plasma effects. To help avoid data measured when the lunar magnetic response is influenced by plasma, individual data sets are selected using criteria: (1) the magnitude of the field external to the moon (measured by the Explorer 35 magnetometer) is greater than 8 gammas; (2) the external field is directed approximately along the sun-earth line; (3) main qualitative features of each event appear in both surface and orbital data in all three vector coordinate axes to minimize use of data with large field gradients between the two magnetometers; and (4) no plasma data are measured above the solar-wind spectrometer instrument threshold. These criteria help discriminate data for those times when the lunar response can be modeled by that of a conducting sphere in a vacuum.

On 20 April 1970 an exceptionally large magnetic transient event was recorded in the lunar environment. The moon was located at high latitude in the north lobe of the geomagnetic tail. Lunar magnetic field and plasma detector measurements indicated the event met all data selection criteria listed above. Analysis of this large selenomagnetic storm event has involved the input Explorer 35 data, convolved with an assumed conductivity profile and compared to the calculated response measured by the Apollo 12 magnetometer. The lunar electrical conductivity profile used to calculate this best fit response is given by Dyal et al. (1976). This profile assumes that the conductivity increases monotonically with depth and that it is a continuous function from the surface to the center of the moon. The best-fit profile rises rapidly from $< 10^{-9}$ mhos/m at the surface to $\sim 10^3$ mhos/m at a depth of 200 to 300 km. Thereafter the conductivity rises more gradually to $\sim 3 \times 10^{-2}$ mhos/m at 900 km depth.

Uncertainties in the lunar conductivity profile determination arise from several causes: (1) the nonuniqueness of profile determination as discussed by Backus and Gilbert (1970), Parker (1970), Phillips (1972), and Hobbs (1973); (2) the penetration

depth allowed by the length and amplitude of the data time series; (3) the frequency response limitations of the Explorer 35 and Apollo magnetometers; (4) inhomogeneities in the external field over the dimensions of the moon; and (5) instrumental errors in the measured fields. The effects of instrumental gain errors in conductivity analyses have been studied in detail by Daily and Dyal (1979). Time independent magnetometer errors such as constant offset errors do not affect this analysis since a field bias is added to one of the data sets to align the data prior to the transient event and the difference between the surface and orbital measurements is the time dependent induced eddy current field. On the other hand, errors in the gain of either magnetometer will affect the analysis results. For example, a gain attenuation of 5% in the Explorer 35 magnetometer would yield a 9.5 γ measurement for an actual 10 γ step transient. The apparent eddy current field would necessarily be modeled by smaller magnitude electrical currents in the lunar interior and result in a lower calculated electrical conductivity for the moon.

2.2 CRUSTAL CONDUCTIVITY

An upper limit has been placed on the average lunar crustal conductivity from an investigation of toroidal ($\nabla \times \underline{B}$) induction in the moon. The toroidal induction mode has been described theoretically by several investigators (Sonett and Colburn, 1967; Schwartz and Schubert, 1969). For the case when the moon is immersed in the solar wind plasma, the external field B_E is constant (eddy current induction vanishes), and the motional solar wind electric field induction drives currents in the moon resulting in a toroidal field B_T . The total field B_A at the surface is

$$B_A = B_E + B_T.$$

Following Schwartz and Schubert (1969), we solve for the toroidal field, B_T , expressed in component form as follows:

$$\begin{aligned} B_{Tx} &= B_{Ax} - B_{Ex}, \\ B_{Ty} &= B_{Ay} - B_{Ey} = AE_z = A(V_x B_{Ey} - V_y B_{Ex}), \\ B_{Tz} &= B_{Az} - B_{Ez} = -AE_y = A(V_x B_{Ez} - V_z B_{Ex}), \end{aligned}$$

where, for a two-layer (core-crust) model of the moon

$$A = \sigma_1 \mu R_m \left(\frac{\frac{1}{2} + \beta + \alpha(1-\beta)}{1 - \beta + \alpha(2+\beta)} \right),$$

$$\alpha = \sigma_1 / \sigma_2,$$

$$\beta = (R_2 / R_m)^3.$$

The components x, y, z are up, east, north ALSEP coordinates at the Apollo 12 site; V is velocity of the moon relative to the solar wind; σ_1 and σ_2 are conductivity of crust and core, respectively; μ is the global permeability; R_2 and R_m are core and lunar radii. For the case where $\sigma_2 \gg \sigma_1$, then

$$A = \sigma_1 \mu R_m \left(\frac{\frac{1}{2} + \beta}{1 - \beta} \right).$$

The components of the toroidal field are calculated by subtracting the components of the external field B_E , measured by an Explorer 35 magnetometer, from the total field B_A , measured at the lunar surface by the Apollo 12 lunar surface magnetometer. We have determined the parameter A by plotting components of toroidal field B_T versus the $V \times B_E$ electric field, using a data set of 100 ten minute averages from a total of 5 lunations, selected from time periods when the solar wind velocities and fields are approximately constant. All data have been selected from time periods when the Apollo 12 magnetometer was on the

REPRODUCIBILITY OF THE
ORIGINAL PAGE IS POOR

lunar nightside, to minimize solar wind compression effects on the surface remanent magnetic field. From these data we calculate a least squares slope $A = (-6.2 \pm 4.3) \times 10^{-2}$ sec/m, where the limits include only random statistical measurement errors. Estimates of systematic errors are based upon comparisons between Apollo 12, LSM Explorer 35-Ames, and Explorer 35-Goddard magnetometers. From this comparison we estimate the systematic error inherent in the analysis. The systematic and random errors result in an upper limit slope of 2×10^{-7} sec/m.

Using this value of slope A, we can determine the upper limit on average crustal conductivity as a function of crust thickness (ΔR). For an average crust thickness $\Delta R = 80$ km (Goins et al., 1977), the conductivity upper limit is 9×10^{-9} mhos/m. We note that the average crust conductivity is not a strong function of crust thickness for thicknesses of the order of 80 km. (A 100 km crust would correspond to a 1.2×10^{-8} mhos/m upper limit, and a 60 km crust would correspond to about 7×10^{-9} mhos/m.) This crustal conductivity upper limit places an important new constraint on the lunar conductivity profile by lowering previous estimates of crust conductivity (based on poloidal induction) by approximately four orders of magnitude.

2.3 LOCAL ANOMALOUS CONDUCTIVITY

A large regional anomaly in the electrical properties of the lunar crust and mantle has been measured by magnetometers emplaced on the lunar surface by the U.S. and the U.S.S.R. This anomaly is indicated by analysis of Lunokhod 2 magnetometer data which has revealed that the magnetic field fluctuations near Mare Serenitatis are strongly linearly polarized in a direction aligned approximately radial to the Mare (Dolginov et al., 1976). The Soviet Lunokhod 2 surface rover is located at the eastern edge of Mare Serenitatis within the Bay Le Monnier at selenographic coordinates 26° North latitude

and 31° East longitude. A similar polarization is reported by Schubert et al. (1974) for the magnetic field oscillations measured at the edge of Mare Imbrium by the U.S. Apollo 15 surface magnetometer. They interpreted this phenomenon as the manifestation of an electrical conductivity anomaly in the lunar crust and upper mantle associated with Mare Imbrium. A similar conductivity anomaly associated with Serenitatis may be expected since both maria contain mascons, are likely to have a similar origin and history, and therefore, probably share similar physical and chemical properties.

To model this conductivity distribution, Vanyan et al. (1979) represented the lunar highlands by a dielectric layer of conductivity less than 10^{-6} S/m and thickness 150 km, between a layer of conductivity 10^{-3} S/m below and the highly conducting solar wind plasma above. Beneath the mare the insulating layer is thicker by an additional 150 km. Magnetic fluctuations between 10^{-2} and 10^{-1} Hz will propagate most readily in the low conducting region, resulting in a concentration of magnetic lines of force in this region beneath the mare. For this model conductivity distribution the magnetic field was calculated which would be measured near the anomaly using a numerical solution to the boundary value problem. Then the data was compared to model calculations by Vanyan et al. (1979) to investigate the proposed electrical conductivity anomaly. The model was adjusted by varying the dielectric thickness beneath Mare Serenitatis until the measured and calculated anisotropy matched at the Lunokhod 2 site. The best agreement was found when the basin was represented by a 150 km thickening of the dielectric layer.

Results of the analysis demonstrate that the magnetic anisotropy measured by the Lunokhod 2 magnetometer may be due to a region of anomalously low conductivity beneath Mare Serenitatis compared to the conductivity beneath adjacent highlands. We

propose a combination of heat transport and chemical differentiation resulting from filling of front-side basins to explain maria conductivity anomalies. According to this hypothesis the magma which filled the front-side basins carried large quantities of heat from deep within the moon to the surface where the heat was dissipated by radiation. The subhighland mantle was cooled by a less efficient process of conduction through the crust. This would leave the maria crust and mantle cooler than that of the adjacent highlands. The magma extruded into the maria seas, and was enriched in heat source radioactive potassium, uranium, and thorium. The magma source regions beneath the maria would therefore be depleted of these heat sources relative to surrounding highland mantle. This depletion of both thermal energy and radioactive heat sources, resulted in cooler submaria mantle in comparison to the subhighland mantle with the cooler material having the lower electrical conductivity. Our hypothesis which relates shallow electrical conductivity structure and mare volcanism has at least two features which may be tested by future lunar experiments: (1) a conductivity anomaly should be associated with all circular lunar maria and (2) the magnitude of each anomaly should be directly related to the volume of magma in the basin suggesting that farside basins which are not flooded by magma should not be associated anomalous lithospheric conductivity.

3.0 LUNAR MAGNETIC PERMEABILITY

3.1 BULK PERMEABILITY MEASUREMENTS

In earlier work on magnetic permeability and iron abundance of the moon (Parkin et al., 1973, 1974), the analytical technique involved use of simultaneous data from the lunar orbiting Explorer 35 magnetometer and the Apollo 12 or 15 surface magnetometer. With the present technique, simultaneous data from the Apollo 15 and 16 surface magnetometers are used, requiring no orbital magnetic field data. This method has the advantages of using only the higher resolution surface magnetometers, and is insensitive to instrument offsets. A representation of the total field at both sites plus a transformation matrix relating fields at the sites, yields a total of 13 equations with 10 unknowns. These equations are solved for the lunar bulk relative magnetic permeability μ_b , expressed as follows:

$$\begin{aligned}\mu_b &= \frac{\Delta B_{2x} - a_{11} \Delta B_{1x}}{a_{12} \Delta B_{1y} + a_{13} \Delta B_{1z}} \\ &= \frac{a_{21} \Delta B_{1x}}{\Delta B_{2y} - a_{22} \Delta B_{1y} - a_{23} \Delta B_{1z}} \\ &= \frac{a_{31} \Delta B_{1x}}{\Delta B_{2z} - a_{32} \Delta B_{1y} - a_{33} \Delta B_{1z}}\end{aligned}$$

REPRODUCIBILITY OF THE
ORIGINAL PAGE IS POOR

where subscripts 1 and 2 denote Apollo sites, e.g. site 1 can be designated Apollo 15 and site 2, Apollo 16; subscripts x, y, z , denote vector components in the ALSEP coordinate system with origin at either site, where \hat{x} is directed radially outward from the lunar surface, and \hat{y} and \hat{z} are tangent to the surface, directed eastward and northward, respectively; a_{ij} is an element in the transformation matrix from site 1 to site 2. Each field-difference term $\Delta B_{ij} = B_{ij}(t_m) - B_{ij}(t_n)$ denotes a difference in a field component measured at the same site at two different times when field values are different. To solve for bulk relative permeability of the moon we perform a regression analysis using over 2000 simultaneous Apollo 15 and Apollo 16 magnetometer data sets, measured during five orbits of the moon through the geomagnetic tail. These data have been carefully selected to eliminate data measured in the plasma sheet or contaminated by other induction modes such as eddy current induction.

Effects of plasma diamagnetism and confinement are minimized by eliminating data points for which the magnitude of the external magnetizing field $H < 7 \times 10^{-5}$ Oe. Since poloidal eddy current induction is dependent upon time rate of change of H , inclusion of poloidal fields is minimized by averaging over 10-min intervals during which Apollo 15 and 16 data peak-to-peak variations are small. Then pairs of data points are selected from different times, and a regression analysis performed. The least-squares best estimate of the slope, calculated using the method of York (1966), is $\mu_b = 1.008 \pm 0.005$. The paramagnetic permeability of the moon, adjusted for ionospheric effects, is $\mu = 1.012^{+0.011}_{-0.008}$. This result is in general agreement with previous measurements using Explorer 35 and Apollo 12 magnetometer data reported by Parkin et al. (1974).

3.2 IRON ABUNDANCE ESTIMATES

Using the value of global lunar magnetic permeability, we can determine free iron and total iron abundances. The free and total iron values are also constrained by lunar density and moment of inertia, and are functions of thermal and compositional models of the lunar interior.

The lunar bulk permeability $\mu = 1.012^{+0.011}_{-0.008}$ is too high to be accounted for by any paramagnetic mineral which is a likely constituent of the lunar interior, implying that some material inside the moon must be in the ferromagnetic state. Assuming the ferromagnetic material is free iron of noninteracting multidomain grains, the lunar free iron abundance can be determined using a thermal model of the lunar interior. The thermal profile is approximated by a two-layer model with the boundary located at the iron Curie point isotherm. We assume the moon is composed of a homogeneous mineral (olivine or orthopyroxene) of uniform density 3.34g/cm^3 , with free iron grains dispersed uniformly throughout the sphere. The iron Curie isotherm radius R_C should be in the range $\lambda > 0.88$, where $\lambda = R_C/R_m$. In our calculations we use $\lambda = 0.88$.

Using $\mu = 1.012^{+0.011}_{-0.008}$ we determine free iron abundance to be $2.5^{+2.3}_{-1.7}$ wt.%. The free iron abundance corresponds to total iron abundance of 6.0 ± 1.0 wt.% for the free iron/olivine lunar model, or 12.5 ± 1.0 wt.% for the free iron/orthopyroxene model. If we assume the lunar composition to be one or a combination of these minerals, the total iron abundance will be between 5.0 and 13.5 wt.%.

3.3 CORE SIZE LIMITS

The moon could have a small highly conducting core with a Cowling time constant of the order of at least a few days which would exclude the external geomagnetic tail field and thus act as a "diamagnetic" region of effective zero permeability. Therefore the lunar magnetic permeability results from magnetometer measurements can be used to place limits on a possible highly conducting core in the moon. In our analysis the moon is represented by a three-layer magnetic model: an outer shell of temperature (T) below the Curie point (T_c), whose permeability μ is dominated by ferromagnetic free iron; an intermediated shell of $T > T_c$ where permeability $\approx \mu_0$, that of free space; and a highly conducting core ($\sigma \gg 10^{-2}$ mhos/m) modeled by $\mu=0$.

For the case of a spherically symmetric permeable moon in a vacuum, immersed in a constant external (geomagnetic high-latitude lobe) field (H) the total magnetic field (B) measured at a surface site, in ALSEP coordinates, is

$$B = \mu_0 \left[(1+2G)H_x \hat{X} + (1-G)H_y \hat{Y} + (1-G)H_z \hat{Z} \right]$$

For the case of a hypothetical highly conducting core $\mu_3=0$.

When $\mu_0=1$

$G=$

$$\frac{-2a^3c^3(\mu-1)^2 + a^3b^3(2\mu+1)(\mu+2) + 2b^6(2\mu+1)(\mu-1) - 2b^3c^3(2\mu+1)(\mu-1)}{-2a^3c^3(\mu+2)(\mu-1) + 2a^3b^3(\mu-1)(\mu+2) + 4b^6(\mu-1)^2 - 2b^3c^3(\mu+2)(2\mu+1)}$$

Where a is the radius of the core, b is the outer radius of the intermediate shell, and c is the radius of the moon and μ is the paramagnetic permeability of the lunar shell.

The magnetic permeability of the outer shell is expressed $\mu = 1 + 4\pi K$; the magnetic susceptibility $K = K_F + K_P$, where K_F is the apparent ferromagnetic susceptibility of free iron (in emu/cm³) and K_P is paramagnetic susceptibility of the rock matrix in the outer shell. We have assumed that the composition of the outer shell is homogeneous, with free iron multidomain, noninteracting grains uniformly distributed throughout a paramagnetic mineral (either olivine or orthopyroxene). All geochemical and geophysical constraints and expressions for K_F and K_P used in our calculations are reported in Dyal et al. (1975).

In order to consider upper limits on such a hypothetical highly conducting lunar core, we impose the extreme (rather unrealistic) condition that the olivine or orthopyroxene matrix has no iron silicate (thus is composed entirely of magnesium silicate). In this extreme case the allowable free iron content is maximized as is the core size. The upper limit core radius consistent with our measurements is 535 km for an orthopyroxene moon and 385 km for an olivine moon. It is noted that for both lunar compositional models the minimum core radius is zero; that is, all our measurements to date do not require the existence of a highly conducting core.

4.0 LUNAR IONOSPHERE AND ATMOSPHERE

The purpose of this work was to present a quantitative model of the lunar ionosphere and its associated atmosphere during the four-day period when the moon is in the geomagnetic tail and thereby shielded from the solar wind plasma. A quantitative description of the lunar atmosphere and ionosphere for times when the moon is shielded from the solar wind is important to our knowledge of the moon's interior. Surface and orbital magnetic data measured in the geotail are used to calculate the lunar electrical conductivity and magnetic permeability (Parkin et al., 1973, 1974). Accurate interpretation of these data requires knowledge of the plasma in the lunar environment.

The concentrations of the constituents of the lunar atmosphere when the moon is in the geomagnetic tail are found to differ substantially from properties in the solar wind, which is a primary source of the lunar atmosphere. This is especially true during 'quiescent' geotail conditions when effects due to external plasma are minimal (e.g., in lobe regions when little or no plasma is detected by Apollo solar wind spectrometers or suprathermal ion detectors). Argon 40 has a source both in the solar wind and the geotail; it is vented from the surface as a radioactive decay product of subsurface ^{40}K . Hydrogen and helium existing in the lunar atmosphere initially as the moon enters the geotail are lost rapidly, primarily through thermal escape, whereas the heavier constituents, neon and argon, are lost very much more slowly through photo-ionization. After two days in the tail, the constituent atmosphere densities are calculated to be as follows: H_2 , $< 10 \text{ cm}^{-3}$; ^4He , $\sim 500 \text{ cm}^{-3}$; ^{36}Ar , $\sim 1.3 \times 10^2 \text{ cm}^{-3}$; ^{40}Ar , $\sim 1.6 \times 10^3 \text{ cm}^{-3}$; and ^{20}Ne , $\sim 3.9 \times 10^3 \text{ cm}^{-3}$.

Ultraviolet radiation from the sun continually ionizes the lunar atmosphere, above the sunlit hemisphere of the moon. When the moon is in the solar wind, these charged particles are quickly and efficiently removed from the lunar environment by the $V \times B$ electric field associated with the solar wind plasma flow past the moon. When the moon is shielded from the solar wind by the geomagnetosphere, conditions are much different. The ionization produces electrons at $\sim 1.5 \times 10^5$ °K and ions at $\sim 370^\circ\text{K}$ from neon and argon, the two most abundant atmospheric species. A hydrostatic treatment of this problem leads to the concept of a Rosseland electric field, which is required to preserve charge neutrality in the presence of the differential competition between gravitational binding and thermal evaporation. A hydrostatically bound ionosphere is one in which the ion pair particle density vanishes at large altitudes. We find that binding requires that the gravitational potential energy exceed the thermal energy. For the conditions appropriate to the moon this does not occur; indeed, the thermal energy exceeds the gravitational energy by a factor of 20. Therefore a hydrostatic treatment is not applicable, and a bound ionosphere does not exist; a hydrodynamic approach is required to describe the lunar ionosphere in the geotail.

At the lunar orbit the earth's magnetic field is nearly uniform and $\sim 10\gamma$. This field corresponds to a magnetic energy density of $\sim 4 \times 10^{-10}$ erg/cm³, a value large in comparison with the energy density of the ionized atmosphere, which is $\sim 2 \times 10^{-13}$ erg/cm³. Therefore the particles flow parallel to the magnetic field lines, forming a cylinder whose base has the lunar diameter. We have developed a hydrodynamic model which predicts ionospheric flow velocities in the range 4-7km/s and corresponding ion pair densities of $\sim 1.2 \times 10^{-2}$ cm⁻³.

From our calculations of ionospheric characteristics we can estimate electromagnetic properties of the ionosphere to determine the influence of the ionosphere on electromagnetic studies of the moon's interior. Our results allow calculation of the lunar ionosphere's plasma energy density $nkT = 2.5 \times 10^{-13}$ erg/cm³, from which we obtain diamagnetic properties of the ionosphere. The magnetization of the plasma is $M = nm$, where the magnetic moment $m = mv^2B/2B^2 = -ktB/B^2$. Because $B = H + 4\pi M = \mu H$ and $\beta = 8\pi nkT^*/B^2$, the relative magnetic permeability is

$$\mu = \frac{1}{(1 + \beta/2)}$$

The quantity β , the ratio of thermal to magnetic energy density, is $\sim 6 \times 10^{-4}$. The corresponding magnetic susceptibility of the ionosphere is $\chi = (\mu - 1)/4\pi \approx -2.5 \times 10^{-5}$ emu/cm³. This value is almost 3 orders of magnitude too low to account for the diamagnetic moment of the moon reported by Russell et al. (1974). Furthermore, the tenuous lunar ionosphere is confined primarily on the lunar sunlit side and is not confined to regions of altitude below 100km. We conclude that the lunar ionosphere contributes only negligibly to the plasma environment near the moon; therefore it is valid to neglect lunar ionospheric effects in studies of electromagnetic properties of the lunar interior.

REFERENCES

- Backus G. E. and Gilbert J. F. (1970) Uniqueness in the Inversion of Inaccurate Gross Earth Data. Phil. Trans. Roy. Soc. A266, 123-192.
- Cisowski S., Fuller M., Rose M. E., and Wasilewski P. J. (1973) Magnetic Effects of Experimental Shocking of Lunar Soil. Proc. Lunar Sci. Conf. 3rd. p. 3003-3017.
- Cisowski S. M., Fuller M., Yee Ming Wu, Rose M. F., and Wasilewski P. J. (1975) Magnetic Effects of Shock and Their Implications for Magnetism of Lunar Proc. Lunar Sci. Conf. 6th. p. 3123-3141.
- Cisowski S. M., Dunn J. R., Fuller M., Yee Ming Wu, Rose M. F., and Wasilewski P. J. (1976) Magnetic Effects of Shock and Their Implications for Lunar Magnetism (II). Proc. Lunar Sci. Conf. 7th. p. 3299-3320.
- Cisowski S. M., Hale C., and Fuller M. (1977) On the Intensity of Ancient Lunar Fields. Proc. Lunar Sci. Conf. 8th. p. 725-750.
- Daily W. D. and Dyal P. (1979) Magnetometer Data Errors and Lunar Induction Studies. J. Geophys. Res., 84,33,13.
- Dolginov Sh. Sh., Eroshenko E. G., Sharova V. A., Vnuchkova T. A., Vanyan L. L., Okulesky B. A., Bazilevsky A. T. (1976) Study of Magnetic Field, Rock Magnetization and Lunar Electrical Conductivity in the Bay Lemonnier. The Moon 15. 3-14.
- Dyal P., Parkin C. W., and Daily W. D. (1975) Lunar Electrical Conductivity and Magnetic Permeability. Proc. Lunar Sci. Conf. 6th, p. 2909-2926.
- Dyal P., Parkin C. W., and Daily W. D. (1976) Structure of the Lunar Interior from Magnetic Field Measurements. Proc. Lunar Sci. Conf. 7th, p. 3077-3095.
- Goins N. R., Dainty A. M., and Toksoz M. N. (1977) The Structure of the Lunar Interior as Determined from Seismic Data (Abs.) In Lunar Science VIII, p. 354-356. The Lunar Science Institute. Houston.
- Hargraves R. B., and Perkins W. E. (1969) Investigations of the Effect of Shock on Natural Remanent Magnetization. J. Geophys. Res., 74. 2576-2589.
- Hide R. (1972) Comments on the Moon's Magnetism. The Moon. 1,39.

- Hobbs B. A. (1973) The Inversion Problem of the Moon's Electrical Conductivity. Earth Planet. Sci. Letters 17. 380-384.
- Hood L., Russell C. T., and Coleman P. J., Jr. (1978) Evidence for a Non-random Magnetization of the Moon. Geophys. Res. Lett. 5, 305-308.
- Hood L. L., and Wilhelms D. E. (1978) Some Evidence on the Source of Lunar Crustal Magnetic Anomalies. Submitted to Science.
- Levy E. H., and Sonett C. P. (1978) Meteorite Magnetism and Early Solar System Fields. Conf. On Protostars and Planets, In Press. Tucson.
- Nagata T., Ishikawa Y., Kinoshita H., Kono M., Syono Y., and Fisher R. M. (1970) Magnetic Properties and Natural Remanent Magnetization of Lunar Materials. Proc. Of The Apollo 11 Lunar Sci. Conf., p. 2325-2340.
- Nagata T., Fisher R. M., Schwerer F. C., Fuller M. D., and Dunn J. R. (1971) Magnetic Properties and Remanent Magnetization of Apollo 12 Lunar Materials and Apollo 11 Lunar Microbreccia. Proc. Lunar Sci. Conf. 2nd. p. 2461-2476.
- Nagata T., Fisher R. M., and Schwerer F. C. (1972) Lunar Rock Magnetism. The Moon 4, 160-185.
- Parker R. L. (1970) The Inverse Problem of Electrical Conductivity in the Mantle. Geophys. J. Roy Astron Soc. 22, 121-138.
- Parkin C. W., Dyal P., Daily W. D. (1973) Iron Abundance in the Moon from Magnetometer Measurements. NASA TMX-62, 279.
- Parkin C. W., Daily W. D., and Dyal P. (1974) Iron Abundance and Magnetic Permeability of the Moon. Proc. Lunar Sci. Conf. 5th, p. 2761-2778.
- Petrova G. N. (1963) The Difference Between Types of Magnetization as a Basis of Study of the Magnetic Stability of Rocks (Disser.). Earth Physics Inst.
- Phillips R. J. (1972) The Lunar Conductivity Profile and the Nonuniqueness of Electromagnetic Data Inversion. Icarus 17. 88-103.
- Russell C. T., Coleman P. J., Jr., Lichtenstein B. R., and Schubert G. (1974) The Permanent and Induced Magnetic Dipole Moment of the Moon. Proc. Lunar Sci. Conf. 5th. p. 2747-2760.
- Schubert G., Schwartz K. (1969) A Theory for the Interpretation of Lunar Surface Magnetometer Data. The Moon 1. 106-117.

- Schubert G., Smith B. F., Sonett C. P., Colburn D. S., and Schwartz K. (1974) Polarized Magnetic Field Fluctuations at the Apollo 15 Site. Possible Regional Influence on Lunar Induction Science 183. 1194-1197.
- Schwartz K., and Schubert G. (1969) Time-Dependent Lunar Electric and Magnetic Fields Induced by a Spatially Varying Interplanetary Magnetic Field. J. Geophys. Res. 74. 4777-4780.
- Sonett C. P., and Colburn D. S. (1967) Establishment of a Lunar Unipolar Generator and Associated Shock and Wake by the Solar Wind Nature 216. 340-343.
- Sonett C. P., Colburn D. S., and Schwartz K. (1968) Electrical Heating of Meteorite Parent Bodies and Planets by Dynamo Induction From Premain Sequence. T Tauri Solar Wind. Nature 219. 924-926.
- Srnka L. J. (1977) Spontaneous Magnetic Field Generation in Hypervelocity Impacts. Proc. Lunar Sci. Conf. 8th. p. 785-792.
- Vanyan L. L. (1977) The Interaction of the Solar Wind With Lunar Magnetic Anomalies. The Moon 16. 321-324.
- Vanyan L. L., Vnuchkova T. A., Yegorov I. V., Basilevsky A. T., Eroshenko E. G., Fainberg E. B., Dyal P., and Daily W. D. (1979) Electrical Conductivity Anomaly Beneath Mare Serenitatis Detected by Lunokhod 2 and Apollo 16 Magnetometers. The Moon and Planets. In Press.
- Wasilewski P. (1972) Magnetic Remanence Mechanisms in Fenico Alloys and the Magnetization of Lunar Rocks and Soil (Abstract). Lunar Science IV. 770. The Lunar Science Institute. Houston.
- Wasilewski P. J. (1973) Shock Remagnetization Associated with Meteorite Impact at Planetary Surfaces. The Moon, 6. 264-291.
- Wasilewski P. J. (1978) Magnetic Properties of Feni Alloys-- Microstructure and Remanent Magnetization Mechanisms (Abstract). In Conf. On Origins of Planetary Magnetism 119-120. Lunar and Planetary Institute. Houston.
- York D. (1966) Least-Squares Fitting of a Straight Line. Canadian J. Phys. 44, 1079-1086.

APPENDIXES

Recent publications and abstracts not contained in previous status reports.

<u>Title</u>	<u>Page</u>
A On the Phase Relationship Between the Energetic Particle Flux Modulation and Current Disc Penetrations in the Jovian Magnetosphere: Pioneer 10 Inbound.	A-1
B Theories for the Origin of Lunar Magnetism . . .	B-1
C Electrical Conductivity Anomalies Associated with Circular Lunar Maria	C-1
D Electromagnetic Properties of the Moon	D-1
E Mare Serenitatis Conductivity Anomaly Detected by Apollo 16 and Lunokhod 2 Magnetometers	E-1
F Lunar Properties from Magnetometer Data: Effects of Data Errors	F-1

APPENDIX A

ON THE PHASE RELATIONSHIP BETWEEN THE ENERGETIC PARTICLE
FLUX MODULATION AND CURRENT DISC PENETRATIONS IN THE
JOVIAN MAGNETOSPHERE: PIONEER 10 INBOUND

ON THE PHASE RELATIONSHIP BETWEEN THE ENERGETIC PARTICLE
FLUX MODULATION AND CURRENT DISC PENETRATIONS IN THE
JOVIAN MAGNETOSPHERE: PIONEER 10 INBOUND

Douglas E. Jones

Department of Physics and Astronomy, Brigham Young University, Provo, Utah 84602

Abstract. The surface defined by the locus of field minima along field lines for an untruncated Jovian model magnetosphere is found to coincide with the surface of the model current disc which provides a good fit to the data. However, when the model is terminated by means of magnetopause currents, preservation of the fit by modifying the current distribution near the outer edge of the disc causes the minimum $|\vec{B}|$ surface to bifurcate. Energetic electron flux time profiles that are based upon such a minimum $|\vec{B}|$ configuration are found to be qualitatively consistent with the inbound Pioneer 10 data.

Introduction

One of the puzzling characteristics of the particle flux modulation observed by the energetic particle measurements aboard Pioneer 10 was that during the inbound leg the electron particle count maxima occurred when the spacecraft was at Jovian System III longitude $\lambda_{III}(1973.92) < 222^\circ$, whereas during the outbound leg they occurred when the spacecraft was at $\lambda_{III}(1973.92) > 42^\circ$ (Van Allen et al., 1974a). It is generally assumed that the 10 hour modulation results from a confinement of the particles to a region near the magnetic equatorial plane (Van Allen et al., 1974b; Simpson et al., 1974; Trainor et al., 1974; Fillius and McIlwain, 1974), although there is strong support for a temporal model, i.e., one in which the particle modulation is strictly a function of time rather than bearing any geometric relation to the location of the current disc that encircles the planet (Chenette et al., 1974; Simpson and McKibben, 1976).

Goertz et al. (1974, 1976) have shown rather convincingly that the Pioneer 10 outbound energetic electron count rate maxima occur as the spacecraft passes through a wobbling current disc and have interpreted the observed particle flux modulation in terms of open and closed field lines. Their study suggests that when the spacecraft is on magnetic field lines that the model magnetosphere predicts as being closed, the energetic particle flux is much greater than when field lines are encountered that the model predicts as being open (or connecting to interplanetary field lines).

Northrop et al. (1974) have considered the azimuthal distortion of the Jovian magnetic field as measured by Smith et al. (1974) and have suggested that the apparent inbound lead of the particle count rate maxima is caused by a slippage of the foot of the magnetic field line in the ionosphere with respect to the Jovian surface. However, if the count rate maxima occur in the magnetic equatorial plane or in the current disc, then the observed change in phase of the occurrence of the maxima in passing from the inbound to the outbound legs of the trajectory requires that the surface of the current disc exhibit a leading type of twist near 10 o'clock local time and a lagging type of twist near the dawn terminator. We find that the magnetic field data are consistent only with a lagging azimuthal twist of the current disc.

In this study we confine ourselves primarily to observations of the flux of ~ 5 to 30 MeV electrons, since the electron flux showed evidence of modulation by Jupiter's rotation during the entire period that Pioneer 10 was within Jupiter's magnetosphere (Simpson et al., 1974).

The Model Studies

Models for Jupiter's current disc have been developed in an attempt to determine if a stationary current configuration in the corotating frame can produce a magnetic field that matches the data, or whether a dynamic model is required, and, if so, what its characteristics are. In addition to such parameters as the thickness, radial extent, and radial dependence of the current, it has been possible to include various types of warping of the current disc, such as twisting, bending, and to some extent fluting. The twisting of the current disc used

in the models is described by the manner in which the axis of each ring increment of current in the disc progressively changes in longitude, or longitude at which the local current disc surface reaches a maximum latitude, as a function of ring radius. It has been found that a warping of the current disc in the form of a lagging type of twist is required to match both the inbound and outbound magnetic field data from Pioneer 10. A linear fit to the twisting of the current disc in the corotating frame has been found to be of the form

$$\lambda_{III}(1973.92) = 232 + 0.4 R/R_J \text{ degrees}$$

for Pioneer 10 inbound, and

$$\lambda_{III}(1973.92) = 36 + 0.9 R/R_J \text{ degrees}$$

for Pioneer 10 outbound, where $\lambda_{III}(1973.92)$ represents the System III longitude dependence of the axis of each current ring on ring radius R . Preliminary results of these model studies have already been reported elsewhere (Jones et al., 1976a,b). [Kivelson et al. (1977, 1978) have more recently described a time dependent configuration for the outbound current disc in terms of propagating Alfvén waves.] Hence, it would appear that the apparent leading nature of the spiralling inferred from the Pioneer 10 inbound electron count rate maxima must result from a discrepancy in the model, from some type of dynamic change that was occurring as Pioneer 10 approached the planet, or from some other cause.

Barish and Smith (1975) have shown that when a dipole plus current ring model for the Jovian magnetosphere is developed to approximate the inbound Pioneer 10 data using Euler potentials, several regions along a field line are observed where the field magnitude exhibits localized minima (see their Fig. 5), and at these field minima, particle flux maxima should occur. Multiple field minima regions are a result of inward compression of the sunward magnetosphere and the presence of the current disc affects where these minima are located. The particular type of minimum $|B|$ contour that results depends upon the current distribution in the disc and the presence of the magnetopause currents. Barish and Smith (1975) have also pointed out that with

a thin, intense azimuthal current disc plus their magnetopause current configuration, there are three discrete minimum $|E|$ regions, whereas with a weak, thick current disc there is only one. Fillius et al. (1975) previously suggested that a bifurcated latitude profile would be a possible means of explaining the abnormally high particle count rates observed during the outbound passage of Pioneer 11.

Following the suggestion of Barish and Smith we have attempted to determine the qualitative effect of terminating our magnetosphere models by means of magnetopause currents in order to see if the resulting configuration of the minimum field surface might offer a clue to resolving the problem of the locations of the particle flux maxima and current disc penetrations.

Unfortunately, fluctuations in the angle between \vec{B} and the Jovian spin axis make it difficult to develop an accurate model of the terminated front side magnetosphere. Therefore, we have studied the effects of magnetopause termination using the Pioneer 10 outbound data because the field was much quieter. However, it should be possible to infer the type of configuration to be expected in the front side magnetosphere by simple scaling.

Figure 1. shows the locus of minima in field magnitude along field lines, displayed in a coordinate system containing the current disc symmetry axis, that is observed in field line tracing related to a spherical boundary terminated magnetosphere for Pioneer 10 outbound and a flat current disc lying in the magnetic equator. In order to maintain the good fit to the middle magnetosphere data when magnetopause currents are included (which contributes a significant southward field) additional current is needed in the disc at or beyond $100 R_J$, although this portion of the current disc is probably much thicker.

Qualitatively, we find that the addition of current near the outer edge of the disc tends to cause the surface representing the locus of local minimum values of the field along field lines, that is normally expected to be in the plane of the current disc, to separate into two surfaces beyond $75 R_J$ for the outbound pass. As a result, a single, sharp minimum occurs in the plane of the current disc out to about $75 R_J$, and beyond $75 R_J$ there are two broad minima- one above and one below the plane of the current disc. One would expect this effect to be much more marked

in the case of Pioneer 10 inbound and the bifurcation to begin much closer to the planet. A simple scaling of the nominal inbound and outbound current disc radii (85 and 130 R_J , respectively) deduced from model studies completed to date suggest that nominal inbound bifurcation may begin within 50 R_J . Solar wind enhancements like that which occurred during the inbound pass, and which pushed the magnetopause in to at least 46.5 R_J (Wolfe et al., 1974) must cause bifurcation to begin even closer to the planet. Other effects that need to be considered which affect the shape of the high latitude minimum $|\vec{B}|$ contours are the tilt of the axis, twisting and bending of the current disc, and the actual shape of the magnetopause.

Figure 2 displays the variation with distance along the current disc of the perpendicular distance between the spacecraft and current disc at the time of measurement of a maximum of energetic (> 5 MeV) electron flux (defined as the midpoint between consecutive minima) and minima as deduced from Figure 3 of Van Allen (1976) using the best fit Pioneer 10 inbound current disc. Figure 3 compares the corresponding variation in longitude of current disc penetrations and particle flux maxima with planet-probe distance.

Five of the seven particle flux peaks observed between 55 and 90 R_J are characterized by a doublet structure which is consistent with the passage of the spacecraft through a local maximum in the particle flux. The particle flux minima were likely relative minima as no doublet features were observed. This is supported by the fact that the spacecraft apparently did not pass through the current disc in this same region of the magnetosphere, which is where the model predicts particle flux minima (see Fig. 2). The absence of double peaks within 46 R_J suggests that the spacecraft did not pass periodically completely through a local maximum in particle flux, which is also consistent with the results displayed in Fig. 2.

These data suggest that a bifurcation of the nominal maximum electron flux surface may have occurred in the vicinity of 50 R_J . The situation is clearly complicated because of inward compression by a solar wind enhancement while the spacecraft was between 46.5 and 53.4 R_J (Wolfe et al., 1974). A similar bifurcation is likely to be found in studies of both sets of the Pioneer 11 energetic particle flux data. The bifurcation effects are found to be absent in the Pioneer 10 outbound data at least out to 80 R_J , which is qualitatively consistent with the

assumption that such effects should occur primarily in the sunward portion of the magnetosphere.

If the minimum $|\vec{B}|$ surfaces are able to trap energetic electrons, then such a configuration might qualitatively explain the discrepancy observed in the Pioneer 10 inbound data when the occurrence of particle flux maxima and penetrations of the current disc are compared. Hence, these results tend to support the spatial model for the modulation of the energetic particle flux.

Although we have found in a separate study that there is clear evidence the current in the azimuthal disc was returning to its quasi-stationary configuration during the time the spacecraft passed inward from about $45 R_J$ to periapsis, nevertheless, the model and correlative studies being reported here suggest that the phase relationship between the particle flux maxima and current disc penetrations was relatively constant during the time interval when the spacecraft passed $40 R_J$ inbound and on out the outbound leg of the trajectory. The longitudinal locations of the current disc penetrations corresponding to the near Jupiter portions of Pioneer 10 inbound and those for the entire outbound portion are smoothly consistent. This also suggests that there are no significant longitudinal discontinuities in the current disc occurring over the 75 degrees separating the inbound and outbound trajectories. Coroniti and Kennel (1977) have postulated the existence of two distinct regions of the magnetosphere based upon a model that combines corotation within about $45 R_J$ and radial outflow beyond. This model would perhaps combine some of the features of both the temporal and spatial models. However, based upon the Pioneer 10 outbound data, no basic changes in the current disc are apparent out to at least $80 R_J$.

Recent studies of ELF chorus in the terrestrial magnetosphere by Tsurutani and Smith (1977) suggest that chorus may originate near the magnetopause in minimum $|\vec{B}|$ pockets as well as in regions near the magnetic equator (see their Figure 14). The flux of energetic particles should be higher in these regions (West, 1974). Hence, it is tempting to suggest that the inclusion of a large current disc would predict the type of latitudinal spatial distribution of energetic particles that is seen in the magneto-

sphere of Jupiter, and also suggests what type of latitude distribution of ELF chorus one would expect to find there.

Acknowledgements. I would like to thank Leverett Davis, Jr. and Edward J. Smith for helpful discussions and comments. This work was supported in part by NASA-Ames contract NAS2-7358 and grant NSG-2082.

References

- Barish, F.D. and R.A. Smith, An analytical model for the Jovian magnetosphere, Geophys. Res. Lett., 2, 269, 1975.
- Chenette, D.L., T.F. Conlon, and J.A. Simpson, Bursts of relativistic electrons from Jupiter observed in Interplanetary space with the time variation of the planetary rotation period, J. Geophys. Res., 79, 3551, 1974.
- Coroniti, F.V. and C.F. Kennel, Possible origins of time variability in Jupiter's outer magnetosphere, Geophys. Res. Lett., 4, 211, 1977.
- Fillius, R.W., and C.E. McIlwain, Radiation belts of Jupiter, Science, 183, 314, 1974.
- Fillius, R.W., C.E. McIlwain and A. Morgro-Campero, Radiation belts of Jupiter: A second look, Science, 188, 465, 1975.
- Goertz, C.K., B.A. Randall and M.F. Thomsen, A model for the Jovian magnetic field, EOS Trans. AGU, 56, 1172, 1974.
- Goertz, C.K., D.E. Jones, B.A. Randall, E.J. Smith and M.F. Thomsen, Evidence for open field lines in Jupiter's magnetosphere, J. Geophys. Res., 81, 3393, 1976.
- Jones, D.E., L. Davis, Jr., E.J. Smith, and J.G. Melville, II, Jupiter's magnetic field and magnetosphere, paper presented at COSPAR, Philadelphia, Penn., June 17, 1976a.
- Jones, D.E., J.G. Melville, II, E.J. Smith, and L. Davis, Jr., Modelling Jupiter's magnetospheric current disc: Pioneers 10 and 11, EOS Trans. AGU, 57, 991, 1976b.
- Kivelson, M.G., P.J. Coleman, Jr., L. Froidevaux, and R.L. Rosenberg, A time dependent model of the Jovian current sheet, UCLA Institute of Geophys. and Planetary Physics Publ. No. 1704, 1977.
- Kivelson, M.G., P.J. Coleman, Jr., L. Froidevaux, and R.L. Rosenberg, A time dependent model of the Jovian current sheet, J. Geophys. Res., 83, 4823, 1978.
- Northrop, T.G., C.K. Goertz, and M.F. Thomsen, The magnetosphere of Jupiter as observed with Pioneer 10, 2. non-rigid rotation of the magnetodisc, J. Geophys. Res., 79, 3579, 1974.

- Simpson, J.A., D. Hamilton, G. Lenk, R.B. McKibben, A. Mogro-Campero, M. Perkins, K.R. Pyle, A.H. Tuzzolino, and J.H. O'Gallagher, Protons and electrons in Jupiter's magnetic field: results from the University of Chicago experiment on Pioneer 10, Science, **183**, 306, 1974.
- Simpson, J.A., and R.B. McKibben, Dynamics of the Jovian magnetosphere and energetic particle radiation, Jupiter, T. Gehrels (Ed.), 738, University of Arizona Press, 1976.
- Smith, E.J., L. Davis, Jr., D.E. Jones, P.J. Coleman, Jr., D.S. Colburn, P. Dyal, C.P. Sonett, and A.M.A. Frandsen, The planetary magnetic field and magnetosphere of Jupiter: Pioneer 10, J. Geophys. Res., **79**, 3501, 1974.
- Trainor, J.H., B.J. Teegarden, D.E. Stilwell, F.B. McDonald, E.C. Roelof, and W.R. Webber, Energetic particle population in the Jovian magnetosphere; a preliminary note, Science, **183**, 311, 1974.
- Van Allen, J.A., D.N. Baker, B.A. Randeall, and D.D. Sentman, The magnetosphere of Jupiter as observed with Pioneer 10; 1, instrument and principal findings, J. Geophys. Res., **79**, 3559, 1974a.
- Van Allen, J.A., D.N. Baker, B.A. Randall, M.F. Thomsen, D.D. Sentman, and H.R. Flindt, Energetic electrons in the magnetosphere of Jupiter, Science, **183**, 309, 1974b.
- Van Allen, J.A., High-energy particles in the Jovian magnetosphere, Jupiter, T. Gehrels (Ed.), 928, University of Arizona Press, 1976.
- West, H.I., Jr., Pitch angle distributions of energetic electrons in the equatorial region of the outer magnetosphere--OGO 5 observations, Magnetospheric Physics, B.M. McCormac (Ed.), 93, D. Reidel, 1974.
- Wolfe, J.H., J.D. Mihalov, H.R. Collard, D.D. McKibbin, L.A. Frank, and D.S. Intriligator, Pioneer 10 observations of the solar wind interaction with Jupiter, J. Geophys. Res., **79**, 3489, 1974.

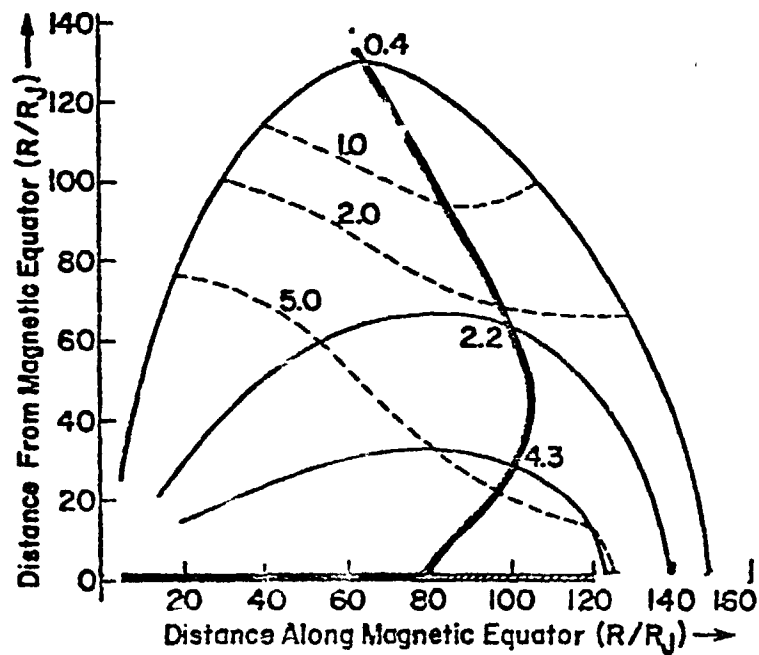


Figure 1

REPRODUCIBILITY OF THE
ORIGINAL PAGE IS POOR

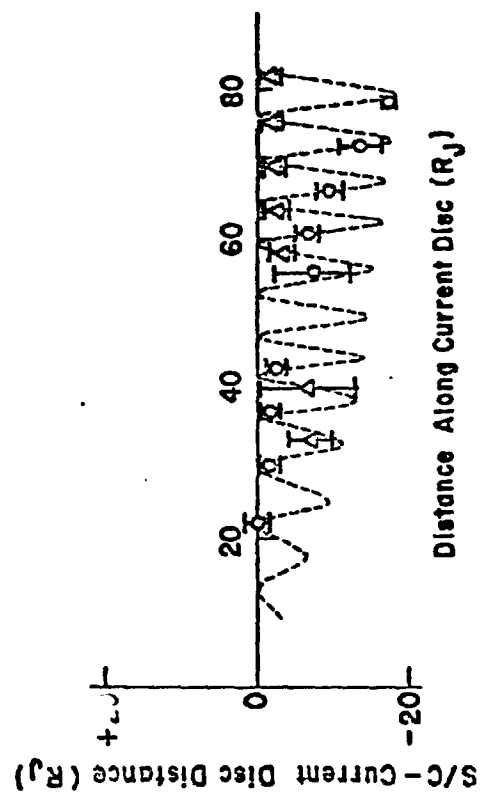


Figure 2

REPRODUCIBILITY OF THE
ORIGINAL PAGE IS POOR

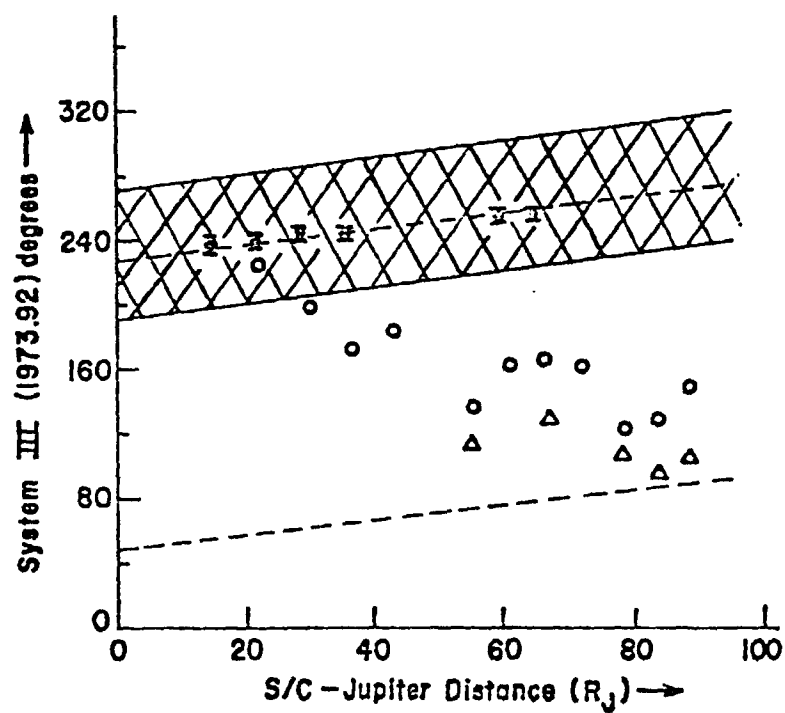


Figure 3

REPRODUCIBILITY OF THE
ORIGINAL PAGE IS POOR

APPENDIX B

THEORIES FOR THE ORIGIN OF LUNAR MAGNETISM

Theories for the Origin of Lunar Magnetism

William D. Daily
Eyring Research Institute
Provo, UT 84601

Palmer Dyal
NASA-Ames Research Center
Moffett Field, CA 94035

Short Title:
Origin of Lunar Magnetism

2 February 1979

Abstract

This paper reviews the major theories which have been proposed to explain the remanent magnetism found in the lunar crust. A total of nine different mechanisms for lunar magnetism are discussed and evaluated in light of the theoretical and experimental constraints pertinent to lunar magnetism. We conclude that none of these theories in their present state of development satisfy all of the known constraints. However, the theories which agree best with our present understanding of the moon are meteorite impact magnetization, thermoelectric dynamo field generation, and an early solar wind field.

1. INTRODUCTION

In this paper we review the theories and hypotheses which have been advanced to explain the remanent magnetization of the lunar crust. Since the reviews of lunar magnetization by Dyal et al. (1974) and Fuller (1974) new concepts have been proposed, old ideas have been developed, and new constraints discovered for these theories. We attempt to include in this review recent theoretical and experimental information pertinent to constraints on these theories. We hope that this review will differentiate those theories which clearly do not satisfy the constraints, from those which are viable and should be investigated in more detail.

Prior to the Apollo landings, the moon was considered magnetically uninteresting, without a global permanent field or appreciable magnetization in its crust. However, analysis of returned samples showed an unexpectedly large natural remanent magnetization (NRM) present in crustal material that is carried by free iron grains (Strangway et al., 1970; Pearce et al., 1971; Collinson et al., 1973). A magnetometer was included in the Apollo 12 experiment package to investigate magnetic fields induced in the moon by the solar wind magnetic field. Measurement of a 38 gamma steady field at the Apollo 12 landing site (Dyal et al., 1970) forced investigators to recognize regional uniformity in crustal magnetism. Based on knowledge of terrestrial remanent magnetism in iron oxides, the lunar remanence in unoxidized iron appears to be a magnetically hard thermoremanent type, acquired as the iron grains cooled in the presence of magnetic fields from about 10^{-3} to 1.6 Oe (Fuller, 1974). Virtually all lunar samples studied contain an NRM of 10^{-6} to 10^{-4} gauss $\text{cm}^3 \text{g}^{-1}$. In addition, remanent magnetic fields up to several hundred gammas (1 gamma = 10^{-5} Oe) are measured over much of the lunar surface (see Dyal et al., 1974 and Fuller, 1974 for reviews). During the ten years since the first lunar landings, many investigators have proposed a wide variety of

mechanisms to explain the magnetization of the moon. Many of these ideas are only hypotheses, some have been developed into theories, but none of them are entirely satisfactory for explaining all the relevant data. It is possible that none of them offer the correct explanation or that there is more than one explanation for the phenomenon. We hope that a review of the theories proposed to date will encourage further work in the field and help identify those processes responsible for lunar remanence.

For convenience in this review we classify the lunar magnetization theories into two groups: (1) Global--those which involve magnetic fields of a scale size comparable to or larger than the moon. (2) Local--those which involve processes or fields of a local nature where small regions are magnetized. The various theories of each classification will be reviewed and evaluated based on present knowledge of lunar remanence as well as lunar evolution.

2. GLOBAL PROCESSES

2.1 Solar Field.

Several authors have suggested that the paleomagnetic fields necessary to magnetize lunar crustal material originated in the early sun (e.g., Nagata et al., 1972). Supporting this idea Banerjee and Mellema (1976) conclude that paleointensity determinations on carbonaceous chondrites and lunar samples are consistent, implying that early solar system fields were responsible for the magnetization of both types of materials. If a large solar field was present during lunar crustal formation, and of dipole character out to the lunar orbit, the crust would have been magnetized uniformly as shown in Figure 1a. The present moon cannot have a uniformly magnetized shell since it would yield a global remanent dipole moment (Figure 1b) 2 to 3 orders of magnitude larger than the limit placed by Russell et al. (1974). On the other hand, if the early solar field was convected from the sun as it is today, the magnetic lines of force near the ecliptic would be preferentially aligned parallel to

Fig. 1

the ecliptic plane in the familiar spiral pattern. Hood et al. (1978) have shown that the magnetization vectors of these source regions tend to be parallel to this plane. This suggests that the regions may have been magnetized by early intense solar wind fields. Sonett et al. (1968) and Levy and Sonett (1978) have suggested that a pre-main sequence T Tauri sun or even an earlier nebular dynamo could have produced such large solar system fields. Freeman (1977) also proposes that a nebular dynamo may arise from induced currents in the plasma. In this model relative motion between the solar magnetic field, which corotates with the sun, and the nebular plasma which moves at Keplerian speed, generates a $\mathbf{V} \times \mathbf{B}$ electric field which drives currents in the equatorial rotation plane. At the surface of these current sheets, fields as large as 1 gauss are estimated.

The main objection to a solar or nebular origin for lunar magnetism is that the magnetizing field must remain constant during the cooling of a large volume of crust if it is to acquire a uniform magnetization. The time scale for fluctuations in an early solar field and for rotation of the moon itself, are probably small compared to the cooling time of large crustal regions. Large units could be uniformly magnetized by a solar wind field only if they were thin enough to cool rapidly. Hood and Wilhelms (1978) identified an extraordinarily thin, highly magnetized deposit at 8° N and 59° W. The Apollo subsatellite magnetometer measures a 21 gamma anomaly (at 20 km altitude) which coincides closely in size, shape, and position to a light deposit known as Reiner γ. The deposit thickness of 10 m is estimated from very small distortion of mare ridges which are observed internal and external to the deposit (D.E. Wilhelms, personal communication, 1979). A layer this thin may have cooled sufficiently fast to be uniformly magnetized by the solar wind magnetic field. If Reiner γ is responsible for the anomaly and it is only 10 m thick, its magnetization must be $5 \times 10^{-2} \text{ gauss cm}^3 \text{ g}^{-1}$ which is 500

times the stable magnetization of most lunar samples. Therefore, magnetization of localized regions in the crust or of thin breccia flows on the surface by an intense solar wind field is plausible, but magnetization of large regions by this mechanism is problematic.

2.2 Terrestrial Field.

Magnetization of lunar rocks by the terrestrial field requires that the moon was once much closer to the earth, that the earth's field was much more intense, or a combination of these two possibilities. If the lunar distance were only 3-4 earth radii, the present terrestrial field would be sufficient to account for the lunar paleointensity determinations of $\sim 10^3$ gammas but cannot account for the paleointensity values as high as 1.6 Oe (e.g., Fuller, 1974). This orbit requires the moon to be dangerously close to the Roche limit (Runcorn et al., 1970). The moon would not remain in this orbit for 1 b.y. (the approximate age span of magnetized lunar samples) because tidal braking would rapidly transfer spin angular momentum from the earth to the moon with an increase in lunar orbit radius to conserve angular momentum (Fuller, 1974).

To explain lunar magnetism with the moon in its present orbit, a terrestrial dipole moment at least 10^2 larger than its present value is necessary. Alfvén and Lindberg (1974) propose a type of terrestrial hydromagnetic dynamo which could produce a field of 1600 gammas at the moon if its distance was 10 to 20 earth radii. Extrapolation of available data does not imply the existence of these large fields. Paleointensity data for the earth is available in some detail for the past 0.4 b.y., and during this time the terrestrial magnetic moment has not increased in strength more than 50% of its present value (Strangway, 1970). Some terrestrial samples as old as 3 b.y. have a remanence similar to that of young rocks, implying that the earth's dynamo has operated much the same for the past 3 b.y. (Strangway, 1978).

Magnetization of the global lunar crust in a terrestrial magnetic dipole leads to a remanent moment in the modern moon larger than the measured limits (Russell et al., 1974). The mechanism for acquisition of this dipole moment is the same as that discussed for the early solar magnetizing field and is depicted in Figure 1. Considering the arguments discussed above, the earth seems to be an unlikely source for the early lunar magnetizing field.

2.3 Ancient Magnetized Core.

Runcorn and Urey (1973) and Strangway et al. (1973) have suggested that crustal remanence may have resulted from a lunar core, magnetized during or shortly after its formation. This core may have acquired a depositional magnetism as it accreted in a proposed 20 gauss field. Alternatively, the core may have acquired an isothermal remanence in this intense solar field or a viscous remanence in a weaker field. The magnetic field of this core is proposed to have thermoremanently magnetized the outer lunar shell as it cooled, 3.2 to 4 b.y. ago. Subsequent radioactive heating of the interior raised the core temperature above the Curie point with a loss of the internal magnetizing field. The proposed scenario is schematically illustrated in Figure 2. Strangway and Sharpe (1974, 1975) and Solomon (1978) have demonstrated that lunar evolution constraints are compatible with this mechanism for an early lunar field. In addition, Runcorn (1975) has shown that a spherical shell magnetized by the field of an internal dipole will have no magnetic moment if the original magnetizing field is removed. However Stephenson (1976) has calculated the residual dipole moment of the spherical shell for the more realistic case where the permeability of the shell and core are different. For this model, the calculated moment of a crust magnetized to a depth of only 35 km is the same order of magnitude as the limit measured by Russell et al. (1974). Srnka and Mendenhall (1978) also calculate a residual shell dipole for the more sophisticated model where the magnetizing dipole

Fig. 2

exponentially decays in strength and the crust is magnetized in layers as the Curie isotherm advances with depth during crustal cooling. For reasonable model parameters the residual dipole moment is 5 times the upper limit allowed by Apollo subsatellite measurements (Russell et al., 1974). It has also been pointed out by Runcorn (1976) that a field from an ancient magnetized core cannot explain paleointensity measurements of 1 Oe and larger derived for some lunar samples.

2.4 Lunar Core Dynamo.

A popular mechanism for the origin of the lunar field is a regenerative dynamo in a small core (e.g., Runcorn et al., 1971; Strangway et al., 1971). This idea is appealing since a hydromagnetic dynamo is the most reasonable source for the earth's field and terrestrial analogies are tempting for lunar phenomena. Remanence in lunar samples 4 b.y. old, requires formation of a small convecting core at least this early in lunar history. However, differentiation of the required iron or iron sulfide core and the lunar crust, seems to require melting of the whole moon (Runcorn, 1976). Melting the lunar core this early requires an extraordinarily intense heat source. For this heat source Runcorn (1977, 1978a) postulates iron soluble super-heavy elements with atomic numbers from 114 to 126 and half lives of $\sim 10^8$ yrs. Paleointensity determinations require this lunar dynamo to generate surface fields 3 times larger than those generated by the terrestrial dynamo. Paleointensity determinations on some samples indicate a decline in the early lunar field as would be expected from a dynamo produced in a cooling core. Paleomagnetic field intensities decreasing from 1.3 gauss to 0.05 gauss between 3.9 and 3.2 b.y. ago is indicated by the data in Figure 3a (Stephenson et al., 1975; Collinson et al., 1976; Runcorn, 1978). Cisowski et al. (1977) question this decline in the paleofield due to the large variation of intensity estimates for rocks of the same age and type. They attribute some of this variation to the

Fig. 3

modification of primary remanence in samples by shock effects (Cisowski et al., 1973; 1977). The apparent decrease of the early lunar field with time is not evident (Fig. 3b) when only paleointensity estimates are plotted for samples with a stable, single phase NRM which exhibits properties of a thermoremanence on alternating field or thermal demagnetization (Cisowski et al., 1977).

Magnetization of an ideal crustal shell by an internal dipole, as shown in Figure 4, results in zero field external to the shell after the magnetizing dipole is removed (Runcorn, 1975). The observed magnetic anomalies above the lunar crust are attributed to cratering or other processes which change the ideal shell. Field lines escape the shell at each crater. However, these field lines contribute to a global dipole moment as well as producing magnetic anomalies. Weiss et al. (1977) have calculated the magnetic dipole moment for a lunar model with the 17 largest basins and craters scooped out of a crustal shell magnetized by an internal dipole. The residual moment was much smaller than the measured upper limit dipole for the moon permitting a dynamo hypothesis to explain magnetic anomalies and satisfy the global dipole constraint.

The field lines that escape the shell at each crater will result in strong correlation of magnetic anomaly and crater location. Figure 5 shows the field magnitude calculated by Weiss et al. (1977) which would be observed 100 km above a shell magnetized by an internal dipole field and later cratered by removal of magnetized crust. The correlation between surface field and crater boundary is obvious yet this correlation has ^{been} searched for without success in lunar magnetic and topographic maps (Russell et al., 1977; Lin, 1978; Hood et al., 1978). This correlation may be destroyed in the highlands by overlapping of craters and by highly magnetized breccia deposits. To minimize these effects Lin (1978) has studied electron reflection magnetic maps for lunar maria. He found no correlation of magnetic field intensity

with craters and concluded that lunar maria are not uniformly magnetized as would be expected from a lunar dynamo field.

Operation of a lunar dynamo depends on the existence of a highly conducting core. Runcorn (1967) argues for a core based on departure of the moon from a hydrostatic equilibrium figure supported by solid convection in the lunar interior. However, Cassen et al. (1978) calculate lunar geometrical distortion from internal convection and find it unlikely that the lunar figure is determined by convection. Bills and Ferrari (1977), also investigating the lunar core, used global moment of inertia, gravitational, topographic, and compositional information to construct a lunar model which is consistent with an FeS_2 core in the moon. Likewise, electrical conductivity studies of Dyal et al. (1975, 1976), Goldstein et al. (1976), and Wiskerchen and Sonett (1977) cannot confirm or rule out the presence of a small highly conducting core. Nakamura et al. (1974) have tentatively proposed a small molten core based on the reduction of the P-wave velocity within 350 km of the lunar center. These observations of a possible phase change in the lunar interior do not require a highly electrical conducting core as needed for dynamo action.

The above experimental evidence for an iron core in the moon is inconclusive. However, if a small iron core is present it is important to examine the feasibility of dynamo action. Gose et al. (1972) have demonstrated that the magnetic Reynolds number is large enough for dynamo action. Levy (1972, 1974) was the first to examine the lunar dynamo in detail. He assumed a Parker type dynamo in the moon similar to that usually proposed for the earth. Scaling of the terrestrial dynamo to the lunar case leads to a rotation rate fast enough to break up the moon. Another dynamo model for the moon driven by a combination of diurnal tides and precession has also been investigated. Dolginov (1975) scales a precessional terrestrial dynamo to match a lunar core of 400 km radius and calculates fields up to 4000 gammas at the lunar surface. Model

calculations by Houben (1978) for a lunar precessional dynamo yield surface fields of a gauss or larger. We may conclude, therefore, that a magnetic dynamo is a reasonable source of global fields, but theory does not clearly predict field generation in a lunar core.

The observable consequences in the moon of an early dynamo magnetic field have been extensively studied. Runcorn (1975) established the important theorem that an external field vanishes from an ideal spherical shell magnetized by an internal dipole field after the dipole is removed (schematically depicted in Figure 4). This was important because it showed that a lunar dynamo magnetizing field is compatible with the present dipole moment limit. Stephenson (1976) extended the results of Runcorn (1975) to a more realistic lunar model by including a permeability difference between the lunar crust, core, and the external plasma. For this model the calculated present residual dipole moment is not zero. For a shell of relative permeability 1.012, and magnetized to a value typical of lunar samples, the residual moment is the same order of magnitude as the upper limit placed by Russell et al. (1974). Prnka (1976) extended the work further by including magnetization of the crust by layers to account for a finite crustal cooling rate. However, this calculation showed that the remanent dipole moment was nearly independent of the thermal history in the crust. Subsequently, Weiss et al. (1977) found that the residual moment for a magnetized crust of asymmetrical thickness was insensitive to simple crust thickness variations. On the other hand, they found that the remanent moment was very sensitive to the position of the magnetizing dipole. For a 100 km thick layer magnetized to an intensity typical of lunar samples, an offset of only 60 km in the magnetizing dipole results in a present dipole moment equal to the measured upper limit moment. Therefore, the ancient lunar dipole must have been centered to within 3% of the planet's radius, whereas the dipole moments of Earth and Jupiter are offset from their centers of

figure 5% to 10% of their radii. Recent modeling by Srnka and Mendenhall (1978) accounts for several other important processes in crustal magnetization. In their model a permeable shell is assumed to be magnetized in layers to simulate a realistic thermal history of the crust and the magnetized dipole is allowed to vary in intensity and direction to simulate dynamo field reversals as well as long term decay in dipole intensity. For a nonreversing magnetizing dipole which exponentially decays in intensity to match the lunar sample paleointensity data shown in Figure 3a, the remanent crustal dipole is at least 4 times larger than the measured upper limit. The calculated moment of the lunar crust for this model, throughout the magnetizing period to the present time, is shown in Figure 6. This model can be compatible with the measured dipole limit by demagnetizing (perhaps by shock) the outer layer of the magnetized shell a few tens of kilometers deep. The final remanent moment in this model can also be made compatible to the measured limit for the moon by simply requiring the magnetizing dipole to remain at 8×10^{24} gauss cm^3 (1 Oe surface field) from 4.6 to 3.9 b.y. ago, followed by an exponential decay with a time constant of 283 million years. A similar remanent moment is obtained by assuming a rise in dipole intensity from zero at 4.6 b.y. to 8×10^{24} gauss cm^3 at 3.9 b.y., followed by the same exponential decline in intensity. Evolution of the global magnetic moment for these two cases is shown by the curves labeled b and c in Figure 6. Another possibility for acquisition of a small but allowable modern crustal dipole, is by reversal of the magnetizing dipole in analogy to the earth's dynamo field reversals. Calculations for almost any model with reversing internal dipoles of period less than $\sim 10^7$ years yield allowable remanent moments. For example, a dipole field reversing direction every 10^7 years with an envelope of exponential decline in intensity (time constant 283×10^6 yr) yields a remanent moment of $\sim 10^{17}$ gauss cm^3 . This work of Srnka and Mendenhall (1978) has demonstrated that the small

Fig. 6

present day lunar magnetic dipole does not rule out a magnetic dynamo in early lunar history.

One of the most severe constraints on the lunar dynamo is that it must have produced large fields only 0.6 b.y. after lunar formation was complete. This requirement has lead Runcorn (1977) to postulate the presence of super heavy elements in the moon to rapidly melt the moon, form the core, and generate early dynamo action. Heating of the deep interior this early in lunar history is difficult to reconcile with much of our understanding of lunar composition and structure. Solomon (1978) examined early core formation in the moon by considering several of these constraints: the present lunar heat flow; the heat source abundance; the melting of the outer shell and differentiation of a 70 km thick crust; and the very constant lunar volume to maintain lithospheric stresses ~ 1 k bar. He concludes that these constraints do not allow core formation during the first 1 b.y. of lunar history without large scale tectonic features in the crust as a result of global volume change during cooling. Evidence of moon-wide compressional fracture is not observed in the lunar crust yet some lunar samples were magnetized during the first 0.7 b.y. of lunar history.

Another constraint on an early global lunar field was suggested by Goswami (1976). A sufficiently strong global field, resulting from a core dynamo or any other source, would divert solar wind plasma around the moon forming a magnetosphere analogous to that of the earth. Implantation of solar wind ions in the lunar crust would not take place under these conditions. Goswami (1976) suggests that a depletion of solar wind ions in lunar breccias with ages greater than 3.2 b.y. would indicate the presence of such a global field. The intrinsic field necessary to establish a lunar magnetosphere capable of shielding the surface from solar plasma depends on the density and bulk velocity of the solar wind. For present solar wind conditions of

5 cm^{-3} and 500 km s^{-1} a dipole moment of about $2.5 \times 10^{21} \text{ gauss cm}^3$ with a surface field of 40 gammas is necessary to stand off the plasma. Goswami (1976) studied three lunar breccias having a formation age greater than 3.0 b.y., which are enriched in solar wind ions in comparison to other lunar samples. These samples were apparently not shielded from solar wind ion flow for any appreciable time since their formation which implies that an early global lunar dipole moment was probably less than about $10^{21} \text{ gauss cm}^3$ (40 gammas at surface). This study does not support a global field of 1 Oe at the surface as required by paleointensity measurements.

In conclusion it is improbable that a dynamo was responsible for the early lunar magnetic field. However, neither experimental or theoretical studies conclusively rule out a small core dynamo field source.

3. LOCAL PROCESSES

3.1 Local Fe-FeS Dynamos.

Pearce et al. (1972) first proposed the idea that small pockets of Fe-FeS eutectic located close to the surface, each acting as a self regenerative magnetic dynamo, may have been responsible for lunar remanence. This hypothesis was developed by Murthy and Banerjee (1973) and incorporated into a particular accretional model of the moon. In this model, local surface melting allowed Fe-FeS melt to accumulate in pockets (Fescons) located preferentially on the front side of the moon at a depth of about 200 km. These massive accumulations, each approximately 10^{-4} lunar mass, with a density of $\sim 5.6 \text{ g cm}^{-3}$ and a diameter of about 130 km, are postulated to account for the mass concentrations beneath the ringed maria. To explain lunar magnetism these bodies of Fe-FeS eutectic at a temperature of $\sim 10^3 \text{ }^\circ\text{C}$ must become self-regenerating dynamos much as the terrestrial core dynamo. The possibility of dynamo action can be determined from the magnetic Reynold's number (R_m) for such a body. Taking the resistivity $\rho = 3 \times 10^5 \text{ emu}$ for iron at its melting point, a characteristic

length $\ell = 130$ km, magnetic permeability $\mu = 1$, fluid velocity $v = 0.2$ cm sec^{-1} , then $R_m (= \ell v 4 \pi \mu / \rho)$ is 100. Since $R_m \gg 1$ self-regeneration is possible in these bodies. These multiple lunar dynamos would have a variety of individual characteristics resulting in the observed wide range of paleointensity determinations from samples. However, because the dynamos are necessarily located beneath maria, mare basalts should be the most highly magnetized rocks. This is directly contrary to sample analysis (Fuller, 1974; Pearce et al., 1973) and subsatellite observations of remanent field intensity (Russell et al., 1977; Lin, 1978). This disagreement with experimental evidence constitutes a serious objection to this theory of lunar magnetism.

3.2 Local Unipolar Dynamo.

Another type of local magnetic dynamo proposed by Nagata et al. (1971) is schematically depicted in Fig. 7. This dynamo operates on the same principle as the whole moon induction unipolar dynamo proposed by Sonett and Colburn (1967). In the proposed local dynamos current is induced in a highly conducting lava basin by the motional, or $\underline{V} \times \underline{B}$ electric field, associated with relative motion of solar wind plasma and moon. Magnetic fields associated with these currents magnetize the crustal material. The electrical circuit is completed by the highly conducting solar wind plasma. Although the theory for whole-moon unipolar induction has been thoroughly investigated (e.g., Schwartz et al., 1969), the theory of unipolar induction on a regional scale has not been developed. Assuming a square lava pool geometry, of thickness D , Nagata et al. (1971) estimate the induced magnetic field to be

$$B \sim \mu_0 (1-K) \sigma E D$$

where K is used to account for less than ideal efficiency in the dynamo, σ is the effective electrical conductivity of the lava, and E is the motional electric field $|\underline{V} \times \underline{B}|$ (\underline{V} is the relative velocity of moon and solar wind and

Fig. 7

B_0 is solar wind magnetic field). For $\sigma \approx 10^{-1} (\Omega \text{ cm})^{-1}$, $D = 10 \text{ m}$, and $E = 1 \text{ V/cm}$ which may be appropriate for the solar wind from an early T Tauri sun, a field of 10^3 gammas is generated at the lava pool surface. This field is comparable to the lower paleointensity values (e.g., Nagata et al., 1971). It is unlikely that this mechanism could generate fields as large as 1 Oe as required by other paleointensity determinations. Operation of this mechanism requires the fortuitous orientation of the motional electric field in the plane of the lava basin. For any other orientation the electrical circuit must include the highly resistive lunar crust which would result in very small currents and fields from the dynamo. Overall evaluation of this model is difficult because little work has been done to define its details. Model calculations need to be performed before this hypothesis is viable.

3.3 Thermoelectric Dynamo.

A magnetic dynamo driven by thermoelectric currents in the cooling lunar crust was first proposed by Dyal et al. (1973) and later developed further by Dyal et al. (1977). As the lunar crust solidified from a primordial magma ocean, meteorite impacts are proposed to have penetrated the solid crust, exposing subsurface magma and forming lava-filled basins. Two such basins in close proximity, formed at approximately the same time, would have been connected below the crust by subsurface magma and above by solar plasma as shown in Fig. 8. Heterogeneous cooling in the crust could have resulted in cooling one basin more rapidly, producing a large temperature difference between the basins. In this model we have the elements of a thermoelectric circuit: two dissimilar conductors (plasma and lava) joined at two junctions (lava basin surfaces) which are at different temperatures. The thermoelectric potential is $E_{AB} = \epsilon_{AB} (\Delta T)$ where E_{AB} is the Seebeck potential, ϵ_{AB} is the relative Seebeck coefficient and ΔT is the temperature difference of the junctions. This electric potential drives currents which result in magnetic

Fig. 8

fields within the crust as shown in Fig. 8. Calculation of the magnetic field intensity requires a knowledge of the relative Seebeck potential of lunar basalts and solar plasma and the thermal history of the solidifying lava basin. The Seebeck potential of lunar samples has not been measured, although Telkes (1950) and Noritomi (1955) found coefficients in various geologic samples to range from -3.2 to $+2.1$ mV/ $^{\circ}$ K. The thermoelectric properties of the solar wind plasma were estimated from an expression given by Ioffe (1957) which represents materials whose conduction electrons, like those of a plasma, obey Maxwell-Boltzmann statistics. A Seebeck coefficient of 3 mV/ $^{\circ}$ K is estimated for an early solar wind such as could be expected from a T-Tauri sun. From these order of magnitude estimates a relative Seebeck potential of 1 mV/ $^{\circ}$ K was chosen for the calculations. Measured temperature profiles of terrestrial lava beds reported by Peck et al. (1964) were used in the calculations and the electrical resistance of the circuit determined from experimental conductivity-temperature relations for basalts given by Presnell et al. (1972). The magnetic field intensity between the two basins is a function of basin size and separation as shown in Fig. 9. For basins as large as 100 to 200 km the calculated magnetic fields are 1 to 3×10^3 gammas which are similar to many paleointensity results.

Fig. 9

There are two principal disadvantages to explaining lunar magnetism by this mechanism. First, paleomagnetic fields as large as 1 Oe, as indicated by some sample analyses, would require extraordinarily large thermoelectric coefficients. Second, the time scale for field generation is uncertain because of unknown cooling rates for lavas under lunar conditions and thermoremanent magnetization of large regions require field generation during their cooling. Critical evaluation of the time scale for field generation in this mechanism will be possible when lava cooling rates in a vacuum are included in the model.

3.4 Volcanic Ash Flow.

Cap (1972) proposed that magnetic fields may have been generated on a local scale at the lunar surface by current systems in ionized volcanic ash flows. In this field generation mechanism, the volcanic dust or ash is triboelectrically ionized, the volcanic gases assuming the opposite charge to maintain electrical neutrality. Differential flow of gas and dust in this neutral plasma is proposed as the source for electrical convection currents which result in the magnetizing fields. Cap estimates the magnetic field produced in this process by calculating the field H at the surface of a long cylindrical current flow of radius $R = 10$ km.

$$H = 3\alpha euR(\rho_r - \rho_g)/2r^3 c \rho_s$$

In this expression the electronic charge is e , the number of electron charges per particle is $\alpha = 10^3$, the relative flow speed of gas and dust is $u = 2$ cm sec⁻¹, the particle, gas and mixture densities are ρ_s , ρ_g , and ρ_m respectively, the particle radius is $r = 10^{-3}$ cm, and the speed of light is c . For $\rho_s = 2.4$ g cm⁻³, $\rho_g \approx 10^{-4}$ g cm⁻³ and 20% of the mixture volume occupied by dust ($\rho_m \approx 0.48$ g cm⁻³) the magnetizing field is about 1000 gammas which is comparable to some of the lower paleointensity values. There are several features of this mechanism which are uncertain. For example, ionization of the volcanic ash particles under lunar conditions has not been established. In addition, convection currents in the flow are possible only when the electrical circuit is complete and the currents close. Completion of the circuit through the lunar crust, one possibility suggested by Cap, is not likely because of the extreme electrical resistivity of the crust. The solar wind plasma (during lunar daytime) or other ionized gas clouds could carry the currents to complete the circuit only if they were of sufficiently high electron density. Currents closing in the gas above the surface would not produce intense fields within the

crust. Lightning discharges inside the flow may reach the surface and result in magnetization of crustal rocks. The cylindrical current model proposed by Cap is also of doubtful usefulness in calculating the magnetic field. Exit of gas from a surface vent into a vacuum is probably not cylindrical. Also field generation by this mechanism would be transient, and a sustained field is necessary to thermoremanently magnetize a large volume of lunar crust. These and other uncertainties about this mechanism remain until a more complete model of the process is investigated.

3.5 Impact Magnetization.

Magnetization of localized regions during impact cratering was among the first mechanisms to explain lunar remanence (e.g., Nagata et al., 1970, 1971). Several different magnetization processes occurring during impact and crater formation have been proposed. It has even been suggested that the thermoremanence measured in lunar samples is actually a peizoremanence acquired by shock propagation in the iron grains. Brecher (1976) is led to this conclusion by the magnetic characteristics of a particular highland breccia which has a direction of NRM related to shear and flow planes in the sample. These textural features may be controlled by stress of the breccia during formation in an impact event. Brecher suggests that shock propagation may align a small fraction ($\sim 10^{-3}$) of the iron domains resulting in a remanence of the magnitude observed in lunar rocks. While this hypothesis is plausible, there are apparently few other samples which suggest a textural remanence. Gose et al. (1978) have been unsuccessful in finding a remanence-texture relationship in lunar samples.

Acquisition of a NRM in ferromagnetic iron oxides due to impulsive stress loads is a well known phenomenon (e.g., Petrova, 1963; Shapiro and Alovera, 1970; Hargraves and Perkins, 1969). The magnetic effects of shock loading in nonoxidized iron and its alloys (the principle carriers of natural remanence in lunar materials) have been only recently studied (e.g., Wasilewski, 1972,

1973, 1978a,b). Magnetic studies of iron oxides cannot always be directly applied to free iron remanence but recent experimental results of shock loads on iron grains in a magnetic field do result in a magnetic remanence. For example, Nagata et al. (1971) were the first to experimentally study the relationship of stress and magnetic properties in lunar samples. They found that a mechanical shock applied in an external field of 3-9 Oe resulted in a shock remanent magnetization (SRM) proportional to the field and shock intensities. Cisowski et al. (1973, 1975, 1976, 1977) report results of a series of experiments extending this work to demonstrate the viability of shock magnetism. In these experiments they find that shock levels of 20 to 100 k bars applied to demagnetized lunar samples in magnetic fields ≥ 0.5 Oe, result in a magnetic remanence comparable to that found in lunar samples. Some of the shock magnetized samples are found to be petrologically and magnetically similar to regolith breccias. This is illustrated by the thermal and alternating field demagnetization of typical shocked samples shown in Fig. 10. These data reveal that shock remanence can exhibit a range of blocking temperatures similar to a partial thermoremanence. The shock acquired remanence is also fairly stable against alternating field demagnetization. At 30 k bars the intensity of the shock remanence is found to be approximately linear with the external field and varies by 10^{-5} gauss $\text{cm}^3 \text{g}^{-1}$ for each Oersted field change. In a constant field of 0.50 Oe Cisowski et al. (1975) report that shock remanence depends on the peak shock level as shown in Fig. 11. It is obvious that SRM is highly dependent on both the external field and the peak shock pressure making future experiments necessary at lunar conditions of low field levels. Until these experiments are performed we must rely on results extrapolated to low field values. Assuming a linear dependence of shock magnetization on field intensity, Cisowski et al. (1973) estimate a remanence of 10^{-4} and 10^{-5} gauss $\text{cm}^3 \text{g}^{-1}$ (similar to that of lunar samples) in a field of 10^3 and 10^2

Fig. 10

Fig. 11

gamma respectively for one sample shocked to 50 k bars. However even these fields are one or two orders of magnitude larger than are common in the present lunar environment. It is possible that larger fields were present during the heavy cratering period. Large transient fields generated during the proposed SRM may have been produced by compression of a small ambient field or from currents in crater ejecta plasma. We now review two mechanisms proposed to generate transient fields during crater impact.

Gold and Soter (1976) proposed that the ambient interplanetary field could be amplified by compression between the moon and the ionized coma of a comet just prior to the comet impact on the lunar surface. Their model is shown schematically in Fig. 12. Model calculations of peak field intensity account for coma composition and size but require several assumptions about ionization of the coma and field diffusion through this ionized component. Fig. 13 shows the relationship they derived between the peak field in gammas and the comet magnitude. According to this model the interplanetary field could be amplified to an intensity of 10^3 gammas by a magnitude 10 comet. Also shown in Fig. 13 is the number of comets expected to impact the moon during 4.6 b.y. (estimated by Everhart, 1969). The large number of observed magnetic anomalies (Russell et al., 1975; Lin et al., 1976) seems inconsistent with only ~ 10 comet impacts expected from this model.

Generation of currents and associated magnetic fields in crater ejecta was first suggested by Hide (1972) as a possible mechanism to produce the large fields necessary to magnetize regions of the lunar crust. This field generation mechanism has been demonstrated in laser-produced plasmas which yield magnetic fields as large as a kilogauss (Stamper et al., 1971 and Bird et al., 1973). Calculations by Widner (1973) and Tidman (1974) indicate that 10^7 gauss may be possible in laser-produced plasmas. Srnka (1977) has investigated this mechanism to evaluate its importance during lunar crater formation.

He considers the magnetic fields arising from drift currents generated by non-aligned temperature and density gradients in the ejecta plasma. These plasma gradients may result from impact in a vertically stratified target as schematically shown in Fig. 14. For a idealized current configuration the field generated is a function of the fractional density change across the plasma cloud and the temperature gradient (see Fig. 15). Fractional density enhancements of 0.5 and temperature gradients of 40°K/m do not seem unreasonable for the initial expansion phase of the ejecta plasma. These parameters yield a field magnitude of 10^3 gammas. More extreme pressure gradients or other current configurations (Sraka, 1977) may result in larger field values.

Experimental confirmation that magnetic fields are generated in impact ejecta has been attempted by Sraka et al. (1976) in an experiment using a high speed projectile fired at a basalt target. At impact a field was measured three times the ambient value. However, experiment design did not allow discrimination between fields generated by plasma currents and compression of the ambient field by expansion of ejecta plasma. In another experiment Martelli and Newton (1977) used the high velocity plasma from an explosive charge to impact a basalt target. They found that plasma was produced in the ejecta, but generation of currents and fields were again uncertain. Both of these impact experiments did confirm, however, the acquisition of shock related remanence.

One objection to explaining lunar magnetism by SRM is the lack of an observable correlation between individual craters and magnetic anomalies. Weiss et al. (1977) demonstrated that this correlation should exist if craters are excavations in a uniformly magnetized shell (see Fig. 5). However, correlation of field anomalies and crater morphology may be complex for a patchy magnetization in an otherwise unmagnetized shell and correlation between individual craters and field anomalies may be entirely absent in the highlands

which are saturated by craters. On the other hand, isolated more craters do not show any correlation with field anomalies (Lin, 1978). This constitutes a serious objection to SRM of the lunar crust.

4. DISCUSSION AND CONCLUSIONS

In this paper we have reviewed the major theories proposed to explain lunar crustal remanent magnetization. None of these theories, at their present level of development, satisfy all of the experimental constraints. However, several of the hypotheses require additional development before they can be realistically evaluated. For example, the shock magnetization mechanism requires experimental study of lunar material shocked in low field lunar conditions. The thermoelectric mechanism requires inclusion of temperature histories for radiatively cooling lunar type lavas. Laboratory measurement of the thermoelectric coefficient for lunar materials is also needed.

Some of the mechanisms reviewed here are unlikely candidates for explaining lunar remanent magnetism. These mechanisms are the terrestrial field, a lunar fossil field, and local Fe-FeS dynamos fields. The most likely mechanisms are meteorite impact magnetization, thermoelectric dynamos, and early solar field magnetization. Hopefully, additional theoretical and experimental work, along with possible future missions to the moon, will clarify our understanding of the origin of lunar remanent magnetism.

Acknowledgements.

The authors thank Drs. P. Cassen and H. Houben of Ames Research Center, Dr. D. Wilhelms of the U.S. Geologic Survey, and L. Hood at the University of California for helpful discussions. We are pleased to acknowledge the support for W.D.D. under NASA Grant NSG-2082.

REFERENCES

- Alfvén, H. and Lindberg, L., 1974. Magnetization of celestial bodies with special application to the primeval earth and moon. The Moon, 10: 323-335.
- Banerjee, S.K. and Mellema, J.P., 1976. A solar origin for the large lunar magnetic field at 4.0×10^9 yr ago? In: R.B. Merrill (Editor), Proc. Lunar Sci. Conf. 7th. Geochim. Cosmochim. Acta, 3: 3259-3270.
- Bills, B.G. and Ferrari, A.J., 1977. A lunar density model consistent with topographic, gravitational, librational, and seismic data. J. Geophys. Res., 82: 1306-1314.
- Bird, R.S., McKee, L.L., Schwirzke, F., and Cooper, A.W., 1973. Pressure dependence of self-generated magnetic fields in laser-produced plasmas. Phys. Rev. A: 1328-1331.
- Brecher, A., 1976. The magnetic characteristics of highland breccia 73215: Evidence for textural control of magnetization. In: R.B. Merrill (Editor), Proc. Lunar Sci. Conf. 7th. Geochim. Cosmochim. Acta, 2: 2217-2231.
- Cap, F.F., 1972. Possible production mechanisms of lunar magnetic fields. J. Geophys. Res., 77: 3328-3333.
- Cassen, P., Young, R.E., and Schubert, G., 1978. The distortion of the moon due to convection, Geophys. Res. Lett., 5: 294-296.
- Cisowski, S., Fuller, M., Rose, M.E., and Wasilewski, P.J., 1973. Magnetic effects of experimental shocking of lunar soil. In: E.A. King, Jr. (Editor), Proc. Lunar Sci. Conf. 3rd. Geochim. Cosmochim. Acta, 3: 3003-3017.
- Cisowski, S.M., Fuller, M., Yee Ming, Wu, Rose, M.F., and Wasilewski, P.J., 1975. Magnetic effects of shock and their implications for magnetism of lunar samples. In: R.B. Merrill (Editor), Proc. Lunar Sci. Conf. 6th Geochim. Cosmochim. Acta, 3: 3123-3141.

- Cisowski, S.M., Dunn, J. R., Fuller, M., Yee Ming, Wu, Rose, M.F., and Wasilewski, P.J., 1976. Magnetic effects of shock and their implications for lunar magnetism (II). In: R.B. Merrill (Editor), Proc. Lunar Sci. Conf. 7th. Geochim. Cosmochim. Acta, 3: 3299-3320.
- Cisowski, S.M., Hale, C., and Fuller, M., 1977. On the intensity of ancient lunar fields. In: R.B. Merrill (Editor), Proc. Lunar Sci. Conf. 8th. Geochim. Cosmochim. Acta, 1: 725-750.
- Collison, D.W., Stephenson, A., and Runcorn, S.K., 1973. Magnetic properties of Apollo 15 and 16 rocks. In: W.A. Gose (Editor), Proc. Lunar Sci. Conf. 4th. Geochim. Cosmochim. Acta, 3: 2963-2976.
- Collinson, D.W., Runcorn, S.K., and Stephenson, A., 1976. On the intensity of the ancient lunar magnetic field (abstract). Lunar Science VII, 166-168, The Lunar Science Institute, Houston.
- Dolginov, Sh. Sh., 1975. On the origin of ancient lunar magnetic fields. The Moon, 14: 255-261.
- Dyal, P., Parkin, C.W., and Sonett, C.P., 1970. Apollo 12 magnetometer: measurement of a steady magnetic field on the surface of the moon. Science, 169: 762-764.
- Dyal, P., Parkin, C.W., and Daily, W.D., 1973. Surface magnetometer experiments: Internal lunar properties. In: W.A. Gose (Editor), Proc. Lunar Sci. Conf. 4th. Geochim. Cosmochim. Acta, 3: 2925-2945.
- Dyal, P., Parkin, C.W., and Daily, W.D., 1974. Magnetism and the interior of the moon, Rev. Geophys. and Space Phys., 12: 568-591.
- Dyal, P., Parkin, C.W., and Daily, W.D., 1975. Lunar electrical conductivity and magnetic permeability. In: R.B. Merrill (Editor), Proc. Lunar Sci. Conf. 6th. Geochim. Cosmochim. Acta, 3: 2909-2926..

- Dyal, P., Parkin, C.W., and Daily, W.D., 1977. Global lunar crust: Electrical conductivity and thermoelectric origin of remanent magnetism. In: R.B. Merrill (Editor), Proc. Lunar Sci. Conf. 8th. Geochim. Cosmochim. Acta, 1: 767-783.
- Everhart, E., 1969. Close encounters of comets and planets. Astron. J., 74: 735-750.
- Freeman, J.W., 1977. The magnetic field in the solar nebula. In: R.B. Merrill (Editor), Proc. Lunar Sci. Conf. 8th. Geochim. Cosmochim. Acta, 1: 751-755.
- Fuller, M., 1974. Lunar magnetism. Rev. Geophys. Space Phys., 12: 23-70.
- Gold, T. and Soter, S., 1976. Cometary impact and the magnetization of the moon. Planet. Space Sci., 24: 45-54.
- Goldstein, B.E., Phillips, R.J., and Russell, C.T., 1976. Magnetic evidence concerning a lunar core. In: R.B. Merrill (Editor), Proc. Lunar Sci. Conf. 7th. Geochim. Cosmochim. Acta, 3: 3321-3341.
- Gose, W.A., Pearce, G.W., Strangway, D.W., and Larson, E.E., 1972. On the magnetic properties of lunar breccias (abstract). Lunar Science, 3: 332-334, The Lunar Science Institute, Houston.
- Gose, W.A., Strangway, D.W., and Pearce, G.W., 1978. Origin of magnetization in lunar breccias: An example of thermal overprinting. Earth and Planet. Sci. Lett., 38: 373-384.
- Goswami, J.N., 1976. Constraints on the nature of the ancient lunar magnetic field. Nature, 261: 675-677.
- Hargraves, R.B. and Perkins, W.E., 1969. Investigations of the effect of shock on natural remanent magnetization. J. Geophys. Res., 74: 2576-2589.
- Hide, R., 1972. Comments on the moon's magnetism. The Moon, 1: 39.
- Hood, L., Russell, C.T., and Coleman, P.J., Jr., 1978. Evidence for a non-random magnetization of the moon. Geophys. Res. Lett., 5: 305-308.

- Hood, L.L. and Wilhelms, D.E., 1978. Some evidence on the sources of lunar crustal magnetic anomalies, submitted to Science.
- Houben, H., 1978. A tidal-precessional dynamo for the terrestrial planets. Submitted to Phys. Earth and Planet. Int., this volume.
- Ioffe, A.F., 1957. Semiconductor thermoelements and thermoelectric cooling. Infosearch, London. 184 pp.
- Levy, E.H., 1972. Magnetic dynamo in the moon: A comparison with earth. Science, 178: 52-53.
- Levy, E.H., 1974. A magnetic dynamo in the moon? The Moon, 9: 49-56.
- Levy, E.H. and Sonett, C.P., 1978. Meteorite magnetism and early solar system fields. Conf. on Protostars and Planets, in press, Tucson.
- Lin, R.P., 1978. A search for impact crater-associated surface magnetic fields in mare regions (abstract). Lunar and Planetary Science IX, 651-653, Lunar and Planetary Institute, Houston.
- Lin, R.P., Anderson, K.A., McQuire, R.E., and McCoy, J.E., 1976. Fine scale lunar surface magnetic fields detected by the electron reflection method (abstract). Lunar Science VII, 492-494, The Lunar Science Institute, Houston.
- Martelli, G. and Newton, G., 1977. Hypervelocity cratering and impact magnetization of basalt. Nature, 269: 478-480.
- Murthy, V.R., and Banerjee, S.K., 1973. Lunar evolution: How well do we know it now. The Moon, 7: 149-171.
- Nagata, T., Ishikawa, Y., Kinoshita, H., Kono, M., Syono, Y., and Fisher, R.M., 1970. Magnetic properties and natural remanent magnetization of lunar materials. In: A.A. Levinson (Editor), Proc. of the Apollo 11 Lunar Sci. Conf. Geochim. Cosmochim. Acta, 3: 2325-2340.

- Nagata, T., Fisher, R. M., Schwerer, F.C., Fuller, M.D., and Dunn, J.R.,
1971. Magnetic properties and remanent magnetization of Apollo 12 lunar materials and Apollo 11 lunar microbreccia. In: A.A. Levinson (Editor), Proc. Lunar Sci. Conf. 2nd. Geochim. Cosmochim. Acta, 3: 2461-2476.
- Nagata, T., Fisher, R.M., Schwerer, F.C., Fuller, M.D., and Dunn, J.R.,
1972. Rock magnetism of Apollo 14 and 15 materials. In: E.A. King, Jr. (Editor), Proc. Lunar Sci. Conf. 3rd. Geochim. Cosmochim. Acta, 3: 2423-2447.
- Nakamura, Y., Latham, G., Lammlein, D., Ewing, M., Duennebier, F., and Dorman, J., 1974. Deep lunar interior from recent seismic data. Geophys. Res. Lett., 1: 137-140.
- Noritomi, K., 1955. Investigation of thermoelectricity for metallic and silicate minerals. Geophysics, 7: 94-101.
- Pearce, G.W., Strangway, D.W., and Larson, E.E., 1971. Magnetism of two Apollo 12 igneous rocks. In: A.A. Levinson (Editor), Proc. Lunar Sci. Conf. 2nd. Geochim. Cosmochim. Acta, 3: 2451-2460.
- Pearce, G.W., Strangway, D.W., and Gose, W.A., 1972. Remanent magnetization of the lunar surface. In: E.A. King, Jr. (Editor), Proc. Lunar Sci. Conf. 3rd. Geochim. Cosmochim. Acta, 3: 2449-2464.
- Pearce, G.W., Gose, W.A., and Strangway, D.W., 1973. Magnetic studies on Apollo 15 and 16 lunar samples. In: D.R. Criswell (Editor), Proc. Lunar Sci. Conf. 3rd. Geochim. Cosmochim. Acta, 3: 3045-3076.
- Peck, D.L., Moore, L.G., and Kojima, G., 1964. Temperatures in the crust and melt of Alae Lava Lake, Hawaii, after the August 1963 eruption of Kilauea Volcano. A preliminary report. U.S. Geol. Survey Prof. Paper 501D, P.D1-D7.

- Petrova, G.N., 1963. The difference between types of magnetization as a basis of study of the magnetic stability of rocks. (Dissert.) Earth Physics Inst.
- Presnall, D.C., Simmons, C.L., and Porath, H., 1972. Changes in electrical conductivity of a synthetic basalt during melting. J. Geophys. Res., 77: 5665-5672.
- Runcorn, S.K., 1967. Convection in the moon and the existence of a lunar core. Proc. Roy. Soc., Ser. A, 296: 270-284.
- Runcorn, S.K., 1975. An ancient lunar magnetic dipole field. Nature, 253: 701-703.
- Runcorn, S.K., 1976. Inferences concerning the early thermal history of the moon. In: R.B. Merrill (Editor), Proc. Lunar Sci. Conf. 7th. Geochim. Cosmochim. Acta, 3: 3221-3228.
- Runcorn, S.K., 1977. Early melting of the moon. In: R.B. Merrill (Editor), Proc. Lunar Sci. Conf. 8th. Geochim. Cosmochim. Acta, 1: 463-469.
- Runcorn, S.K., 1978a. On the possible existence of superheavy elements in the primeval moon. Earth and Planet. Sci. Lett., 39: 193-198.
- Runcorn, S.K., 1978b. The ancient lunar dynamo (abstract). Conf. on Origins of Planet. Mag., 81-83, Lunar and Planetary Institute, Houston.
- Runcorn, S.K. and Urey, H.C., 1973. A new theory of lunar magnetism. Science, 180: 636-638.
- Runcorn, S.K., Collinson, D.W., O'Reilly, W., Battey, M.H., Stephenson, A.A., Jones, J.M., Manson, A.J., and Readman, P.W., 1970. Magnetic properties of Apollo 11 lunar samples. In: A.A. Levinson (Editor), Proc. Apollo 11 Lunar Sci. Conf. Geochim. Cosmochim. Acta, 3: 2369-2387.
- Runcorn, S.K., Collinson, D.W., O'Reilly, W., Stephenson, A., and Battey, M.H., Manson, A.J., and Readman, P.W., 1971. Magnetic properties of Apollo 12 lunar samples, Proc. Roy. Soc. London, Ser. A, 325: 157-174.

- Russell, C.T., Coleman, P.J., Jr., Lichtenstein, B.R., and Schubert, G., 1974. The permanent and induced magnetic dipole moment of the moon. In: W.A. Gose (Editor), Proc. Lunar Sci. Conf. 5th. Geochim. Cosmochim. Acta, 3: 2747-2760.
- Russell, C.T., Coleman, P.J., Jr., Fleming, B.K., Hilburn, L., Ionnidis, G., Lichtenstein, B.R., and Schubert, G., 1975. The fine-scale lunar magnetic field. In: R.B. Merrill (Editor), Proc. Lunar Sci. Conf. 6th. Geochim. Cosmochim. Acta, 3: 2955-2969.
- Russell, C.T., Weiss, H., Coleman, P.J., Jr., Soderblom, L.A., Stuart-Alexander, D.E., and Wilhelms, D.E., 1977. Geologic-magnetic correlations on the moon: Apollo subsatellite results, In: R.B. Merrill (Editor), Proc. Lunar Sci. Conf. 8th. Geochim. Cosmochim. Acta, 1: 1171-1185.
- Schwartz, K., Sonett, C.P., and Colburn, D.S., 1969. Unipolar induction in the moon and a lunar limb shock mechanism. The Moon, 1: 7-30.
- Shapiro, V.A. and Alovera, N.I., 1970. Characteristics of the dynamic remanent magnetization of ferromagnetic rocks at temperatures from 0 to 600 °C. Izv., Earth Physics, 11: 95-98.
- Solomon, S.C., 1978. Lunar thermal history versus lunar magnetism, or how to box in a hypothesis and build a coffin (abstract). Conf. on Origins of Planetary Magnetism, 98-99, Lunar and Planetary Institute, Houston.
- Sonett, C.P., and Colburn, D.S., 1967. Establishment of a lunar unipolar generator and associated shock and wake by the solar wind. Nature, 216: 340-343.
- Sonett, C.P., Colburn, D.S., and Schwartz, K., 1968. Electrical heating of meteorite parent bodies and planets by dynamo induction from premain sequence, T Tauri solar wind. Nature, 219: 924-926.
- Srnka, L.J., 1976. On the global TRM of the lunar lithosphere. In: R.B. Merrill (Editor), Proc. Lunar Sci. Conf. 7th. Geochim. Cosmochim. Acta, 3: 3357-3372.

- Srnka, L.J., 1977. Spontaneous magnetic field generation in hypervelocity impacts. In: R.B. Merrill (Editor), Proc. Lunar Sci. Conf. 8th. Geochim. Cosmochim. Acta, 1: 785-792.
- Srnka, L.J. and Mendenhall, M.H., 1978. Theory of global thermoremanent magnetization of planetary lithospheres in dipole fields. Submitted to J. Geophys. Res.
- Srnka, L.J., Martelli, G., Cisowski, S.M., and Fuller, M.D., 1976. Magnetic field effects and permanent magnetization in a hypervelocity impact experiment. Lunar Science VII, 1092-1094, The Lunar Science Institute, Houston.
- Stamper, J.A., Papadopoulos, K., Sudan, R.N., Dean, S.O., McLean, E.A., and Dawson, J.M., 1971. Spontaneous magnetic fields in laser-produced plasmas. Phys. Rev. Lett., 26: 1012-1015.
- Stephenson, A., 1976. The residual permanent magnetic dipole moment of the moon. The Moon, 15: 67-81.
- Stephenson, A., Runcorn, S.K., and Collinson, D.W., 1975. On changes in the intensity of the ancient lunar magnetic field. In: R.B. Merrill (Editor), Proc. Lunar Sci. Conf. 6th. Geochim. Cosmochim. Acta, 3: 3049-3062.
- Strangway, D.W., 1970. History of the earth's magnetic field. McGraw Hill, New York, 168 pp.
- Strangway, D.W., 1978. The record of magnetic fields in the early solar system. The Moon and Planets, 18: 273-279.
- Strangway, D.W. and Sharpe, H.A., 1974. Lunar magnetism and an early cold moon. Nature, 249; 227-230.
- Strangway, D.W. and Sharpe, H.A., 1975. A model of lunar evolution. The Moon, 12: 369-397.
- Strangway, D.W., Larson, E.E., and Pearce, G.W., 1970. Magnetic studies of lunar samples - breccia and fines. In: A.A. Levinson (Editor), Proc. Apollo 11 Lunar Sci. Conf. Geochim. Cosmochim. Acta, 3: 2435-2451.

- Strangway, D.W., Pearce, G.W., Gose, W.A., and Timme, R.W., 1971. Remanent magnetization of lunar samples. Earth Planet. Sci. Lett., 13: 43-52.
- Strangway, D.W., Gose, W.A., Pearce, G.W., and Carnes, J.G., 1973. Magnetism and the early history of the moon. Proc. of the 18th Annual Conf. on Magnetism and Magnetic Materials, J. Applied Phys., 2: 1178.
- Telkes, M., 1950. Thermoelectric power and electrical resistivity of minerals. Am. Mineralogist, 35, no. 7.
- Tidman, D.A., 1974. Strong magnetic fields produced by composition discontinuities in laser-produced plasmas. Phys. Rev. Lett., 32: 1179-1181.
- Wasilewski, P., 1972. Magnetic remanence mechanisms in FeNi Co alloys and the magnetization of lunar rocks and soils (abstract). Lunar Science IV, 770, The Lunar Science Institute, Houston.
- Wasilewski, P.J., 1973. Shock remagnetization associated with meteorite impact at planetary surfaces. The Moon, 6: 264-291.
- Wasilewski, P.J., 1978a. Magnetic properties of FeNi alloys-microstructure and remanent magnetization mechanisms (abstract). In Conf. on Origins of Planetary Magnetism, 119-120. Lunar and Planetary Institute, Houston.
- Wasilewski, P.J., 1978b. Shock induced effects in fine particle iron (abstract). In Conf. on Origins of Planetary Magnetism, 121-122. Lunar and Planetary Institute, Houston.
- Weiss, H., Hood, L.L., and Coleman, P.J., Jr., 1977. Extended analysis of the cratered shell model of the moon's permanent magnetic field. In: R.B. Merrill (Editor), Proc. Lunar Sci. Conf. 8th. Geochim. Cosmochim. Acta, 1: 757-766.
- Widner, M.M., 1973. Self-generated magnetic fields in laser produced plasmas. Phys. Rev. Lett., 32: 1179-1181.
- Wiskerchen, M.J. and Sonett, C.P., 1977. A lunar metal core? In: R.B. Merrill (Editor), Proc. Lunar Sci. Conf. 8th. Geochim. Cosmochim. Acta, 1: 515-535.

FIGURE CAPTIONS

- Figure 1. Magnetization of the lunar crust by a uniform external field. (a) As the moon cools a crust is formed and is magnetized by an external magnetic field of solar or terrestrial origin. At the lunar orbit either of these fields may be approximately uniform. (b) A constant magnetization is acquired by the crustal shell which results in a dipole field external to the lunar sphere.
- Figure 2. Magnetization of the lunar core by an external magnetic field. (a) The early lunar core is magnetized by a uniform magnetic field of solar or terrestrial origin. The outer shell (crust) is too hot to be magnetized. (b) A constant magnetization is acquired by the core which results in a dipole field capable of magnetizing the outer shell as it cools. (c) The core temperature rises high enough to erase its magnetization but the shell continues cooling and retains a magnetization everywhere parallel to the magnetizing dipole field. No external magnetic field results from the magnetization in this shell.
- Figure 3. Paleomagnetic field intensity of the moon. The magnetic field intensity in Oe is plotted as a function of age in billions of years. The sample numbers identify each data point. (a) Paleointensity determinations of Runcorn (1978) indicating a decline in the ancient magnetizing field. (b) Paleointensity determinations of Cisowski et al. (1977) which do not indicate a decline in the ancient magnetizing field. Sample 70019 is a soil breccia with a young compaction age.

Figure 4. Magnetization of the lunar crust by a lunar core dynamo dipole field. (a) Early heating of the deep interior allows formation of a small iron core which begins regenerative dynamo action producing a dipole magnetic field. (b) As the outer shell cools in the presence of this dipole field it is magnetized everywhere parallel to the magnetizing field. No external magnetic field results from magnetization in this shell.

Figure 5. Remanent field-crater correlation calculated for a shell magnetized by an internal dipole field. Ten of the prominent lunar impact basins are simulated in the model by voids in the magnetized shell. The basins are outlined by the heavy circular lines. Magnetic field intensity contours in gammas delineate where fields larger than 1 gamma would be measured from an altitude of 100 km.

Figure 6. Calculated global remanent magnetic moment of the moon as a function of time for three different models of the magnetizing dipole field (after Srnka and Mendenhall, 1978). The present lunar dipole moment is limited by measurements of Russell et al. (1974) to values below the shaded region. Negative moments indicate that the remanent dipoles are antiparallel to the magnetizing dipole moment. (a) Magnetic moment of the magnetized shell is shown for a 9.5×10^{25} gauss cm^3 magnetizing moment 4.6 b.y. ago, which exponentially decays in intensity with a time constant of 283×10^6 yr. (b) The shell magnetic moment is shown for a magnetizing dipole moment 8×10^{24} gauss cm^3 from 4.6 to 3.9 b.y. ago before an exponential decay with a

time constant of 283×10^6 yr. (c) The shell magnetic moment is shown for a magnetizing dipole moment increasing from zero at 4.6 b.y. ago to 8×10^{24} gauss cm³ at 3.9 b.y., followed by an exponential decay with a time constant of 283×10^6 yr.

Figure 7. Local unipolar generator. The motional or $\underline{V} \times \underline{B}$ electric field of the solar wind drives electrical currents in a highly conducting lava pool on the lunar surface. The electrical circuit is completed by the solar wind plasma. Magnetic fields resulting from the induced currents magnetize the cooling lunar crust.

Figure 8. Magnetic field generation by thermoelectric currents. A thermoelectric potential, resulting from the temperature difference of two lava basins, drives currents through the highly conducting lunar interior and solar wind. The resulting magnetic field magnetizes the cooling lunar crust.

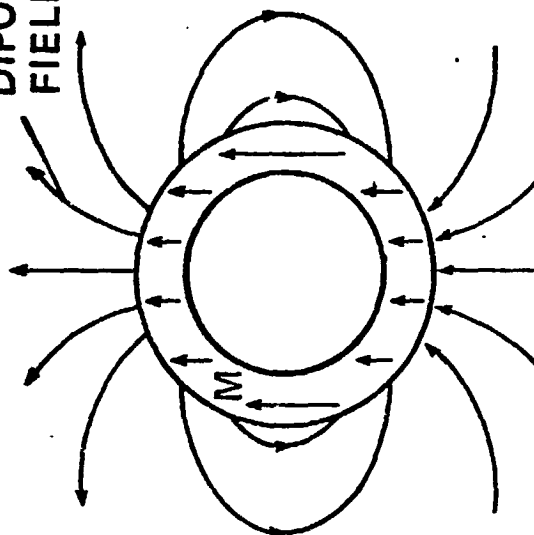
Figure 9. Thermoelectrically generated magnetic fields. The maximum calculated field is plotted as a function of basin size and separation for an assumed thermoelectric potential of 1 mv/°C. (after Dyal et al., 1977).

Figure 10. Demagnetization curves for lunar samples magnetized during shock loading in the earth's field. (a) Magnetization as a function of temperature is shown for samples shocked to 50 k bar and 100 k bar. For comparison, the thermal stability is plotted for a sample given a partial thermoremanence by cooling from 350 to 20 °C in a 0.5 Oe field. (b) Magnetization is

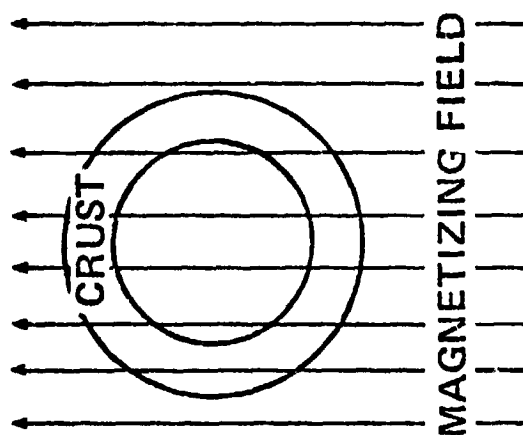
shown as a function of peak field during alternating field demagnetization for samples shocked to several levels. (after Cisowski et al., 1975).

- Figure 11. Acquisition of remanence by lunar soils as a function of peak shock pressure. The experiments were carried out in a 0.5 Oe magnetic field. (after Cisowski et al., 1975)
- Figure 12. Enhancement of an ambient magnetic field by compression between the plasma of a comet coma and a plasma sheath at the lunar surface.
- Figure 13. Results of model calculations illustrating the feasibility of magnetic field amplification prior to comet impact on the moon. Estimates of the number of comet impacts with the moon during its 4.6 b.y. history are from Everhart (1969).
- Figure 14. Schematic representation of a simplified current and field configuration in an impact event. Hypervelocity impact in a vertically stratified target may be capable of generating a current and field system such as this.
- Figure 15. Model calculation results for magnetic fields generated in hypervelocity impact ejecta. Magnetic fields are generated in this model when temperature and density gradients are not parallel as may be the case for the ejecta from a stratified target.

EXTERNAL
DIPOLE
FIELD



(b)



(a)

Figure 1

REPRODUCIBILITY OF THE
ORIGINAL PAGE IS POOR

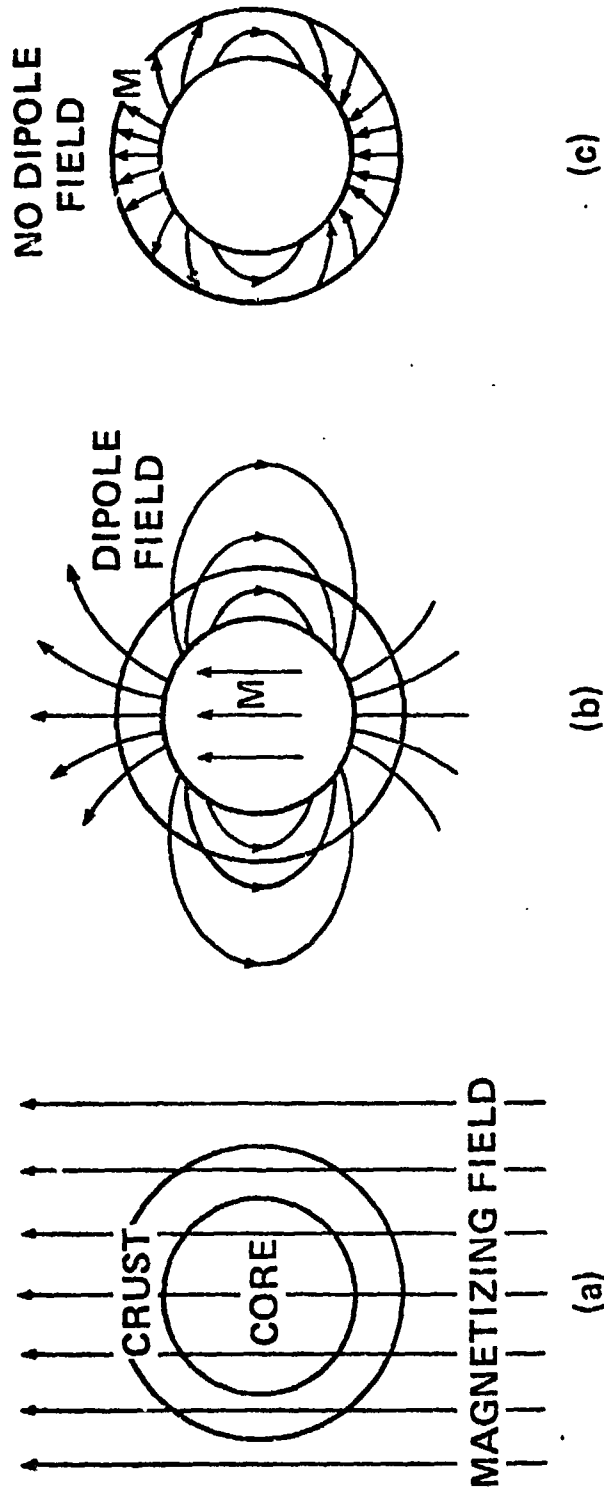
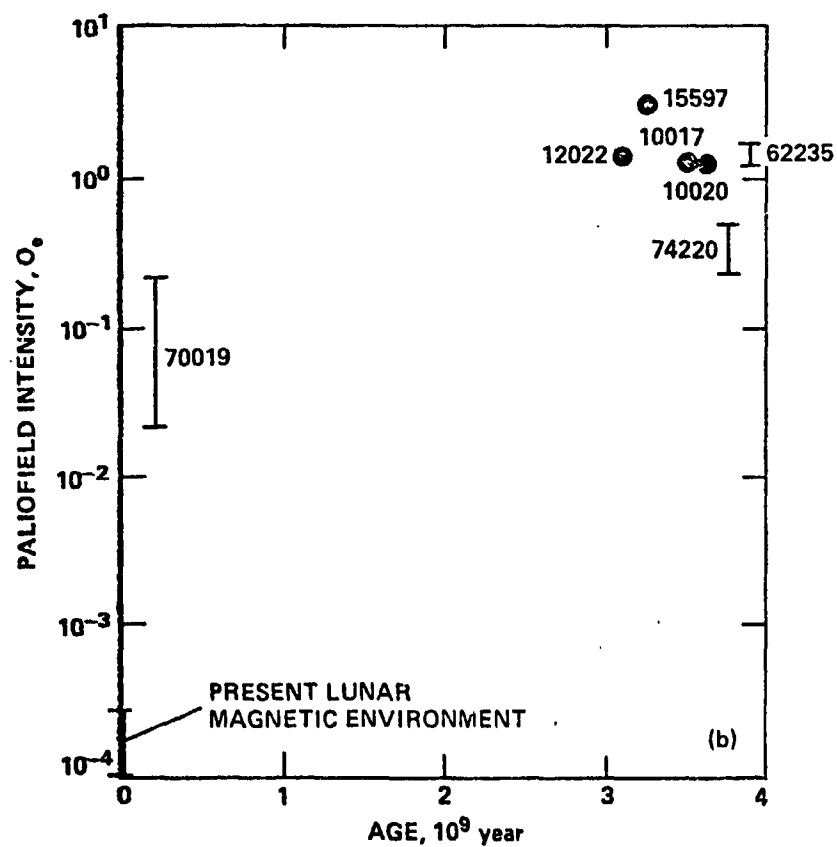
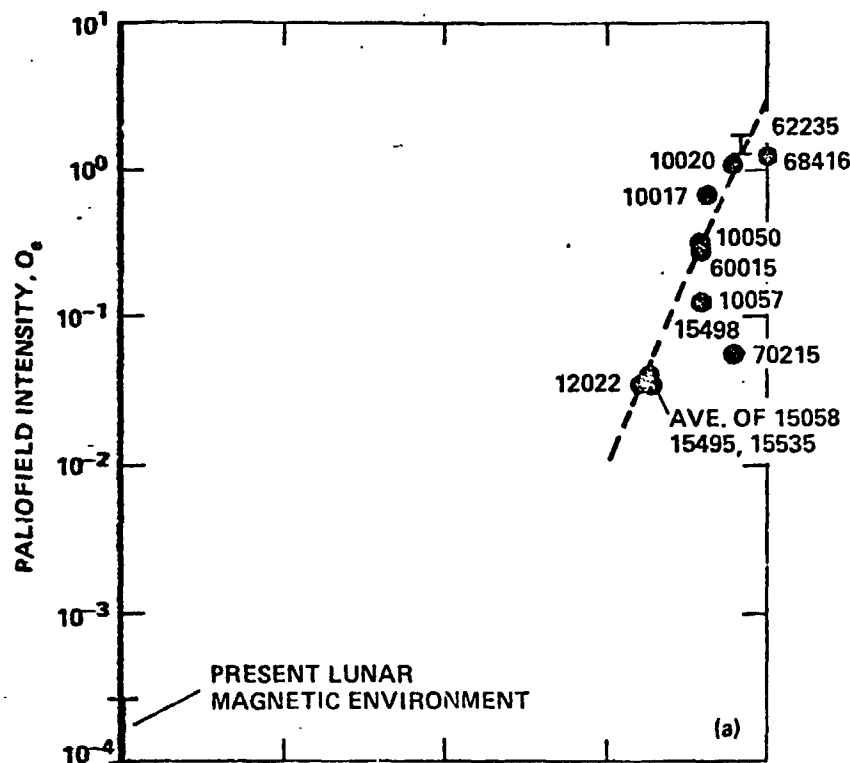


Figure 2



REPRODUCIBILITY OF THE
ORIGINAL PAGE IS POOR

Figure 3

REPRODUCIBILITY OF THE
ORIGINAL PAGE IS POOR

B-41

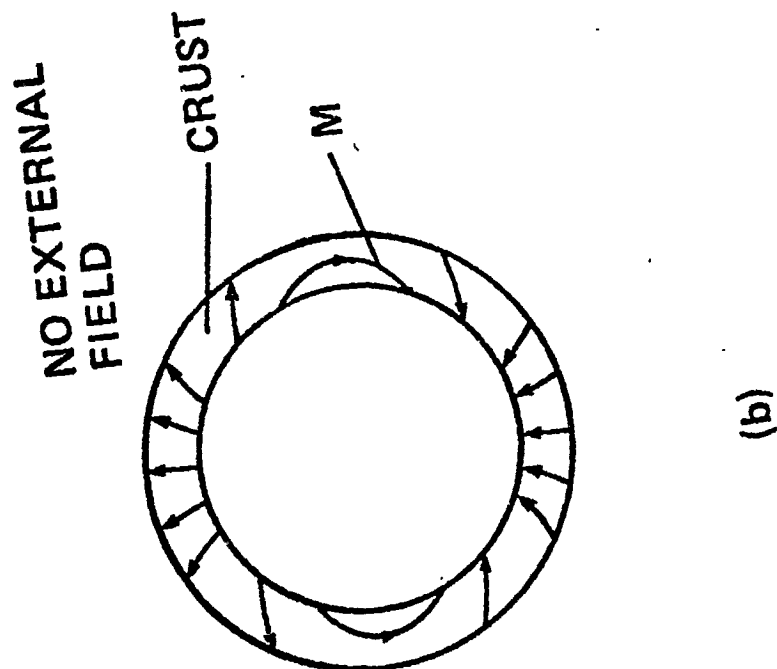
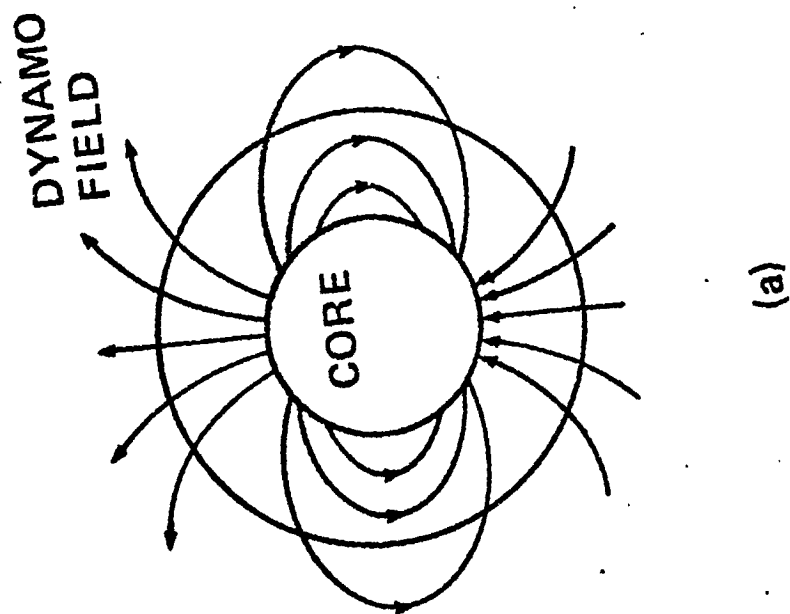


Figure 4

REPRODUCIBILITY OF THE
ORIGINAL PAGE IS POOR

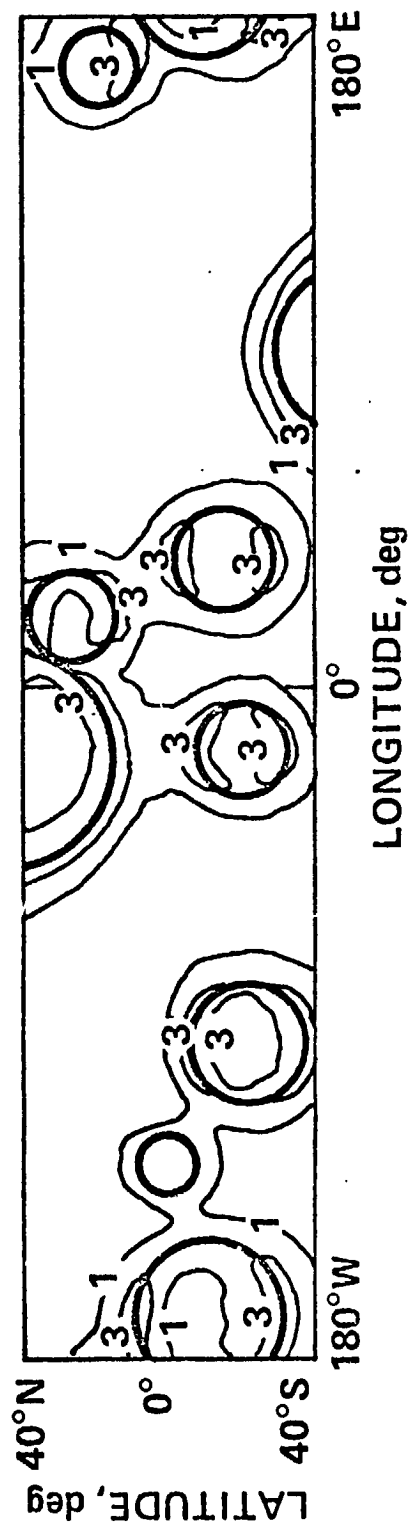


Figure 5

REPRODUCIBILITY OF THE
ORIGINAL PAGE IS POOR

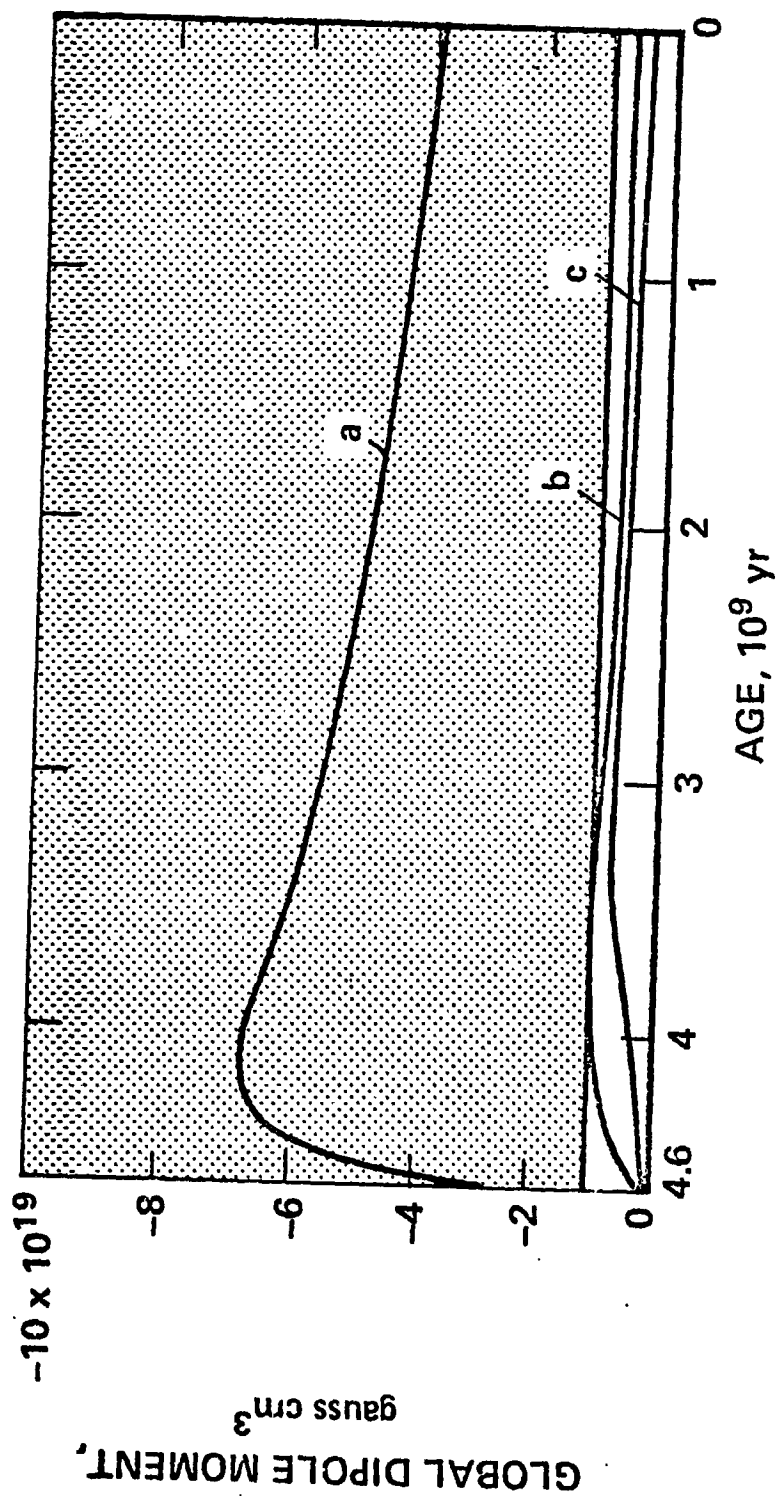


Figure 6

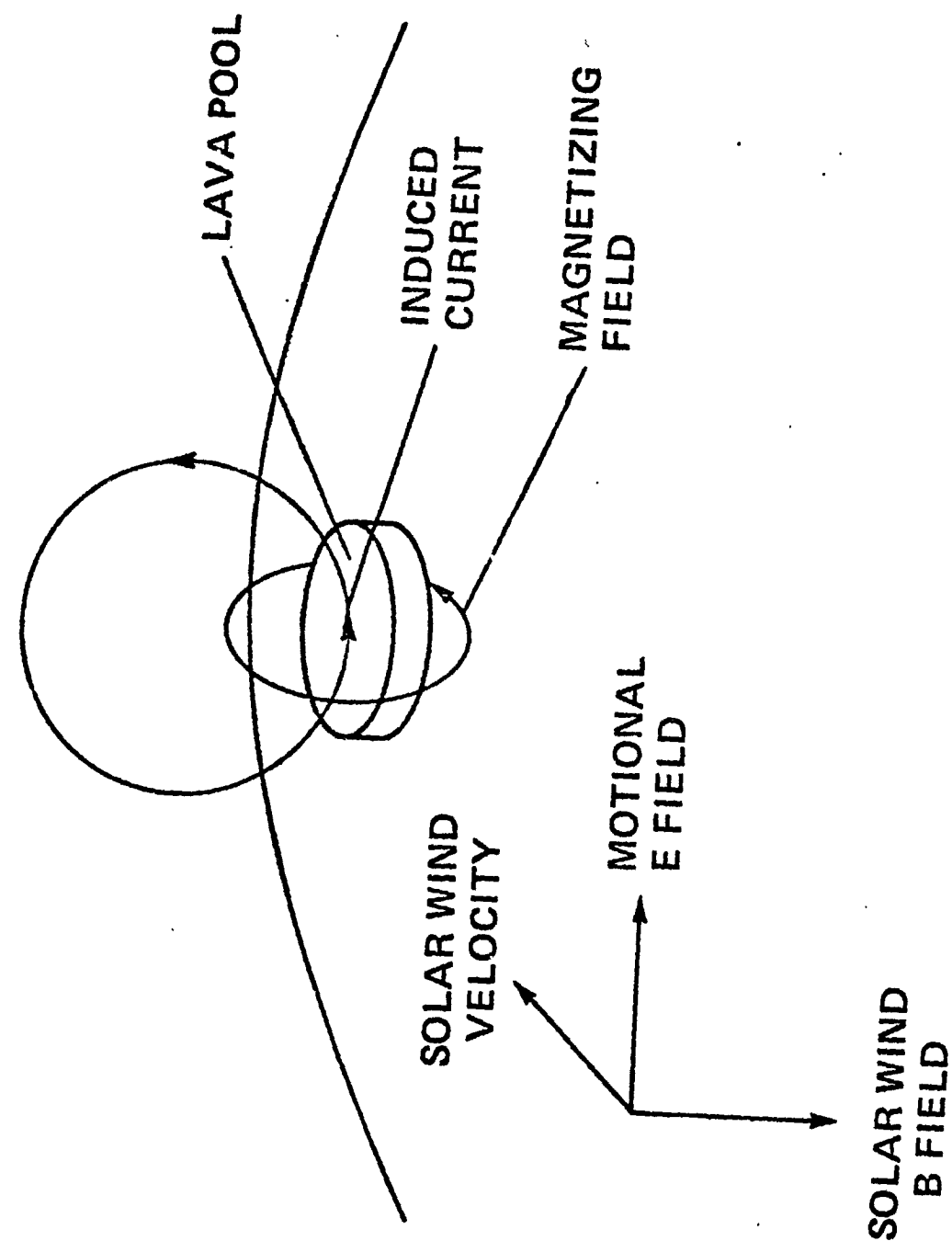


Figure 7

REPRODUCIBILITY OF THE
ORIGINAL PAGE IS POOR

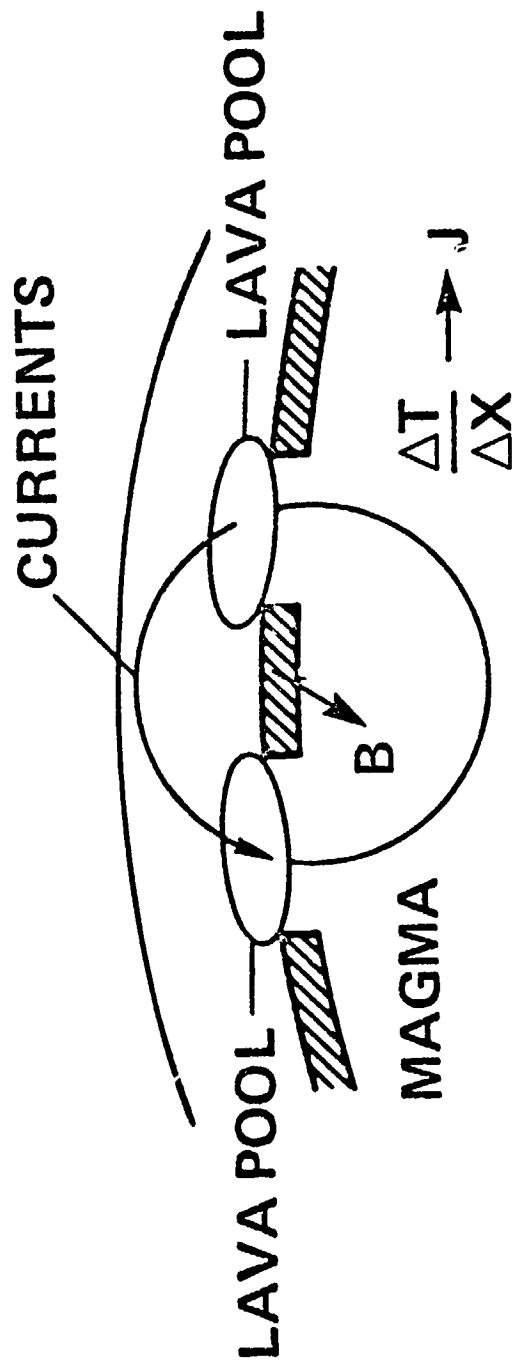


Figure 8

Figure 8

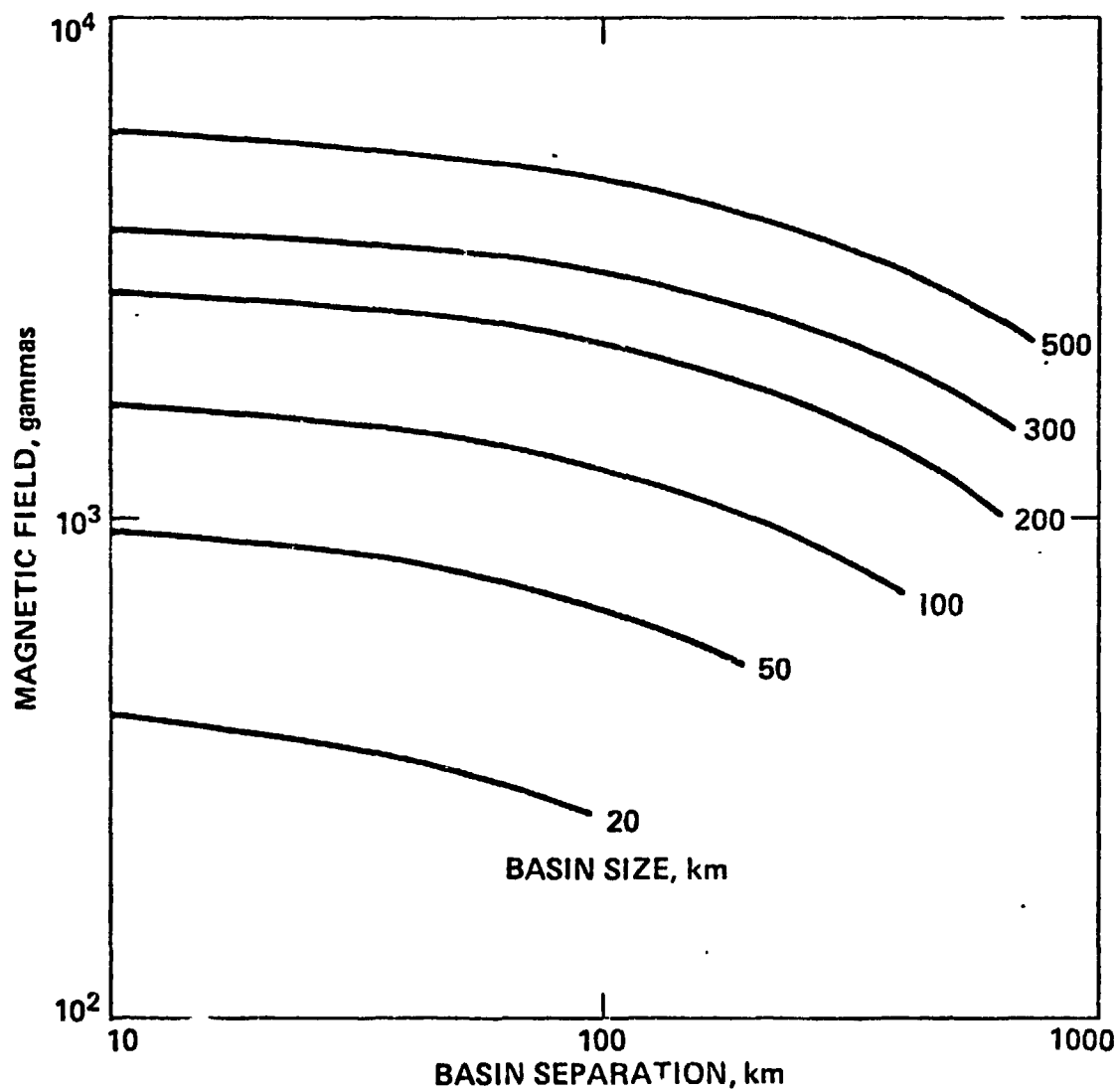
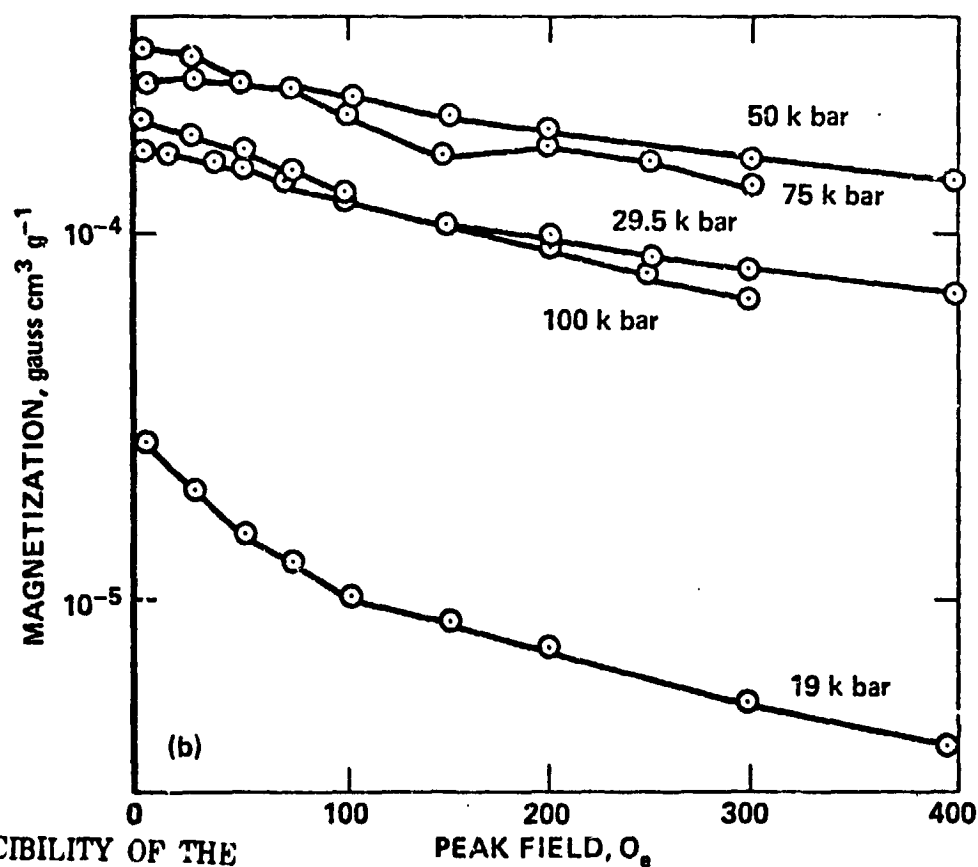
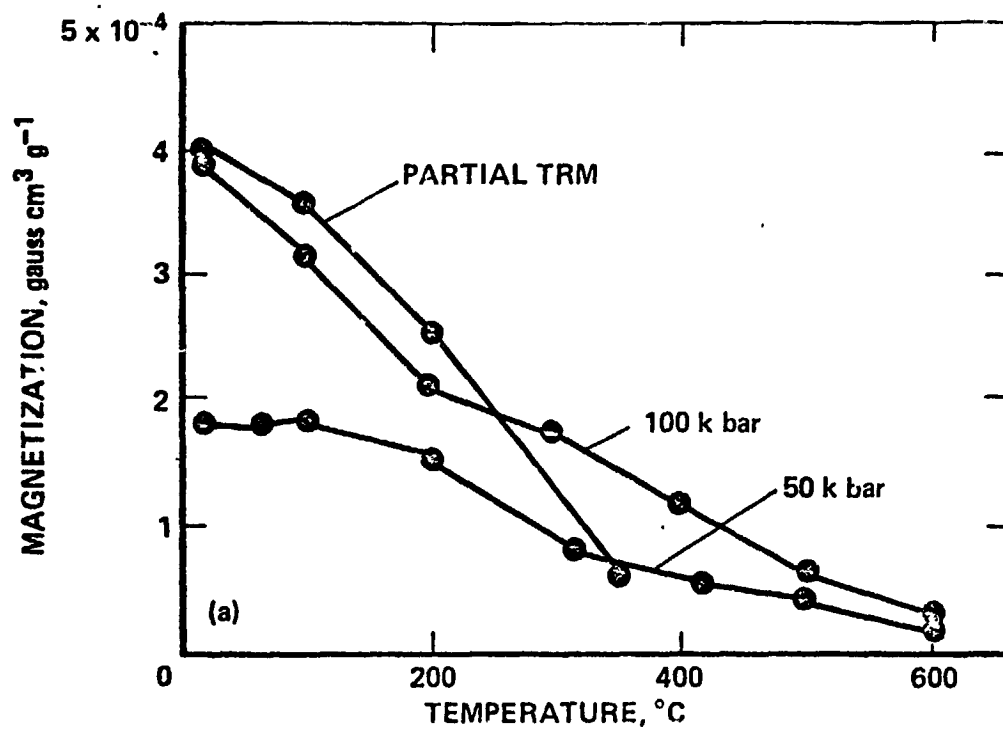


Figure 9

REPRODUCIBILITY OF THE
ORIGINAL PAGE IS POOR



REPRODUCIBILITY OF THE
ORIGINAL PAGE IS POOR

Figure 10

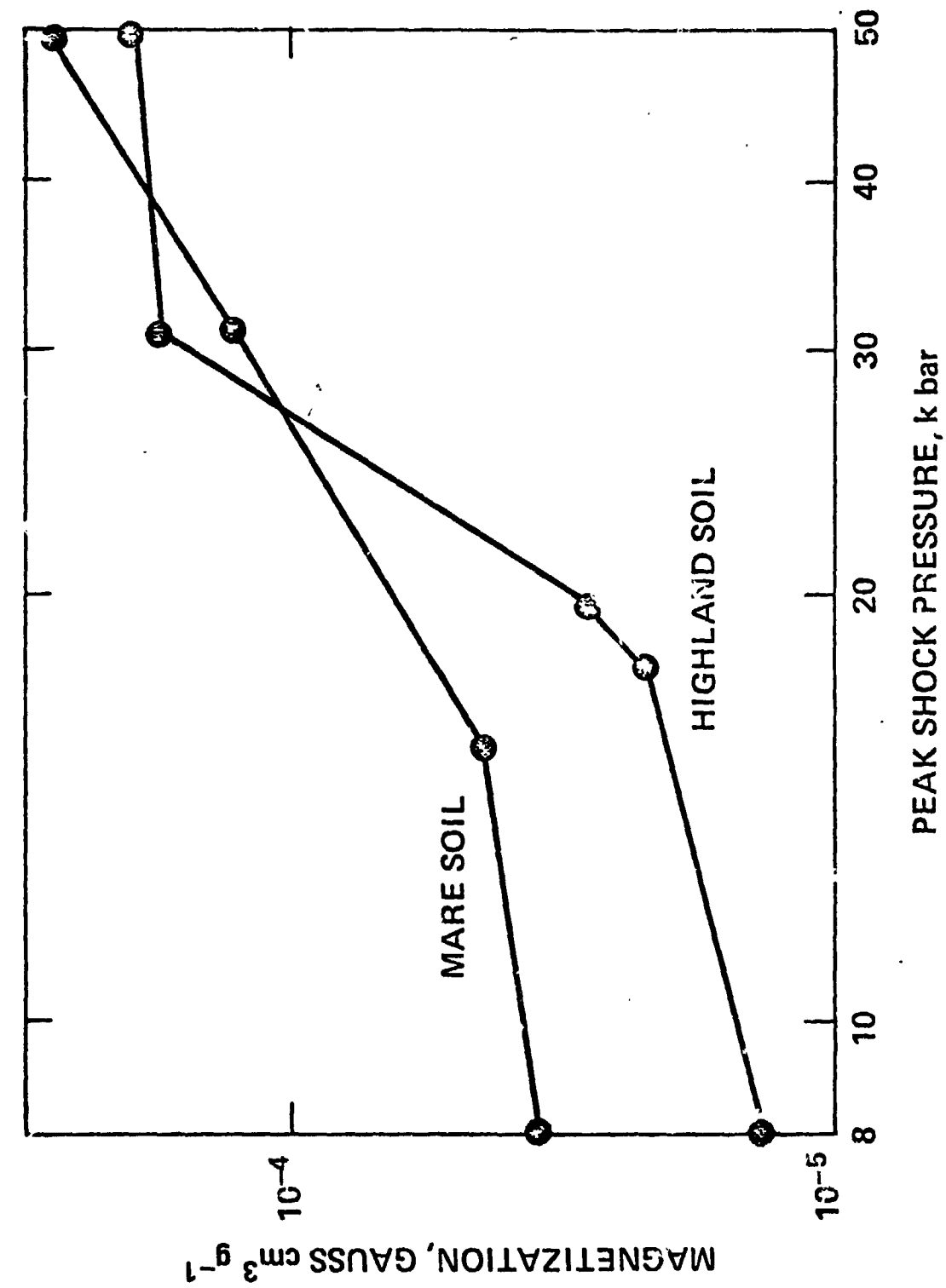


Figure 11

REPRODUCIBILITY OF THE
ORIGINAL PAGE IS POOR

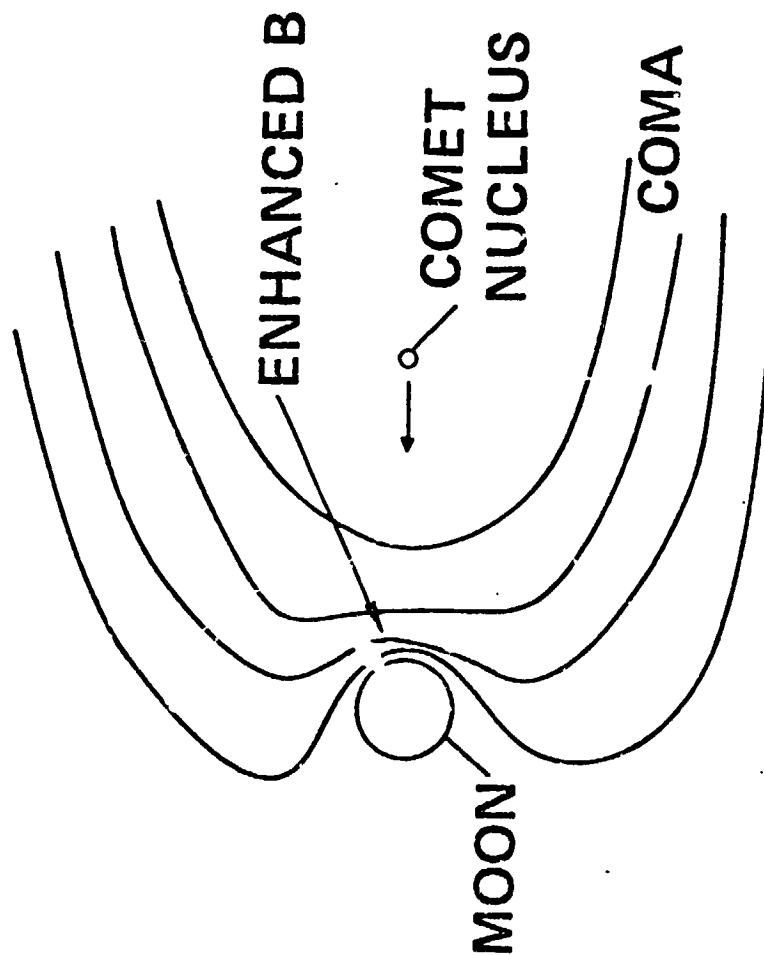


Figure 12

REPRODUCIBILITY OF THE
ORIGINAL PAGE IS POOR

REPRODUCIBILITY OF THE
ORIGINAL PAGE IS POOR

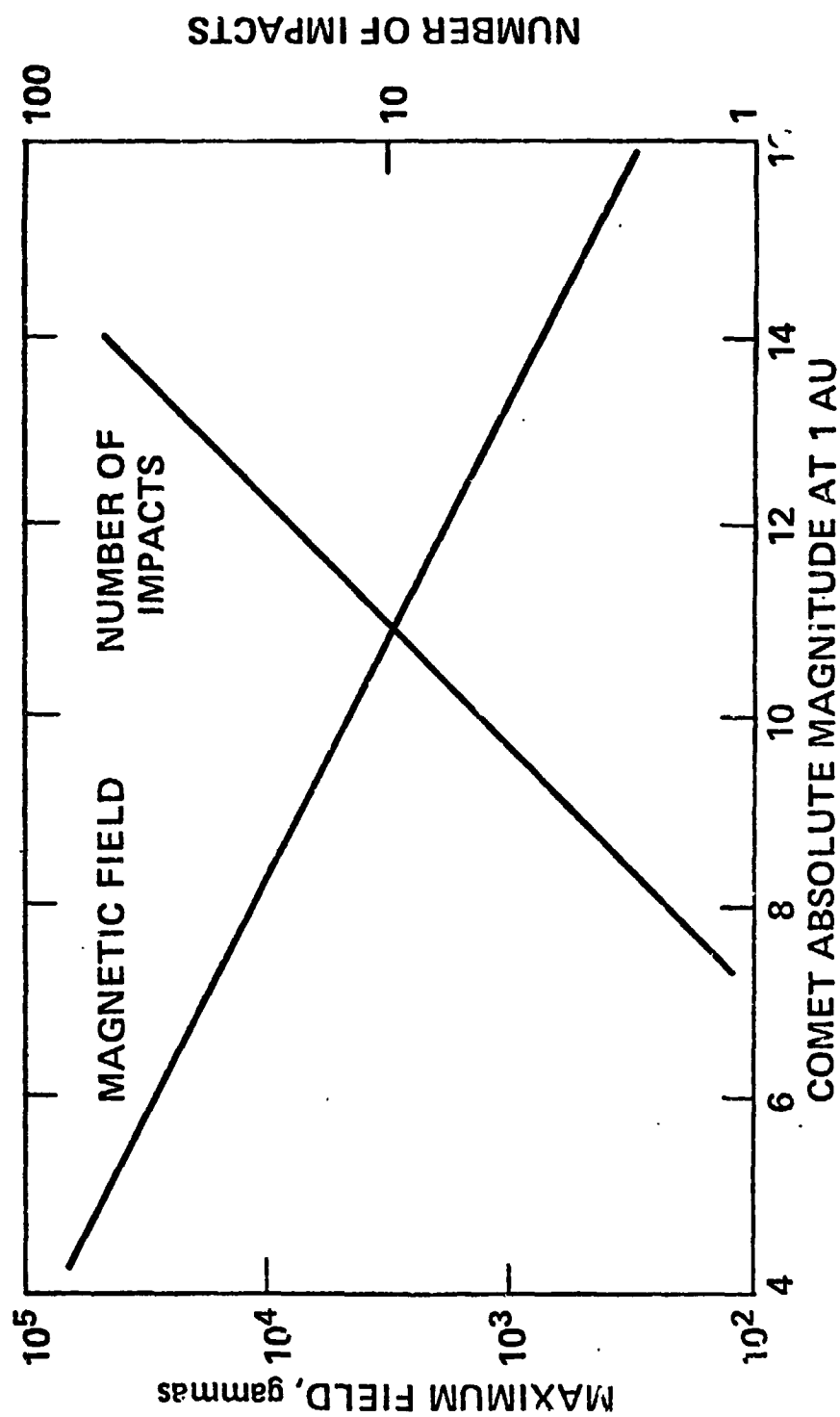


Figure 13

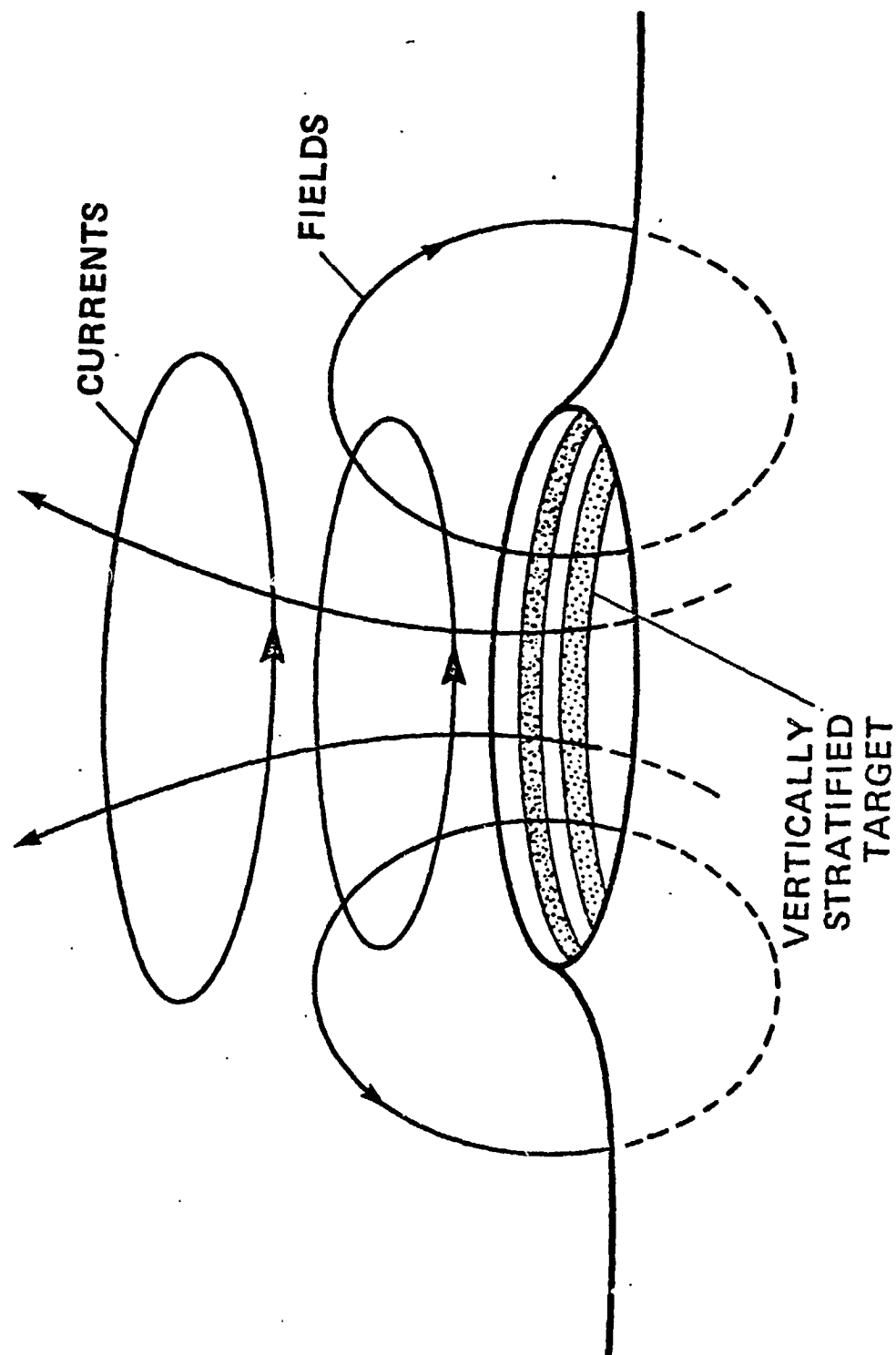


Figure 14

REPRODUCIBILITY OF THE
ORIGINAL PAGE IS POOR

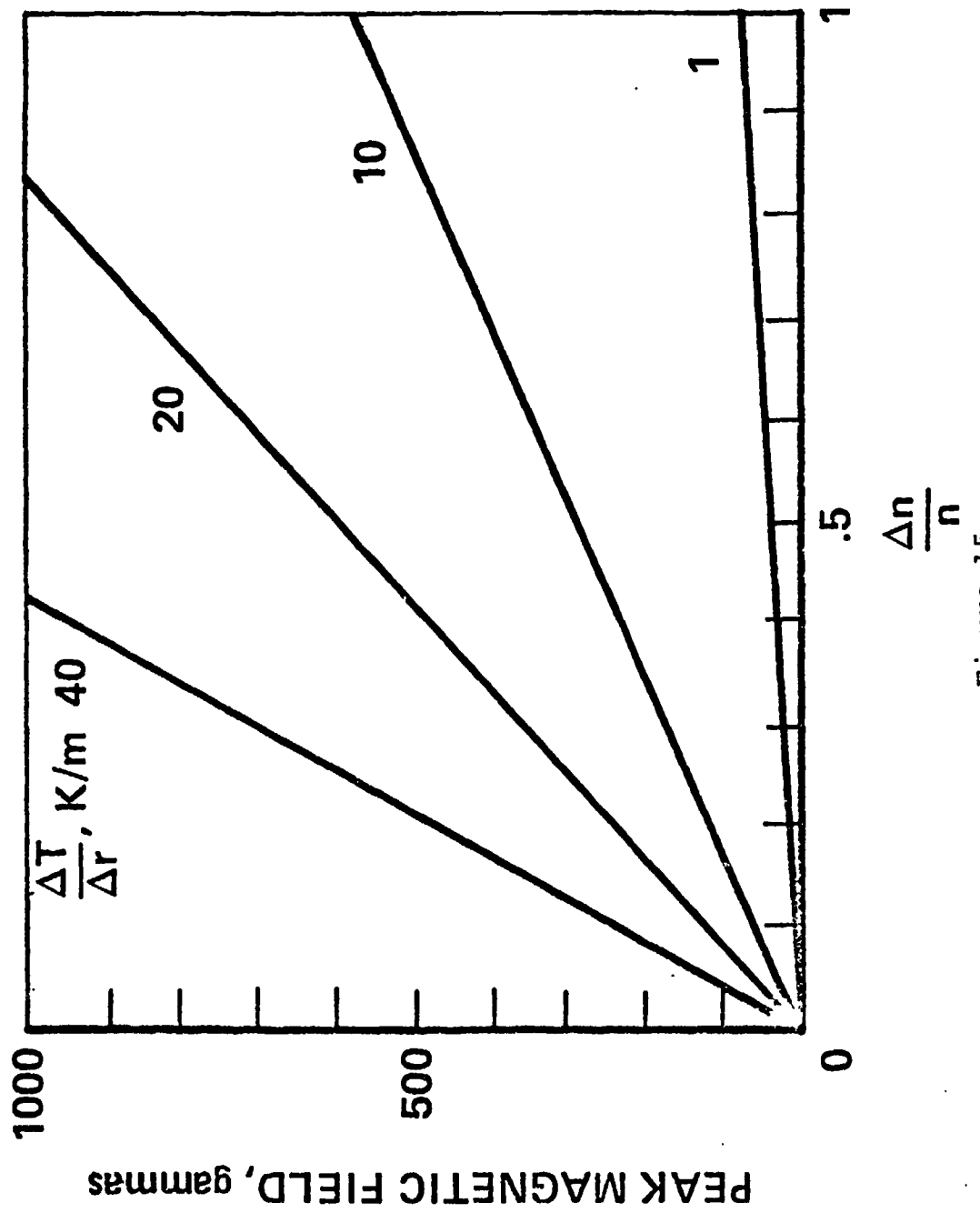


Figure 15

REPRODUCIBILITY OF THE
ORIGINAL PAGE IS POOR

APPENDIX C

ELECTRICAL CONDUCTIVITY ANOMALIES ASSOCIATED
WITH CIRCULAR LUNAR MARIA

**Electrical Conductivity Anomalies Associated
with Circular Lunar Maria**

**Palmer Dyal
NASA-Ames Research Center
Moffett Field, CA 94035**

**William D. Daily
Eyring Research Institute
Provo, UT 84601**

Revised

15 June 1979

Submitted to Proc. Lunar Planet. Sci. Conf. 10th

Abstract - A strong anisotropy is observed in magnetic field fluctuations measured by the Lunokhod 2 magnetometer located on the eastern edge of Mare Serenitatis. This anisotropy can be explained by a regional anomaly in the subsurface electrical conductivity distribution associated with the mare similar to the proposed conductivity anomaly associated with Mare Imbrium. The Serenitatis magnetic field anisotropy is compared to the field fluctuation measured by the Apollo 16 magnetometer 1100 km to the south, and this comparison indicates that the subsurface conductivity distribution can be modeled by a nonconducting layer in the lunar lithosphere which is 150 km thick beneath the highlands and 300 km thick beneath Serenitatis. The decrease in electrical conductivity of the upper mantle beneath the mare may result from lower temperatures due to transport of thermal energy and radioactive heat sources to the surface during mare flooding. This proposed anomaly, along with that proposed for Mare Imbrium, strengthens the possibility of regional anomalies in electrical conductivity associated with all circular lunar maria.

INTRODUCTION

A large regional anomaly in the electrical properties of the lunar crust and mantle has been measured by magnetometers emplaced on the lunar surface by the U.S. and the U.S.S.R.. This anomaly is indicated by analysis of Lunokhod 2 magnetometer data which has revealed that the magnetic field fluctuations near Mare Serenitatis are strongly linearly polarized in a direction aligned approximately radial to the Mare (Dolginov et al., 1976). The Soviet Lunokhod 2 surface rover is located at the eastern edge of Mare Serenitatis within the Bay Le Monnier at selenographic coordinates 26° North latitude and 31° East longitude. A similar polarization is reported by Schubert et al. (1974) for the magnetic field oscillations measured at the edge of Mare Imbrium by the U.S. Apollo 15 surface magnetometer. They interpreted this phenomenon as the manifestation of an electrical conductivity anomaly in the lunar crust and upper mantle associated with Mare Imbrium (Sonett et al., 1974). A similar conductivity anomaly associated with Serenitatis may be expected since both maria contain mascons; are likely to have a similar origin and history; and therefore, probably share similar physical and chemical properties. In this section we present evidence for a region of anomalous electrical conductivity in the upper mantle beneath Mare Serenitatis. We begin by presenting a model of the conductivity anomaly used by Vanyan et al. (1979) to interpret the magnetometer data. The data analysis is then described and the model compared to the data to yield an estimate of the size and location of the anomaly. Implications of this model on the structure and evolution of Serenitatis are then discussed.

THEORETICAL MODEL FOR CONDUCTIVITY ANOMALY

The polarization of magnetic fluctuations observed at the Lunokhod site

may be explained by a region of either anomalously low or high electrical conductivity beneath Serenitatis. However, this interpretation is not unique and the polarization may result from some other source. It is unlikely that this other source is Mare Imbrium because the Apollo 12 magnetometer, at the same distance from Imbrium as the Lunokhod magnetometer, does not measure a field anisotropy which could be attributed to the Imbrium anomaly. We hypothesize that the electrical conductivity distribution beneath Serenitatis is responsible for the observed field polarization. To model this conductivity distribution, Vanyan et al. (1979) represented the lunar highlands by a dielectric layer of conductivity less than 10^{-6} S/m and thickness 150 km, between a layer of conductivity 10^{-3} S/m below and the highly conducting solar wind plasma above (Figure 1a). Beneath the mare the insulating layer is thicker by an additional 150 km. Magnetic fluctuations between 10^{-2} and 10^{-1} Hz will propagate most readily in the low conducting region, resulting in a concentration of magnetic lines of force in this region beneath the mare (see Figure 1a). Schubert et al. (1974) use a similar model in which subsurface currents were represented by two current layers in which the anomalously low conductivity beneath Imbrium is represented by a hole in the upper current layer (Figure 1b).

For the model conductivity distribution shown in Figure 1a Vanyan et al. (1979) calculated the magnetic field which would be measured near the anomaly using a numerical solution to the boundary value problem assuming that the fluctuations external to the moon are circularly polarized (isotropic). The ellipses shown in Figure 2 represent the calculated elliptically polarized (anisotropic) horizontal fields at several locations near the anomalies. In the model the insulating layer thickness increases from 150 km beneath the highlands to 300 km beneath the maria as indicated by the figure. The ellipses major axes are radial to the basins indicating an anisotropy in amplitude of field fluctuations similar to that measured at the Lunokhod 2 and Apollo 15 sites.

DATA ANALYSIS AND RESULTS

For quantitative comparison of these model calculations with the data we have computed the power spectral density of horizontal fields as a function of direction measured by Apollo 15 and Lunokhod 2 magnetometers. Figure 3 shows this distribution of power at 4×10^{-2} Hz at these two sites and at the Apollo 16 site. At the Apollo 15 and Lunokhod 2 sites on the margins of Imbrium and Serenitatis respectively the horizontal field fluctuations are distinctly anisotropic when compared to the fluctuations measured at the Descartes site 1100 km south of Serenitatis by the Apollo 16 magnetometer. Comparison of Figures 2 and 3 reveals that the measured power anisotropies qualitatively agree with the model calculations. This agreement supports our hypothesis of conductivity anomalies associated with these large maria. Therefore, we use this model to estimate depth and size characteristic of the proposed anomalies.

Sonett et al. (1974) demonstrated that the anisotropy measured by Apollo 15 was strongly frequency dependent. At frequencies less than 5×10^{-3} Hz the power distribution at the surface is similar to that measured external to the moon by the lunar orbiting Explorer 35 magnetometer. At frequencies greater than 10^{-2} Hz the anisotropy in the surface field fluctuations is independent of the power distribution external to the moon and is oriented radial to the Imbrium basin. Direct comparison of surface field anisotropy near Serenitatis and the extra lunar field power distribution is not possible since simultaneous Lunokhod 2 and Explorer 35 data are not available. Fortunately, under certain conditions, the Apollo 16 surface magnetometer, located in the Descartes highlands, can be used to measure the field external to the moon. At frequencies greater than 10^{-2} Hz the field fluctuations at Apollo 16 represent the external field variations (Dyal et al., 1978), however below this frequency the Apollo 16 surface fluctuations are dominated by interaction of the 234 gamma remanent field with the solar wind plasma. Observation of simultaneous

Fig.

Lunokhod 2 and Apollo 16 data at frequencies greater than 10^{-2} Hz show that the external field fluctuations are nearly isotropic whereas the Lunokhod 2 field fluctuations are highly anisotropic and aligned with Serenitatis as shown in Figure 3.

This data has been compared to model calculations by Vanyan et al. (1979) to investigate the proposed electrical conductivity anomaly associated with Serenitatis. The model described in the previous section was adjusted by varying the dielectric thickness beneath Mare Serenitatis until the measured and calculated anisotropy matched at the Lunokhod 2 site. The best agreement was found when the basin was represented by a 150 km thickening of the dielectric layer as shown in Figure 2.

DISCUSSION AND CONCLUSIONS

Results of the above analysis demonstrate that the magnetic anisotropy measured by the Lunokhod 2 magnetometer may be due to a region of anomalously low conductivity beneath Mare Serenitatis compared to the conductivity beneath adjacent highlands. However, as Schubert et al. (1974) have pointed out, this interpretation of the field anisotropy is not unique since both high and low conductivity anomalies beneath a mare basin result in identical magnetic polarization at the mare edge. The following hypotheses have been proposed to explain conductivity anomalies associated with lunar maria: (1) Schubert et al. (1974) suggest that the Imbrium associated anomaly may be due to deep faults concentric with the impact basin. Basin excavation certainly resulted in fracturing of subsurface material, however, below 200 km the lithospheric pressure exceeds the rock strength and only closed fracturing is possible at these depths for temperatures of 800-1200 °C (Toksöz et al., 1973). These closed fractures will be sealed by diffusion in the time period from their formation to the present. (2) Although heat generated by impact during basin formation could account for an increased conductivity, this near surface heat

would probably be dissipated by now. (3) Sonett et al. (1974) suggested that chemical differentiation may account for a conductivity contrast between submare and subhighland mantle.

We propose a combination of heat transport and chemical differentiation resulting from filling of front-side basins to explain maria conductivity anomalies. According to this hypothesis the magma which filled the front-side basins carried large quantities of heat from deep within the moon to the surface where the heat was dissipated by radiation. The subhighland mantle was cooled by a less efficient process of conduction through the crust. This would leave the submaria crust and mantle cooler than that of the adjacent highlands. The magma extruded into the maria seas, was also enriched in heat source radioactive potassium, uranium, and thorium. The magma source regions beneath the maria would therefore be depleted of these heat sources relative to surrounding highland mantle. This depletion of both thermal energy and radioactive heat sources, resulted in cooler submaria mantle in comparison to the subhighland mantle with the cooler material having the lower electrical conductivity. The resulting thermal structure of typical submare and subhighland mantle is schematically depicted in Figure 4. The magma generation zones for mare basalts are estimated to be at a 100 to 450 km depth from petrology studies of returned samples and from thermal history calculations (e.g., Toksöz et al., 1973, Solomon, 1975; Hubbard & Minear, 1975). This estimate is in general agreement with our depth for the conductivity anomaly. Our hypothesis which relates shallow electrical conductivity structure and mare volcanism has at least two features which may be tested by future lunar experiments: (1) a conductivity anomaly should be associated with all circular lunar maria and (2) the magnitude of each anomaly should be directly related to the volume of magma in the basin suggesting that farside basins which are not flooded by magma should not be associated anomalous lithospheric conductivity.

Fig. 4

Acknowledgements--The authors are grateful to M. Legg of Diversified Computer Applications for programming and analysis support. Research support for W.D.D. under NASA Grant NSG-2082 is gratefully acknowledged.

REFERENCES

- Dolginov Sh.Sh., Eroshenko E.G., Sharova V.A., Vnuchkova T.A., Vanyan L.L., Okulesky B.A., Bazilevsky A.T. (1976) Study of magnetic field, rock magnetization and lunar electric conductivity in the Bay, Lemonnier. The Moon 15, 3-14.
- Dyal P., Daily W.D., and Vanyan L.L. (1978) Crustal evolution inferred from Apollo magnetometer measurements. Proc. Lunar Planet. Sci. Conf. 9th, p. 231-248.
- Hubbard N.J., and Miner J.W. (1975) A physical and chemical model of early lunar history. Proc. Lunar Sci. Conf. 6th, p. 1057-1085.
- Schubert G., Smith B.F., Sonett C.P., Colburn D.S., and Schwartz K. (1974) Polarized magnetic field fluctuations at the Apollo 15 site: Possible regional influence on lunar induction. Science 183, 1194-1197.
- Solomon S.C. (1975) Mare volcanism and lunar crustal structure. Proc. Lunar Sci. Conf. 6th, p. 1021-1042.
- Sonett C.P., Smith B.F., Schubert G., Colburn D.S., and Schartz K. (1974) Polarized electromagnetic response of the moon. Proc. Lunar Sci. Conf. 5th, p. 3073-3089.
- Toksöz M.N., Dainty A.M., Solomon S.C., and Anderson K.R. (1973) Velocity structure and evolution of the moon. Proc. Lunar Sci. Conf. 4th, p. 2529-2547.
- Vanyan L.L., Vnuchkova T.A., Egorov I.V., Basilevsky A.T., Eroshenko E.G., Fainberg E.B., Dyal P., and Daily W.D. (1979) Electrical conductivity anomaly beneath Mare Serenitatis detected by Lunokhod 2 and Apollo 16 magnetometers. The Moon and Planets in press.

FIGURE CAPTIONS

- Figure 1. Conductivity anomaly models. Electrical conductors are shaded while dielectrics are unshaded. The magnetic field is denoted by B . (a) The conductivity structure under Serenitatis is modeled by a thickening dielectric layer between highly conducting plasma and mantle. (b) Schubert et al. (1974) modeled the Imbrium anomaly by a hole in a current sheet between the solar plasma and another current layer.
- Figure 2. Model and calculation results for lunar conductivity anomaly at Mare Serenitatis and Mare Imbrium. Thickness t in kilometers of the dielectric layer is indicated by the contours. The calculated anisotropy in magnetic fluctuations tangential to the surface is shown by the ellipses at various locations near the basins. A circularly polarized (isotropic) field is assumed external to the moon.
- Figure 3. Distribution of power in magnetic field fluctuations measured at Lunokhod 2, Apollo 15, and Apollo 16 landing sites. The power spectral density at 4×10^{-2} Hz is plotted for the horizontal magnetic field as a function of azimuth at each site.
- Figure 4. Schematic representation of proposed thermal and electrical conductivity structure beneath circular maria and surrounding highlands. Movement of thermal energy and radioactive heat sources to the surface during basin filling resulted in a cooler submaria mantle relative to the adjacent subhighlands mantle as indicated by shading of the mantle regions. The electrical conductivity beneath the maria would therefore be lower than beneath the highlands.

C-2

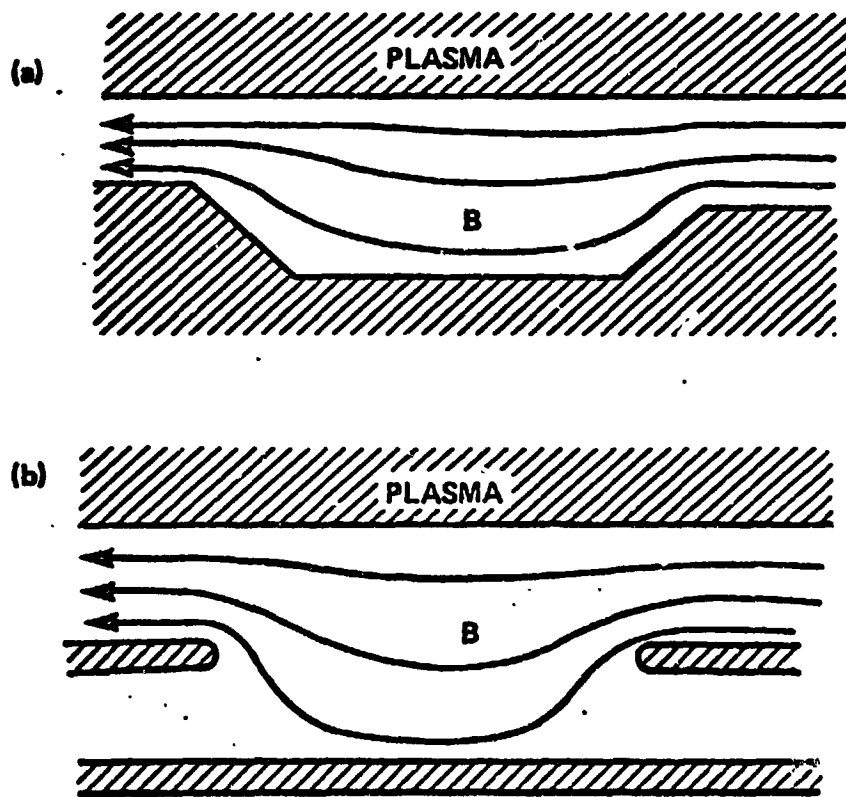


Figure 1

REPRODUCIBILITY OF THE
ORIGINAL PAGE IS POOR

REPRODUCIBILITY OF THE
ORIGINAL PAGE IS POOR

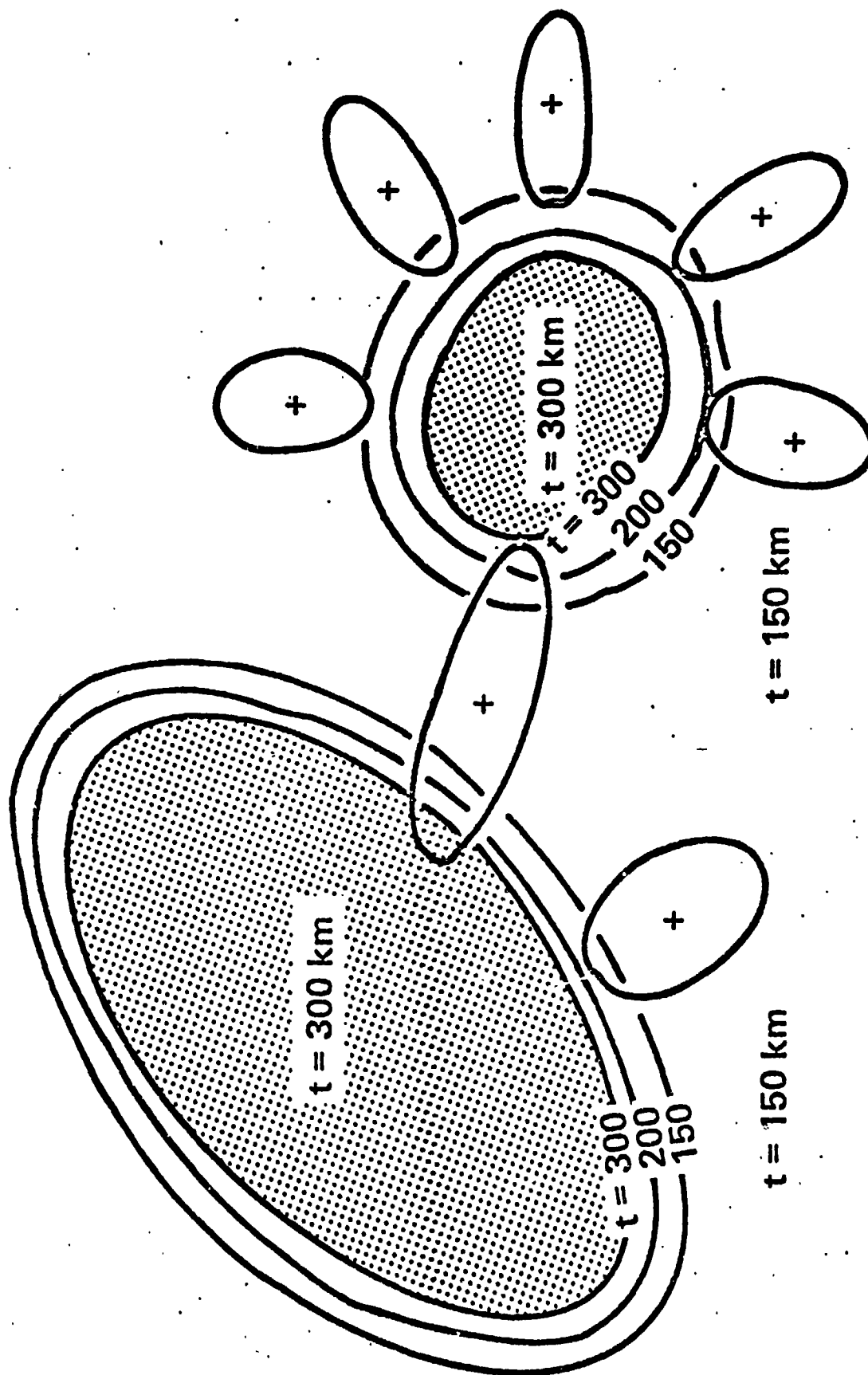


Figure 2

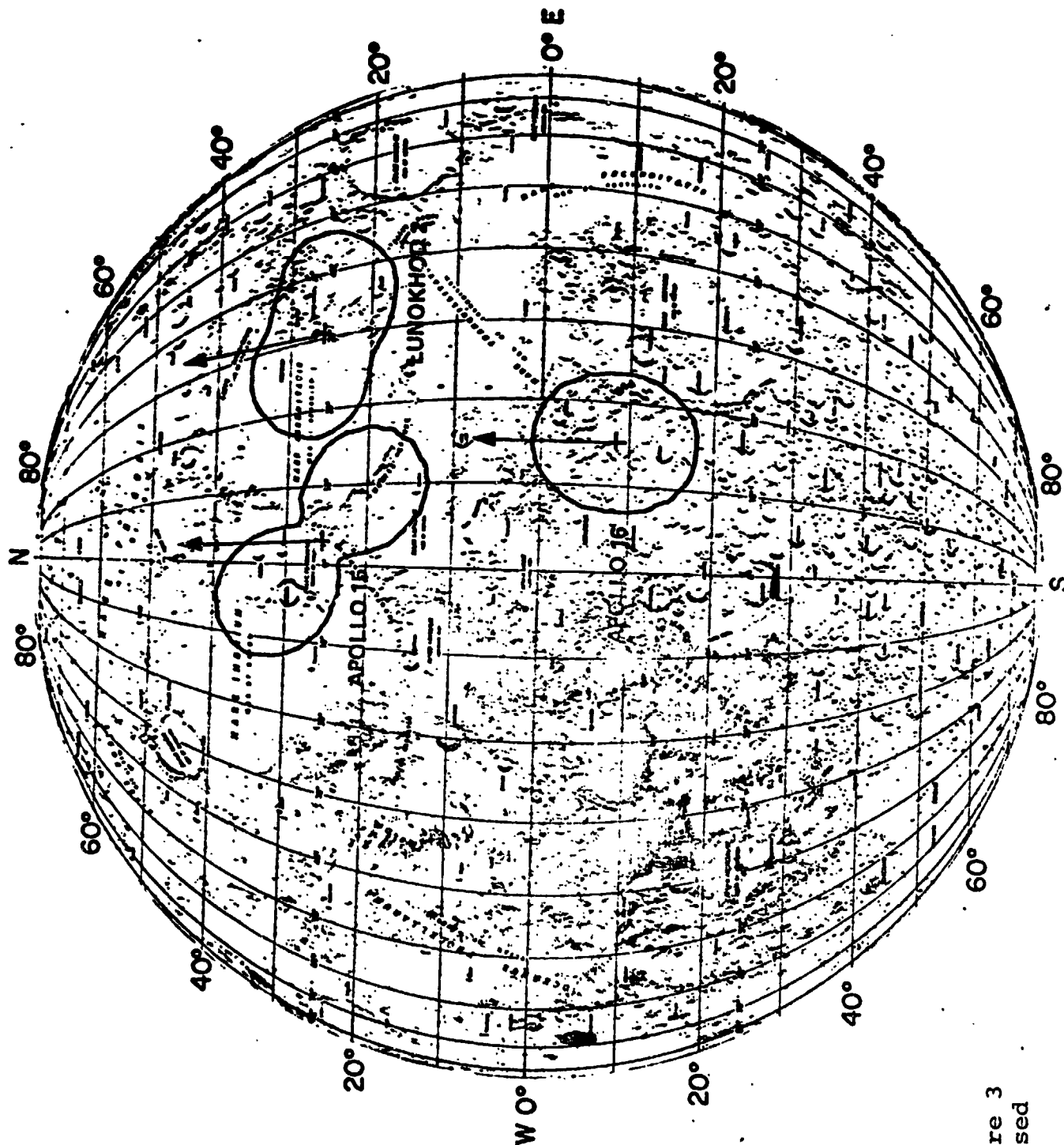
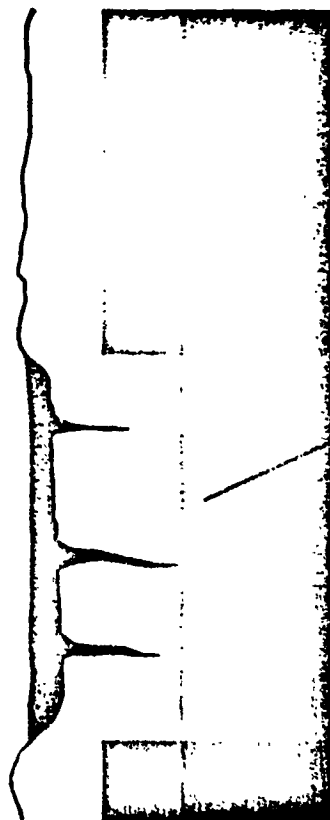


Figure 3
Revised

REPRODUCIBILITY OF THE
ORIGINAL PAGE IS POOR

MARE:
HIGH HEAT LOSS
BY CONVECTION

HIGHLANDS:
LOW HEAT LOSS
BY CONDUCTION



TEMPERATURE
INCREASES
WITH DEPTH

LOWER
TEMPERATURE
AND CONDUCTIVITY

Figure 4
Revised

REPRODUCIBILITY OF THE
ORIGINAL PAGE IS POOR

APPENDIX D

- ELECTROMAGNETIC PROPERTIES OF THE MOON

CHAPTER 12

Electromagnetic Properties of the Moon

Palmer Dyal

NASA-Ames Research Center

Moffett Field, CA 94035

William D. Daily

Eyring Research Institute

Provo, UT 84601

15 May 1979

Abstract

During the time from 1961 to 1972, 11 magnetometers were placed on the lunar surface or in lunar orbit. The purpose of this paper is to review what has been learned about the electromagnetic properties of the moon from analysis of data from the Explorer 35, Apollo, and Lunokhod magnetometers. Local remanent magnetic fields have been measured from 3 to 327 gamma at 4 Apollo landing sites where magnetometers were deployed. A map of the remanent fields obtained from orbiting Explorer magnetometer data, indicates that these surface fields are generally more intense over lunar highlands than over maria. Simultaneous magnetic and plasma data show that the Apollo 12 and 16 remanent fields interact with the solar wind plasma flow and this interaction has been used to determine the scale size of the local fields at these sites. At the Apollo 12 site the field scale size is 18.5 km and at the Apollo 16 site it is 5.7 km. Remanent magnetism in much of the lunar crust is likely characterized by spatial variations as small as a few kilometers. Explorer 35 and Apollo 12 magnetometer data have been used to measure the induced magnetization moment in the moon, from which global lunar permeability is calculated to be 1.012 ± 0.011 . This permeability measurement is used to calculate a model dependent lunar free iron abundance from 0 to 5.8 wt. % with a total iron abundance from 3.5 to 13.9 wt. %. Global eddy current fields have been analyzed to calculate electrical conductivity profiles for the lunar interior. Results from the most recent analysis indicate that lunar conductivity rises rapidly from $< 10^{-9}$ mhos/m at the surface to $\sim 10^{-3}$ mhos/m at a depth of 200 to 300 km. From 300 to 900 km depth the conductivity rises more gradually to 3×10^{-2} mhos/m. From electrical conductivity analyses, lunar thermal profiles have been calculated using laboratory measurements of the relation between conductivity and temperature for various geologic materials.

CONTENTS

	Page
Introduction	1
Explorer 35, Apollo, and Lunokhod Magnetometers	1
Lunar Remanent Magnetism	2
Surface Apollo Site Measurements	2
Orbital Mapping Measurements	3
Solar Wind Interaction with Remanent Fields	4
Theories for the Origin of Lunar Remanent Fields	6
Lunar Magnetic Permeability	14
Introduction	14
Explorer and Apollo Magnetometer Measurements of Global Permeability	15
Lunar Iron Abundance and Structure Inferred from Permeability Measurements	18
Lunar Electrical Conductivity	21
Introduction	21
Explorer and Apollo Magnetometer Measurements of Lunar Global and Regional Conductivity	22
Lunar Thermal Profile and Structure Inferred from Conductivity Measurements	29
Appendix A: Theory for Interaction of Remanent Magnetic Fields and Solar Wind Plasma	31
Appendix B: Theory for Lunar Permeability and Iron Abundance Analysis	34
Appendix C: Theory for Lunar Electrical Conductivity Analysis	38

INTRODUCTION

Magnetometers placed in lunar orbit and on the surface have returned a significant quantity of information about the moon. During the time of the first field measurements near the moon, investigators studied the lunar interaction with the solar wind plasma (Ness et al., 1967; Colburn et al., 1967; Spreiter et al., 1970). Later, after magnetometers were emplaced on the moon and in near lunar orbit, studies were concentrated on the properties of the lunar crust and interior (Dyal et al., 1970b; Dyal and Parkin, 1971a; Sonett et al., 1971b; Schubert et al., 1973 ; Coleman et al., 1972a; Russell et al., 1974; Vanyan, 1977). Using simultaneous magnetic field measurements from orbit and the lunar surface these investigators were able to calculate the lunar permeability and iron content, the electrical conductivity profile and corresponding temperature profile, map the remanent fields associated with the lunar crust, and determine the interaction between the solar wind and these remanent fields.

EXPLORER 35, APOLLO, AND LUNOKHOD MAGNETOMETERS

A total of eleven (11) magnetometers have been placed in lunar orbit or on the lunar surface to measure the magnetic fields associated with the moon. In addition the particles experiment on the Apollo 15 and 16 subsatellites used an electron reflection technique to produce the highest resolution crustal remanent field map to date, (Lin et al., 1975). The Luna 10 (Dolginov et al., 1966) and the Explorer 35 magnetometers (Ness et al., 1967; Sonett et al., 1967) were the first lunar orbiting experiments to make substantive measurements of fields in the lunar environment. These experiments were followed by orbiting magnetometers onboard the Apollo 15 and 16 subsatellites (Coleman et al., 1972a,b) and by Luna 22. Stationary surface magnetometers were deployed by astronauts at the Apollo 12, 15, and 16 landing sites and portable instruments were used at the Apollo 14 and 16 sites, (Dyal et al.,

1974). An automated lunar rover Lunokhod 2 was deployed in Le Monnier Bay to obtain vector field measurements during a traverse of several kilometers (Dolginov et al., 1976). A list of some of the lunar magnetometer characteristics is given in Table 1 and detailed instrumental descriptions are given in the references accompanying this table.

LUNAR REMANENT MAGNETISM

Surface Apollo Site Measurements

The permanent magnetic fields associated with the lunar crust have been measured by surface magnetometers at four Apollo sites and one Lunokhod 2 site and by orbiting magnetometers on Explorer 35, and Apollo 15 and 16 particle and field experiments. In addition the returned lunar samples from the Apollo and Lunokhod landing sites exhibit a natural remanent magnetism (NRM) (reviewed by Fuller, 1974).

The remanence discovered in the analyses of Apollo 11 lunar samples (Strangway et al., 1970) first indicated that there may be a permanent magnetic field associated with the moon. Measurements from orbiting magnetometers had not been interpreted to indicate the presence of permanent lunar fields prior to the Apollo 12 landing in November 1969. A local remanent magnetic field was measured by the Apollo 12 stationary magnetometer deployed on the eastern edge of Oceanus Procellarum. The permanent field magnitude was measured to be $38 \pm 3 \gamma$ and was attributed to localized ordered magnetized sources in the subsurface material (Dyal et al., 1970a; Barnes et al., 1971). A remanent field this large was unexpected, and the origin of magnetized regions on the moon yet remains a central problem in lunar magnetism. Subsequent to this measurement of an intrinsic lunar magnetic field, surface magnetometers have measured fields at the Apollo 14, 15, and 16 sites. Fields of 103 ± 5 and $43 \pm 6 \gamma$, at two sites located about a kilometer apart, were measured by the Apollo 14 lunar portable magnetometer at Fra Mauro. A steady field of

$3.4 \pm 2.9 \gamma$ was measured near Hadley Rille by the Apollo 15 magnetometer. At the Apollo 16 landing site both a portable and a stationary magnetometer were deployed; magnetic fields ranging between 112 and 327 γ were measured at five different locations over a total distance of 7.1 km at the Descartes landing site. These are the largest lunar fields yet measured. All the remanent field vectors have components pointing downward except the one at site 5 near Stone Mountain, which points upward. This anomalous measurement suggests, among other possibilities, that the material underlying Stone Mountain has undergone different geological processes than that underlying the Cayley plains and North Ray crater. In fact, Strangway et al. (1973a) proposed the possibility that the light-colored relatively smooth Cayley formation is magnetized roughly vertically; the difference in the vertical component at site 5 is explained as an edge effect at the Cayley plains-Stone Mountain boundary. A summary of all remanent lunar fields measured by the magnetometers deployed on the surface is given in Table 2.

Orbital Mapping Measurements

Subsequent to the discovery of the field at the Apollo 12 site there were a number of orbital experiments developed to map the fields. Data from the Explorer 35 spacecraft were the first to be used to map surface remanent fields. From the interaction of solar wind plasma with some regions near the limb of the moon, Barnes et al. (1971), Mihalov et al. (1971), and Sonett and Mihalov (1972) inferred surface field strengths and scale sizes. Their techniques were based on the concept that the highly conducting solar wind plasma may interact with high field regions on the moon, when the regions are near the limb, to produce a weak local shock or 'limb compression'. Such shocks could be detected downstream from the moon by the Explorer 35 magnetometer. These magnetic events were interpreted by Mihalov et al. (1971) to infer locations and relative field strengths of surface field concentrations.

Mihalov et al. concluded that there may be magnetic concentrations covering much of the lunar surface, with stronger concentration of magnetized sources on the lunar far side than on the near side and in highlands rather than maria. Limb compressions were also observed by the close orbiting Apollo 15 and 16 subsatellite magnetometers. Using data from these magnetometers, Russell et al. (1973) have confirmed that the source regions for the limb compressions tend to be concentrated in the lunar highlands and especially in the Tsiolkovsky area on the lunar far side.

Direct measurements of the lunar surface fields have been made over about 5% of the lunar surface by the Apollo 15 and 16 subsatellite magnetometers (Coleman et al., 1972b). At the subsatellite altitudes of about 100 km the surface field magnitudes are generally less than 0.5 γ (although sometimes they are as much as 2.5 γ). By averaging data from several orbits that pass over the same surface area, measurements of the fields were made along the entire orbit. Then successive orbits were combined to produce magnetic maps of the regions over which the satellite passed. By using an empirical relation between the height and strength of the field, the orbital values were then referenced to 100 km altitude, and contours of equal intensity drawn for this altitude.

An electron reflection technique was used by Lin et al. (1975) to map a much larger percentage of the lunar surface. These maps indicated large regions of relatively low magnetic field strength on the nearside and regions of higher field intensity with greater variability on the lunar far side. To date there has been very little correlation found between the magnetic fields and surface geological features. Exceptions are the correlations found between remanent fields and Rima Sirsalis (Anderson et al., 1977) and Reiner Gamma (Lin et al., 1979; and Hood et al., 1979).

Solar Wind Interaction with Remanent Fields

The interaction of these crustal remanent magnetic fields with the solar wind has been used by Dyal et al. (1978) to determine the scale lengths of

fields at the Apollo landing sites. This interaction has been modeled by Vanyan (1977) who assumes the crustal magnetic fields propagate into the solar plasma by diffusion. This model is described in Appendix A (See Figure 1).

Fig. 1

The scale sizes of surface remanent fields have been calculated using this model. Measurements used in this analysis were obtained from several different lunar surface and orbital instruments: Apollo 12, 15, and 16 lunar surface magnetometers, Apollo 14 and 16 lunar portable magnetometers, Lunokhod 2 magnetometer, Apollo 12 and 15 solar wind spectrometers, Explorer 35 magnetometer and the Apollo 15 and 16 subsatellite magnetometers.

To theoretically model the interaction consider the magnetic field of a magnetized layer, at a depth d below the lunar surface. Magnetization is proportional to $\cos mz$ where $m = 2\pi/L$ and L is the scale size characteristic of the magnetization. The x axis is directed radially outward from the surface; the y and z axes are tangential to the surface, directed eastward and northward respectively. As shown in Appendix A the distorted and undistorted field at the surface, \underline{B} and \underline{B}_R respectively, are related by

$$B_x - B_{Rx} = -\frac{q-m}{q+m} B_{Rx} \equiv -f(n,L)B_{Rx}$$

for the radial component and

$$B_z - B_{Rz} = \frac{q-m}{q+m} B_{Rz} \equiv f(n,L)B_{Rz}$$

for the tangential component where $q^2 = m^2 + \delta^2$ and δ is the ratio of the plasma frequency and the speed of light. This correlation between the field perturbations and plasma density seen in the Apollo 12 and 16 data can be used to calculate the remanent field scale lengths L at these sites. Results of the remanent field analyses discussed above are summarized in Figure 2.

Fig. 2

Remanent field change tangential to the surface at the Apollo 12, 15, and 16 landing sites is plotted as a function of the measured solar wind density.

For each site the averaged data is compared to the diffusion model calculations with three different scale lengths for the local field values. It is apparent that the Apollo 12 and 16 analyses are relatively sensitive to the model scale lengths. The scale size characteristic of the remanent field at the Apollo 12 site is 18.5 km and at the Apollo 16 site is 5.7 km. The field-plasma interaction at Apollo 15 is negligible, in accordance with the diffusion model, indicating a very low magnitude field in the Hadley landing site region.

Theories for the Origin of Lunar Remanent Fields

The origin of the lunar remanent fields remains an unknown at this time. Many theories have been proposed to explain the NMR found in lunar samples and remanent fields measured by surface and orbiting magnetometers. A complete review of these theories has just been completed by Daily and Dyal (1979b).

For convenience we classify the lunar magnetization theories into two groups: (1) Global--those which involve magnetic fields of a scale size comparable to or larger than the moon. (2) Local--those which involve processes or fields of a local nature where small regions are magnetized.

Several authors have suggested that the paleomagnetic fields necessary to magnetize lunar crustal material originated in the early sun (e.g., Nagata et al., 1972). If a large solar field was present during lunar crustal formation, and of dipole character out to the lunar orbit, the crust would have been magnetized uniformly. The present moon cannot have a uniformly magnetized shell since it would yield a global remanent dipole moment 2 to 3 orders of magnitude larger than the limit placed by Russell et al. (1974). On the other hand, if the early solar field was convected from the sun as it is today, the magnetic lines of force near the ecliptic would be preferentially aligned parallel to the ecliptic plane in the familiar spiral pattern. Hood et al. (1978) have shown that the magnetization vectors of these source regions tend to be parallel to this plane. This suggests that the regions may have been

magnetized by early intense solar wind field. Sonett et al. (1968) and Levy and Sonett (1978) have suggested that a pre-main sequence T Tauri sun or even an earlier nebular dynamo could have produced such large solar system fields.

The main objection to a solar or nebular origin for lunar magnetism is that the magnetizing field must remain constant during the cooling of a large volume of crust if it is to acquire a uniform magnetization. The time scale for fluctuations in an early solar field and for rotation of the moon itself, are probably small compared to the cooling time of large crustal regions. Large units could be uniformly magnetized by a solar wind field only if they were thin enough to cool rapidly. Hood and Wilhelms (1978) identified an extraordinarily thin, highly magnetized deposit at 8 °N and 59 °W. The Apollo subsatellite magnetometer measures a 21 gamma anomaly (at 20 km altitude) which coincides closely in size, shape, and position to a light deposit known as Renneri γ. Magnetization of localized regions in the crust or of thin breccia flows on the surface by an intense solar wind field is plausible, but magnetization of large regions by this mechanism is questionable.

Magnetization of lunar rocks by the terrestrial field requires that the moon was once much closer to the earth, that the earth's field was much more intense, or a combination of these two possibilities. If the lunar distance were only 3-4 earth radii, the present terrestrial field would be sufficient to account for the lunar paleointensity determinations of $\sim 10^3$ gammas but cannot account for the paleointensity values as high as 1.6 Oe (e.g., Fuller, 1974).

To explain lunar magnetism with the moon in its present orbit, a terrestrial dipole moment at least 10^2 larger than its present value is necessary. Alfvén and Lindberg (1974) propose a type of terrestrial hydromagnetic dynamo which would produce a field of 1600 gammas at the moon if its distance was 10 to 20 earth radii. Paleointensity data for the earth is available in some detail

for the past 0.4 b.y., and during this time the terrestrial magnetic moment has not increased in strength more than 50% of its present value (Strangway, 1970). Some terrestrial samples as old as 3 b.y. have a remanence similar to that of young rocks, implying that the earth's dynamo has operated much the same for the past 3 b.y. (Strangway, 1978).

Magnetization of the global lunar crust in a terrestrial magnetic dipole leads to a remanent moment in the modern moon larger than the measured limits (Russell et al., 1974). The mechanism for acquisition of this dipole moment is the same as that discussed for the early solar magnetizing field. Considering the arguments discussed above, the earth seems to be an unlikely source for the early lunar magnetizing field.

Runcorn and Urey (1973) and Strangway et al. (1973b) have suggested that crustal remanence may have resulted from a lunar core, magnetized during or shortly after its formation. The magnetic field of this core is proposed to have thermoremanently magnetized the outer lunar shell as it cooled, 3.2 to 4 b.y. ago. Subsequent radioactive heating of the interior raised the core temperature above the Curie point with a loss of the internal magnetizing field. In addition, Runcorn (1975) has shown that a spherical shell magnetized by the field of an internal dipole will have no magnetic moment if the original magnetizing field is removed. However Stephenson (1976) has calculated the residual dipole moment of the spherical shell for the more realistic case where the permeability of the shell and core are different. For this model, the calculated moment of a crust magnetized to a depth of only 35 km is the same order of magnitude as the limit measured by Russell et al. (1974). Srnka and Mendenhall (1978) also calculate a residual shell dipole for the more sophisticated model where the magnetizing dipole exponentially decays in strength and the crust is magnetized in layers as the Curie isotherm advances with depth during crustal cooling. For reasonable model parameters the

residual dipole moment is 5 times the upper limit allowed by Apollo sub-satellite measurements. It has also been pointed out by Runcorn (1976) that a field from an ancient magnetized core cannot explain paleointensity measurements of 1 Oe and larger derived for some lunar samples.

A popular mechanism for the origin of the lunar field is a regenerative dynamo in a small core (e.g., Runcorn et al., 1971; Strangway et al., 1971). This idea is appealing since a hydromagnetic dynamo is the most reasonable source for the earth's field. Remanence in lunar samples 4 b.y. old, requires formation of a small convecting core at least this early in lunar history. However, differentiation of the required iron or iron sulfide core and the lunar crust, seems to require melting of the whole moon (Runcorn, 1976). Melting the lunar core this early requires an extraordinarily intense heat source. For this heat source Runcorn (1977, 1978a) postulates iron soluble super-heavy elements with atomic numbers from 114 to 126 and half lives of $\sim 10^8$ yrs. Paleointensity determinations require this lunar dynamo to generate surface fields 3 times larger than those generated by the terrestrial dynamo. Paleointensity determinations on some samples indicate a decline in the early lunar field as would be expected from a dynamo produced in a cooling core.

Magnetization of an ideal crustal shell by an internal dipole, results in zero field external to the shell after the magnetizing dipole is removed (Runcorn, 1975). The observed magnetic anomalies above the lunar crust are attributed to cratering or other processes which change the ideal shell. Field lines escape the shell at each crater. However, these field lines contribute to a global dipole moment as well as producing magnetic anomalies. Weiss et al. (1977) have calculated the magnetic dipole moment for a lunar model with the 17 largest basins and craters scooped out of a crustal shell magnetized by an internal dipole. The residual moment was much smaller than the measured upper limit dipole for the moon permitting a dynamo hypothesis to

explain magnetic anomalies and satisfy the global dipole constraint.

The field lines that escape the shell at each crater will result in strong correlation of magnetic anomaly and crater location. The field magnitude as calculated by Weiss et al. (1977) which would be observed 100 km above a magnetized shell would be highly correlated with crater location. This correlation has been searched for without success in lunar magnetic and topographic maps (Russell et al., 1977; Lin, 1978; Hood et al., 1978). In conclusion it is improbable that a dynamo was responsible for the early lunar magnetic field. However, neither experimental or theoretical studies conclusively rule out a small core dynamo field source.

Pearce et al. (1972) first proposed the idea that small pockets of Fe-FeS eutectic located close to the surface, each acting as a self regenerative magnetic dynamo, may have been responsible for lunar remanence. This hypothesis was developed by Murthy and Banerjee (1973) and incorporated into a particular accretional model of the moon. In this model, local surface melting allowed Fe-FeS melt to accumulate in pockets (Fescons) located preferentially on the front side of the moon at a depth of about 200 km. These massive accumulations, each approximately 10^{-4} lunar mass, with a density of $\sim 5.6 \text{ g cm}^{-3}$ and a diameter of about 130 km, are postulated to account for the mass concentrations beneath the ringed maria. However, because these dynamos are necessarily located beneath maria, mare basalts should be the most highly magnetized rocks. This is directly contrary to sample analysis (Fuller, 1974; Pearce et al., 1973) and subsatellite observations of remanent field intensity (Russell et al., 1977; Lin, 1978). This disagreement with experimental evidence constitutes a serious objection to this theory of lunar magnetism.

A magnetic dynamo driven by thermoelectric currents in the cooling lunar crust was first proposed by Dyal et al. (1973) and later developed further by Dyal et al. (1977). As the lunar crust solidified from a primordial magma

ocean, meteorite impacts are proposed to have penetrated the solid crust, exposing subsurface magma and forming lava-filled basins. Two such basins in close proximity, formed at approximately the same time, would have been connected below the crust by subsurface magma and above by solar plasma. Heterogeneous cooling in the crust could have resulted in cooling one basin more rapidly, producing a large temperature difference between the basins. In this model we have the elements of a thermoelectric circuit: two dissimilar conductors (plasma and lava) joined at two junctions (lava basin surfaces) which are at different temperatures. The magnetic field intensity between the two basins as a function of basin size and separation has been calculated. For basins as large as 100 to 200 km the calculated magnetic fields are 1 to 3×10^3 gammas which are similar to many paleointensity results.

There are two principal disadvantages to explaining lunar magnetism by this mechanism. First, paleomagnetic fields as large as 1 Oe, as indicated by some sample analyses, would require extraordinarily large thermoelectric coefficients. Second, the time scale for field generation is uncertain because of unknown cooling rates for lavas under lunar conditions and thermo-remanent magnetization of large regions require field generation during their cooling. Critical evaluation of the time scale for field generation in this mechanism will be possible when lava cooling rates in a vacuum are included in the model.

Magnetization of localized regions during impact cratering was among the first mechanisms to explain lunar remanence (e.g., Nagata et al., 1970, 1971). Several different magnetization processes occurring during impact and crater formation have been proposed.

Acquisition of a NRM in ferromagnetic iron oxides due to impulsive stress loads is a well known phenomenon (e.g., Petrova, 1963; Shapiro and Alovera, 1970; Hargraves and Perkins, 1969). The magnetic effects of shock loading in

nonoxidized iron and its alloys (the principle carriers of natural remanence in lunar materials) have been only recently studied (e.g., Wasilewski, 1972, 1973, 1978a,b). Magnetic studies of iron oxides cannot always be directly applied to free iron remanence but recent experimental results of shock loads on iron grains in a magnetic field do result in a magnetic remanence. For example, Nagata et al. (1971) were the first to experimentally study the relationship of stress and magnetic properties in lunar samples. They found that a mechanical shock applied in an external field of 3-9 Oe resulted in a shock remanent magnetization (SRM) proportional to the field and shock intensities. Cisowski et al. (1973, 1975, 1976, 1977) report results of a series of experiments extending this work to demonstrate the viability of shock magnetism. Assuming a linear dependence of shock magnetization on field intensity, Cisowski et al. (1973) estimate a remanence of 10^{-4} and 10^{-5} gauss cm³ g⁻¹ (similar to that of lunar samples) in a field of 10^3 and 10^2 gamma respectively for one sample shocked to 50 k bars. However even these fields are one or two orders of magnitude larger than are common in the present lunar environment. It is possible that larger fields were present during the heavy cratering period. Large transient fields generated during the proposed SRM may have been produced by compression of a small ambient field or from currents in crater ejecta plasma. Generation of magnetic fields in crater ejecta was first suggested by Hide (1972). Srnka (1977) has further investigated this mechanism to evaluate its importance during lunar crater formation. He considers the magnetic fields arising from drift currents generated by nonaligned temperature and density gradients in the ejecta plasma. Calculations yield a field magnitude of 10^3 gammas. More extreme pressure gradients or other current configurations (Srnka, 1977) may result in larger field values.

None of the above theories, at their present level of development, satisfy

all of the experimental constraints. However, several of the hypotheses require additional development before they can be realistically evaluated. The most likely mechanisms are impact magnetization, thermoelectric dynamos, and early solar field magnetization. Hopefully, additional theoretical and experimental work, along with possible future missions to the moon, will clarify our understanding of the origin of lunar remanent magnetism.

LUNAR MAGNETIC PERMEABILITY

Introduction

Magnetic permeability and iron abundance of the moon can be determined by analysis of magnetization fields induced in the permeable material of the moon. When the moon is immersed in an external field it is magnetized; the induced magnetization is a function of the type and distribution of permeable material in the interior. Figure 3 illustrates how the lunar magnetic permeability is measured using Explorer 35 orbiting and Apollo surface magnetometer data. When the moon is immersed in a uniform external magnetic field H (the geomagnetic tail field), a dipolar magnetization field is induced (modeled here by a two layer sphere) so that the total field B at the surface is the sum of the external and induced field. Measurement of H by the Explorer 35 magnetometer and B by the Apollo surface magnetometer allow calculation of the induced magnetic dipole moment and effective whole body magnetic permeability. Under the assumption that the permeable material in the moon is predominately free iron and iron-bearing minerals, the lunar iron abundance can be calculated from the lunar permeability for assumed compositional models of the interior. Since the amount of iron present in the lunar interior should be consistent with the measured global magnetic permeability, the permeability in effect places a constraint on the physical and chemical composition of the moon's interior.

In this section we will review the theoretical model used in the calculation of lunar permeability using Explorer and Apollo magnetometer data. Then we present the most recent results of the bulk magnetic permeability. The interpretation of these results for lunar iron abundance will then be presented, including a discussion of the model used for calculating free and total iron abundance.

Explorer and Apollo Magnetometer Measurements of Global Permeability

Using data from the Explorer 35 Goddard magnetometer, Behannon (1968) first placed an upper limit on the bulk lunar permeability. In this analysis, Behannon used data measured when the moon was in steady-field regions of the geomagnetic tail, where it was assumed that the external field was uniform over the region of space near the moon and plasma effects were negligible. Under these conditions, for a moon of spherically symmetric permeability distribution, the induced magnetization moment would be dipolar, with the dipole axis oriented along the external field. Explorer 35 field measurements were compared when the moon was above the neutral sheet (with the induced dipole oriented along the field pointing sunward) and below the neutral sheet (with the dipole oriented away from the sun); differences in the data pairs, on the average over many Explorer orbits, were considered to represent a measurement of the induced field. At the Explorer 35 periselene the induced field was found to be less than the experimental error. Using the experimental error as the upper limit of the induced field at the surface, Behannon calculated an upper limit of 1.8 for the bulk magnetic permeability of the moon.

Deployment of Apollo magnetometers on the lunar surface allowed simultaneous measurements of the external inducing field H (by Explorer 35) and the total response field at the lunar surface B (by an Apollo magnetometer). For this analysis consider the lunar interior modeled by a chemically homogeneous sphere which has an iron Curie (T_c) isotherm at some depth R/R_{moon} . The sphere is assumed to be composed of a paramagnetic mineral with free iron distributed throughout. The free iron is ferromagnetic in the outer shell where $T < T_c$, and paramagnetic in the core where $T > T_c$. The permeability μ_2 of the core therefore corresponds to paramagnetic material only, while μ_1 of the shell combines contributions from ferromagnetic iron and paramagnetic mineral.

Following Jackson (1962) the total field on the outer surface of the sphere can be expressed (see Appendix B for details):

$$\underline{B} = H_x(1 + 2F)\hat{x} + H_y(1 - F)\hat{y} + H_z(1 - F)\hat{z} \quad (1)$$

where

$$F = \frac{(2\eta + 1)(\mu_1 - 1) - \lambda^3(\eta - 1)(2\mu_1 + 1)}{(2\eta + 1)(\mu_1 + 2) - 2\lambda^3(\eta - 1)(\mu_1 - 1)} \quad (2)$$

Here $\eta = \mu_1/\mu_2$; μ_1 and μ_2 are relative permeability of shell and core respectively (permeability of free space $\mu_0 = 1$); $\lambda = R_c/R_m$, where R_c = radius of the core and R_m = radius of the whole sphere. \underline{B} is expressed in the ALSEP coordinate system which has its origin on the lunar surface at a magnetometer site. The x-axis is directed radially outward from the lunar surface; the y and z axes are tangential to the surface, directed eastward and northward, respectively.

A plot of any component of equation (1) will result in a B - H hysteresis curve. Equation (2) relates the slope of the hysteresis curve to the lunar permeability. The whole-moon permeability μ is calculated from the hysteresis-curve slope with $\mu_1 = \mu_2 = \mu$:

$$F = \frac{\mu - 1}{\mu + 2} \quad (3)$$

The hysteresis-curve method of permeability analysis was first employed by Dyal and Parkin (1971b) to calculate the whole-moon permeability of 1.03 ± 0.13 . Subsequent analyses have attempted to reduce the uncertainty of this measurement and thereby better constrain this physical parameter of the moon. The procedure has been to select data for the analysis which is less contaminated by the principle noise sources: poloidal and toroidal mode field induction (discussed below) and gradients in the external magnetizing field.

Fluctuations of the extra lunar field ($\partial \underline{B}_E / \partial t$) drive time-dependent eddy currents in the lunar interior. These in turn result in a poloidal magnetic field (TE induction) which is the largest of the electromagnetic induction

fields measured at the surface. In the limit of low-frequency or small-amplitude driving field fluctuations, $\partial B_E / \partial t \rightarrow 0$ and induction from the poloidal mode vanishes. Therefore restrictions placed on the peak-to-peak variations of surface and external fields, discriminate against data obviously contaminated by eddy current fields. In the lobes of the geomagnetic tail the moon is in a relatively constant field environment so that data for permeability analyses is selected from this magnetically quiet region to minimize effects of poloidal induction fields.

Relative motion of the moon and the geomagnetic field results in a motional electric field $\underline{E}_m = \underline{V} \times \underline{H}$ in the lunar reference frame, where \underline{V} is the relative lunar velocity and \underline{H} is the external field. Currents driven by \underline{E}_m set up magnetic fields (TM induction) that are toroidal about the electric field. Theoretically this magnetic field is everywhere tangent to the lunar surface so that the ALSEP x-components, which contain minimal toroidal induction are used for permeability analyses requiring surface field measurements.

The induced magnetization field given by equation (1) assumes a uniform external magnetizing field. Under this assumption the induced field is dipolar; higher order multipoles contribute when inhomogeneities are present in the external field. Uniformity of the ambient geotail field cannot be guaranteed with the available data. However, it is possible to discriminate against data from nonuniform tail fields by requiring magnetic conditions at both surface and orbiting instruments simultaneously to be steady over long time intervals. If the geomagnetic field and moon are in relative motion with a speed characterized by $V \sim L/T$, where L is the distance between Explorer 35 and Apollo magnetometers and T is the time over which the field is steady, then any nonuniformities can be detected as magnetic fluctuations at either instrument. Various criteria on the peak-to-peak fluctuations at both magnetometers have been used to select data in an attempt to assure uniformity in the magnetizing

field. Furthermore, data from the plasma free geomagnetic tail is necessary in permeability analyses using surface measurements to minimize noise due to the interaction between plasma flow and local lunar fields.

Application of these data selection techniques have been used by Parkin et al. (1973, 1974) to accurately measure the bulk lunar permeability from Explorer and Apollo magnetometer data. In the most recent orbit-surface magnetometer results (Parkin et al., 1974), a hysteresis curve was constructed using 2703 data sets and is shown in Figure 4. Since the external magnetizing field is small (~ 10 gammas), the familiar "S" shape of the hysteresis curve degenerates to a straight line (Ellwood, 1934). The data were fit by a least-squares technique which yields the best-estimate slope of 1.008 ± 0.004 . Using this value with the radial (x) component of equations (1) and (3), the whole-moon permeability is 1.012 ± 0.006 (2σ error limits). Both extrema are greater than 1.0, implying that the moon, as a whole, acts as a paramagnetic or weakly ferromagnetic sphere. King and Ness (1977) have questioned the validity of this global permeability measurement, contending that limits in data accuracy make measurements difficult for induction fields as small as 0.1 gamma. Daily and Dyal (1979a) have examined in detail the relative data errors in the Explorer 35 and Apollo surface magnetometers and estimated the effects of these errors on previous permeability analyses. Adjustment of the above bulk permeability results to account for magnetometer gain uncertainties yields a lunar permeability of $\mu = 1.012 \pm 0.011$.

Fig. 4

Lunar Iron Abundance and Structure Inferred from Permeability Measurements

Iron abundance estimates for solar system objects are usually based on geochemical and geophysical properties calculated for bodies of planetary size (Urey, 1962; Reynolds and Summers, 1969; Urey and MacDonald, 1971) or on measured compositions of meteorites (Wänke et al., 1973). However, Parkin et al. (1973, 1974) and Dyal et al. (1975) used global lunar permeability,

determined from magnetic field measurements, to calculate lunar iron abundance for the moon. In these calculations the moon was modeled by a homogeneous paramagnetic rock matrix (olivine and orthopyroxene models were used), in which free metallic iron is uniformly distributed. Pyroxenes and olivines have been reported to be major mineral components of the lunar surface fines and rock samples (Nagata et al., 1971; Zussman, 1972; Weeks, 1972), with combined iron present as the paramagnetic Fe^{2+} ion. The ferromagnetic component of lunar samples is primarily metallic iron which is sometimes alloyed with small amounts of nickel and cobalt (Nagata et al., 1972; Pearce et al., 1971). This free iron is thought to be native to the moon (because of its low nickel content) rather than meteoritic in origin (Strangway et al., 1973b). Orthopyroxene and olivine models are consistent with geochemical studies (Urey et al., 1971; Wood et al., 1970; Ringwood and Essene, 1970; Green et al., 1971) and geophysical studies.

Since the susceptibility of free iron changes several orders of magnitude at the iron Curie temperature (T_c), a two layer model is used with the core-shell boundary R_c at the Curie isotherm (see Figure 3). For $R > R_c$, T is less than T_c , and for $R < R_c$, T is greater than T_c . Therefore, for $R > R_c$ any free iron is ferromagnetic while at greater depths where $T > T_c$, the free iron is paramagnetic. The Curie isotherm location is determined from the thermal profile used for a particular model. Several thermal profiles were used in the model to span the range of likely temperatures in the lunar interior. In the outer shell there are both ferromagnetic and paramagnetic contributions to the total magnetic permeability $\mu_1 = 1 + 4\pi K_1$. The susceptibility of the shell is $K_1 = K_{1c} + K_{1a}$, where K_{1a} is "apparent" ferromagnetic susceptibility and K_{1c} is paramagnetic susceptibility. The ferromagnetic component is metallic free iron, assumed to be multidomain, noninteracting grains; the paramagnetic component is Fe^{2+} in the orthopyroxene or olivine. The ferromagnetic susceptibility

of the shell material is an apparent value which differs from the intrinsic ferromagnetic susceptibility of the iron due to the self-demagnetization of the iron grains and the volume fraction of iron in the shell. For $R < R_c$ the lunar material is paramagnetic only, with susceptibility $K_2 = K_{2c} + K_{2a}$; K_{2c} is the contribution of paramagnetic chemically combined iron and K_{2a} is the apparent susceptibility of free paramagnetic iron above the Curie temperature. (For details of this model see Appendix B.)

From the magnetic properties of lunar compositional and thermal models, iron abundances for the moon are calculated consistent with measured global permeability. From the data shown in Figure 4 and model calculations discussed above, the free iron abundance best value is 2.5 ± 2.0 wt. %. However, the total iron abundance best value is 9.0 ± 4.7 wt. %. As discussed in the previous section, uncertainties in Explorer 35 and Apollo 12 magnetometer gains have required that the above lunar permeability estimate be revised to 1.012 ± 0.011 (see Daily and Dyal, 1979a). Although this new confidence interval does not include a permeability $\mu = 1.0$, it is clear that a nonmagnetic lunar sphere is not entirely ruled out by magnetometer data alone. However, other physical and chemical constraints requires a bulk lunar composition of paramagnetic materials such as orthopyroxene and olivine. For a moon of orthopyroxene composition ($0.25 \text{ FeSiO}_3 \cdot 0.75 \text{ MgSiO}_3$) the bulk permeability is 1.001 which is consistent with the new lower bound of lunar permeability. This lunar model has no free iron but is 13.9 wt. % combined iron. The revised upper bound on lunar permeability allows a lunar model of free iron/orthopyroxene composition with a free iron abundance of 5.8 wt. % and a total iron abundance of 11.3 wt. %.

Introduction

Electrical conductivity of the moon has been calculated from global eddy current response to changes in the magnetic field external to the moon. When the moon is subjected to a change in the external field, an eddy current field is induced in the moon which opposes the change (see Figure 5). The induced field responds with a time dependence which is a function of the electrical conductivity distribution in the lunar interior. Simultaneous measurements of the transient driving field by an Explorer 35 magnetometer and the lunar response field by an Apollo surface magnetometer allow calculation of the lunar conductivity. Since the electrical conductivity of geologic materials is a strong function of their temperature, a thermal profile can be calculated from the conductivity profile for a given compositional model of the lunar interior.

When the moon is in the solar wind, lunar eddy current fields form an induced lunar magnetosphere which is distorted in a complex manner due to flow of solar wind plasma past the moon. The eddy current field is compressed on the dayside of the moon and is swept downstream and confined to a cavity on the lunar nightside. Because of the complex boundary conditions necessary to model these processes, early analysis included a time dependent theory for transient response of a sphere in a vacuum to model lunar response as measured on the lunar nightside (Dyal et al., 1970; Dyal and Parkin, 1971a; Sill, 1972) and a frequency dependent harmonic theory of a sphere totally confined by the solar wind to model response as measured on the lunar dayside (Sonett et al., 1971a, 1972; Kuckes, 1971; Sill, 1972). Both the transient and the harmonic techniques have subsequently been further developed. Transient analyses have evolved to include effects of plasma cavity confinement on the lunar nightside data and time dependent analyses of magnetic step transients measured on the lunar dayside (Dyal et al., 1973). Harmonic analyses have

Fig. 5

been developed to model asymmetric confinement of the fields by the solar plasma (Schwartz and Schubert, 1973), correct for diamagnetic effects in the solar wind (Kuckes et al., 1974) and extend the analysis to lower frequencies (Wiskerchen and Sonett, 1977).

Time-dependent poloidal response of a sphere in a vacuum has been applied to data measured in the geomagnetic tail where plasma confinement effects are minimized. In this section lunar electrical conductivity from transient-response and harmonic analysis results are reviewed with emphasis on this time dependent geomagnetic tail technique. We begin with a review of the theory used and then present the data analysis and results most recently reported by Dyal et al. (1976). Harmonic analyses of magnetic fields measured on the lunar dayside, with the moon in the solar wind, are then reviewed. Discovery of local anomalies in lunar conductivity, apparently associated with circular maria, is also discussed.

Explorer and Apollo Magnetometer Measurements of Lunar Global and Regional Conductivity

Lunar electrical conductivity is calculated using measurements of global fields induced by changes in the extra lunar field. Data for the analysis is selected from measurements obtained in the lobes of the geomagnetic tail, during times when there is no indication of plasma effects. To help avoid data measured when the lunar magnetic response is influenced by plasma, individual data sets are selected using criteria: (1) the magnitude of the field external to the moon (measured by the Explorer 35 magnetometer) is greater than 8 gammas; (2) the external field is directed approximately along the sun-earth line; (3) main qualitative features of each event appear in both surface and orbital data in all three vector coordinate axes to minimize use of data with large field gradients between the two magnetometers; and (4) no plasma data are measured above the solar-wind spectrometer instrument threshold. These criteria help discriminate data for those times when the lunar

response can be modeled by that of a conducting sphere in a vacuum. Details of the vacuum theory are discussed in Appendix C.

On 20 April 1970 an exceptionally large magnetic transient event was recorded in the lunar environment. The moon was located at high latitude in the north lobe of the geomagnetic tail. Lunar magnetic field and plasma detector measurements indicated the event met all data selection criteria listed above. Simultaneous magnetic observations on earth indicated a geomagnetic storm sudden commencement (peak K_p of 8+) eleven minutes prior to its detection at the moon. The earth orbiting Vela satellite measured a solar wind velocity up to 400 km/sec during the passage of this large event, which accounts for the 11 minute lag between the commencement of the event at the earth and moon. This event is most probably the result of perturbations on the geomagnetic tail boundary by the transport of the solar disturbance through the magnetosheath. This is the largest selenomagnetic storm event recorded under nearly ideal conditions observed in over six years of lunar magnetic field measurements.

Analysis of this large selenomagnetic storm event has involved the input Explorer 35 data, convolved with an assumed conductivity profile and compared to the calculated response measured by the Apollo 12 magnetometer. The radial component of measured external and response fields, along with a calculated response field which best fit the measured response, are shown in Figure 6. The lunar electrical conductivity profile used to calculate this best fit response is shown in Figure 7. This profile assumes that the conductivity increases monotonically with depth and that it is a continuous function from the surface to the center of the moon. The best-fit profile rises rapidly from $< 10^{-9}$ mhos/m at the surface to $\sim 10^3$ mhos/m at a depth of 200 to 300 km. Thereafter the conductivity rises more gradually to $\sim 3 \times 10^{-2}$ mhos/m at 900 km depth.

Fig. 6

Fig. 7

Uncertainties in the lunar conductivity profile determination arise from several causes: (1) the nonuniqueness of profile determination as discussed by Backus and Gilbert (1970), Parker (1970), Phillips (1972), and Hobbs (1973); (2) the penetration depth allowed by the length and amplitude of the data time series; (3) the frequency response limitations of the Explorer 35 and Apollo magnetometers (4) inhomogeneities in the external field over the dimensions of the moon; and (5) instrumental errors in the measured fields. Those profiles which gave calculated response fields which were acceptable fits to the measured response, lie within the shaded region of Figure 7. Criteria for these fits were chosen after empirical examination of the complex error propagation in profile determination due to instrumental errors, data reduction and analysis errors, and assumptions and approximations in lunar modeling (Dyal et al., 1976).

The effects of instrumental gain errors in conductivity analyses have been studied in detail by Daily and Dyal (1979a). The limit in accuracy that can be expected from analyses using Explorer 35 and Apollo 12 magnetometer data are well represented by this shaded region in Figure 7. Therefore this envelope is representative of the practical limit of accuracy in the analysis since other error sources would tend only to widen it.

Constraints on the conductivity profiles in Figure 7 can be placed by investigation of the toroidal induction in the moon. This mode has been described theoretically by several investigators (Sonett and Colburn, 1967; Schwartz and Schubert, 1969; Schubert and Schwartz, 1969; Sill and Blank, 1970). For the case when the moon is immersed in the solar wind plasma, the external field \underline{B}_E is constant (eddy current induction vanishes), and the motional solar wind electric field induction drives currents in the moon resulting in a toroidal field \underline{B}_T , the total field \underline{B}_A at the surface is $\underline{B}_A = \underline{B}_E + \underline{B}_T$. Following Schubert and Schwartz (1969), the toroidal field,

B_T , is $B_{Tx} = B_{Ax} - B_{Ex}$, $B_{Ty} = B_{Ay} - B_{Ey} = AE_z = A(V_x B_{Ey} - V_y B_{Ex})$, $B_{Tz} = B_{Az} - B_{Ez} = -AE_y = A(V_x B_{Ex} - V_z B_{Ex})$, where, for a two-layer (core-crust) model of the moon

$$A = \sigma_1 \mu R_m \left(\frac{\frac{1}{2} + \beta + \alpha(1 - \beta)}{1 - \beta + \alpha(2 + \beta)} \right),$$

$$\alpha = \sigma_1 / \sigma_2,$$

$$\beta = (R_2 / R_m)^3.$$

The components x, y, z are up, east, north ALSEP coordinates at the Apollo 12 site; V is velocity of the moon relative to the solar wind; σ_1 and σ_2 are conductivity of crust and core, respectively; μ is the global permeability; R_2 and R_m are core and lunar radii. For the case where $\sigma_2 \gg \sigma_1$, we have

$$A = \sigma_1 \mu R_m \left(\frac{\frac{1}{2} + \beta}{1 - \beta} \right).$$

The components of the toroidal field are calculated by subtracting the components of the external field \underline{B}_E , measured by an Explorer 35 magnetometer, from the total field \underline{B}_A measured at the lunar surface by the Apollo 12 lunar surface magnetometer. The parameter A was studied by Dyal et al. (1977) by plotting components of toroidal field \underline{B}_T versus the $\underline{V} \times \underline{B}_E$ electric field.

The measured value of $A = (-6.2 \pm 4.3) \times 10^{-2}$ sec/m where the limits include only random statistical errors. Systematic Apollo 12 and Explorer 35 magnetometer errors were included in an error analysis to yield an upper limit of $A = 2 \times 10^{-7}$ sec/m. Using this value of slope A, Dyal et al. determined the upper limit on average crustal conductivity as a function of crust thickness. For an average crust thickness of 80 km (Goins et al., 1977) the conductivity

fluctuations at the Apollo 15 site were strongly linearly polarized in a direction tangent to the lunar surface and radial to the circular Imbrium basin. Simultaneous measurements, by the Explorer 35 showed that the external field was not polarized. The Apollo 15 magnetic field oscillations were Fourier analyzed and polar plots made of the power in the horizontal magnetic field as a function of direction at the site. The power at the surface and at Explorer 35 have qualitatively similar directional behavior below about 5×10^{-8} Hz. At these frequencies the Apollo 15 magnetic fields appear to reflect the global lunar response to electromagnetic induction. At 7.45 mhz and at higher frequencies, a dramatic change occurs in the directional properties of the Apollo power relative to the Explorer 35 power which maximizes about 20° to 40° east of north. However, the surface field power shifts to a maximum 20° to 30° north of west. The directional power of magnetic field fluctuations at the Apollo 15 site, at frequencies above about 5 mhz, is invariably a maximum approximately northwest-southeast, independent of the directional character of the interplanetary field power.

Schubert et al. (1974) and Vanyan et al. (1979) have developed models for electromagnetic induction in regions of anomalous electrical conductivity on the moon. A circular region of uniform thickness and anomalously low conductivity will concentrate the magnetic fluctuations at higher frequencies causing fluctuations at the anomaly edge to be linearly polarized, with the polarization direction radial to the anomaly center. For this reason Schubert et al. (1974) and Sonett et al. (1974) have concluded that the Apollo 15 and Explorer 35 magnetometer data indicate that regions of anomalous electrical conductivity in the lunar crust and upper mantle are associated with Mare Imbrium and perhaps with Serenitatis. Subsequent analysis of Lunokhod 2 and Apollo 16 surface magnetometer data by Vanyan et al. (1979) and Dyal and Daily (1979) have demonstrated that magnetic field fluctuations at the edge of Mare Serenitatis

upper limit is 9×10^{-9} mhos/m. We note that the average crust conductivity is not a strong function of crust thickness for thicknesses of the order of 80 km. (A 100 km crust would correspond to a 1.2×10^{-8} mhos/m upper limit, and a 60 km crust would correspond to about 7×10^{-9} mhos/m.) This crustal conductivity upper limit places an important constraint on the lunar conductivity profiles of Figure 7. The toroidal induction results lower the crust conductivity upper limit by approximately four orders of magnitude.

The electrical conductivity of the moon has also been studied by analysis of magnetometer data in the frequency domain. This harmonic analysis has generally been applied to data measured on the lunar dayside with the moon in the solar wind plasma. The theoretical modeling is based on the assumption that any global induced field is excluded from the oncoming solar wind by currents induced in the highly conducting solar plasma; it is assumed that in effect the solar wind completely confines the induced field in the lunar interior and in a thin region above the lunar surface. In early modeling the confinement current was considered to be a surface current providing a boundary condition of total confinement by currents around the whole moon, permitting solution of Maxwell's equations at the lunar surface. Basic theoretical development for the case where induction fields are totally confined to the moon are given by Backus and Gilbert (1967), Parker (1970), Schubert and Schwartz (1969), Sill and Blank (1970), and Kuckes (1971). More recent modeling of the poloidal induction for the moon in the solar wind has accounted for the asymmetric confinement of the induction fields by the solar plasma (Schwartz and Schubert, 1973; Horning and Schubert, 1975). However, none of these theoretical models considers the interaction of remanent magnetic fields at the surface magnetometer site with the solar wind plasma. This interaction has been shown to yield a magnetic signal of the same order of magnitude as the induced eddy current fields (Dyal et al., 1978).

Once the poloidal fields have been derived, the frequency-dependent transfer function is calculated from the data:

$$A_i(f) = \frac{b_{Ei}(f) + b_{Pi}(f)}{b_{Ei}(f)}$$

$i = x, y, z$, where the A_i are transfer functions of components of frequency-dependent magnetic fields, expressed in the orthogonal coordinate system with origin on the surface of the moon (r is the radial and θ and ϕ are tangent to the surface); $b_{Ei}(f)$ is the Fourier transform of the external driving magnetic field; and $b_{Pi}(f)$ is the Fourier transform of the induced global poloidal field.

The harmonic data analysis involves Fourier-analyzing simultaneous data from the Apollo 12 lunar surface magnetometer, taken during lunar daytime, and the orbiting Explorer 35 magnetometer. Then ratios of the surface data to orbital data are used to calculate a lunar transfer function. The form of the transfer function is determined by the internal conductivity distribution in the moon; therefore, a "best fit" conductivity profile can be obtained by numerically fitting the measured and theoretical transfer functions. The "best fit" conductivity profile of Sonett et al. (1972) obtained in this manner is characterized by a large "spike" of maximum conductivity about 1500 km from the lunar center. Other conductivity profiles have been calculated using the Sonett et al. (1972) transfer function, showing that the spike profile is not unique but that the frontside transfer function can be fitted by simpler two- and three-layer models (Kuckes, 1971; Sill, 1972; Sonett et al., 1972; Reisz et al., 1972; Phillips, 1972).

Local anomalies in the shallow electrical conductivity of the moon have been discovered by analysis of surface and orbital magnetic data. Schubert et al. (1974) reported that above approximately 5×10^{-3} Hz, magnetic field

are also highly linearly polarized in the direction aligned with the mare center. This anisotropy is also interpreted as the effect of a regional anomaly in the subsurface conductivity, therefore Vanyan et al. (1979) propose an anomaly associated with Mare Serenitatis similar to that proposed for Imbrium. Vanyan et al. (1979) and Dyal and Daily (1979) have suggested a mechanism to explain a regional effect on electrical conductivity associated with circular maria. According to this hypothesis the magma which filled the front side basins moved large quantities of heat from within the moon to the surface where the heat was radiatively dissipated. The subhighland mantle was cooled by the slower process of conduction through the crust. Therefore, the submaria crust and mantle would be cooler than the adjacent highlands. The magma extruded into the maria was also enriched in heat source radioactive potassium, uranium, and thorium. The magma source regions beneath the maria would then be depleted of these heat sources relative to surrounding highland mantle. This depletion of both thermal energy and radioactive heat sources, could result in cooler submaria mantle in comparison to the subhighland mantle. The cooler material would have a lower electrical conductivity. This hypothesis implies that a conductivity anomaly should be associated with all circular lunar maria and that the magnitude of each anomaly should be directly related to the volume of magma in the basin.

Lunar Thermal Profile and Structure Inferred from Conductivity Measurements

From the electrical conductivity profile of the moon an internal temperature distribution can be inferred for an assumed lunar material composition (see Rikitake, 1966). The electrical conductivity of many geologic materials has been shown to be an exponential function of temperature:

$$\sigma = \sum_i E_i \exp(-a_i/kT)$$

where a_i are the activation energies of impurity, intrinsic, and ionic modes, expressed in electron volts; E_i are material-dependent constants; and k is Boltzmann's constant (see Duba et al., 1972). It should be emphasized that the electrical conductivity $\sigma(a, E, T)$ is a strong function of the material composition; therefore uncertainties in knowledge of the exact composition of the sphere limits the accuracy of the temperature profile calculated from the electrical conductivity profile.

Laboratory measurements relating conductivity to temperature for various minerals which are good geochemical candidates for the lunar interior, have been presented by many investigators (e.g., England et al., 1968; Schwerer et al., 1972; Olhoeft et al., 1973; Duba et al., 1972; Duba and Ringwood, 1973). The work by Duba et al. (1972) on the electrical conductivity of olivine have been used to convert the conductivity profile of Dyal et al. (1974) to a temperature profile, shown as number 5 on Figure 8. Also included in this figure are a selection of temperature profiles calculated by other investigators from lunar thermal history models.

In addition to the lunar thermal profile, the electrical conductivity measurements have been used to investigate the deep lunar interior to detect the presence of a small core. The time dependent analysis of Dyal et al. (1976) on a 6 hour data set from Apollo and Explorer instruments indicates that a lunar core of conductivity ≥ 10 mhos/m must be smaller than about 530 km in radius. However, there is no indication in this analysis that any highly conducting core need exist in the moon. This same conclusion is reached by Wiskerchen and Sonett (1977) from a frequency dependent study of 390 hours of simultaneous Explorer 35 and Apollo 12 data.

Acknowledgments: Support of W.D.D. under NASA Grant NSG-2082 is gratefully acknowledged.

Appendix A: Theory for Interaction of Remanant Magnetic Fields and Solar Wind Plasma

To model field diffusion into the plasma we consider the magnetic field of a magnetized layer, the top of which is at a depth d below the lunar surface. Magnetization M in the layer is $2a \cos mz$ where $m = 2\pi/L$ and L is the scale size characteristic of the magnetization. We use the Apollo coordinate system which has its origin on the lunar surface at the landing site. The x axis is directed radially outward from the surface; the y and z axes are tangential to the surface, directed eastward and northward respectively. The magnetic field in the nonconducting lunar half space $x < 0$ satisfies Maxwell's equation $\nabla \times \underline{B} = (4\pi/c)\underline{j} = 0$ which becomes Laplace's equation $\nabla^2 \underline{B} = 0$ with the solution

$$B_x = (ae^{-m(d+x)} + be^{mx})\cos mz$$

where c is the velocity of light and \underline{j} is the current. In the plasma the field is given by $\nabla \times \underline{E} = -(1/c)\partial \underline{B}/\partial t$ and Ohm's law $\underline{j} = \sigma \underline{E}$ which together yield the diffusion equation

$$\frac{\partial \underline{B}}{\partial t} = \frac{c^2}{4\pi\sigma} \nabla^2 \underline{B}$$

where \underline{E} is the electric field. The electrical conductivity of a collisionless plasma is $\sigma = ine^2/(\bar{m}\omega)$ where the electron density, charge, and mass are n , e , and \bar{m} respectively and ω is the frequency (see Jackson, 1962). Diffusion of the field into the plasma is by a transverse electromagnetic wave propagating along the x axis $\underline{B} = \underline{B}_0 e^{-\beta x} e^{i\alpha x - i\omega t}$, where the propagation constant is $k = \alpha + i\beta$. For these conditions

$$\nabla^2 \underline{B} = \delta^2 \underline{B}$$

with $\delta^2 = \omega_p^2/c^2$ ($\omega_p^2 = 4\pi ne^2/\bar{m}$, the plasma frequency). For $\omega < \omega_p$, k becomes purely imaginary, and the wave does not propagate in the plasma but decays with a length of δ^{-1} . In the limit as $\omega \rightarrow 0$, $B_{x,z} = ce^{-qx}\cos mz$ where $q^2 = m^2 + \delta^2$. From the magnetic boundary conditions at the lunar surface it can be shown that

the distorted and undistorted lunar field \underline{B} and \underline{B}_R respectively are related by

$$B_z - B_{Rz} = \frac{q-m}{q+m} B_{Rz} = f(n,L) B_{Rz}$$

for the radial component and

$$B_z - B_{Rz} = \frac{q-m}{q+m} B_{Rz} \equiv f(n,L) B_{Rz}$$

for the tangential component. Note that for the more general case with two field components tangent to the surface the above equation is valid, the total tangential fields replacing the z components. The theory is linear so that the sum of two solutions is also a solution. Superposition of solutions can be used to model the interaction data with magnetization characterized by two different scale sizes.

The undistorted remanent field \underline{B}_R at each Apollo site is measured when the moon is in the geomagnetic tail and thereby shielded from the solar plasma. The distorted field is calculated from the difference in the field measured at the surface by an Apollo surface magnetometer and the field measured in lunar orbit by the Explorer 35 magnetometer or the Apollo subsatellite magnetometer. This difference is $\underline{B} = \underline{B}_A - \underline{B}_E = \underline{B}_P + \underline{B}_R + \underline{B}_D$ is the field measured at the surface and \underline{B}_E is the field external to the moon measured by a lunar orbiting magnetometer. The undistorted remanent field is \underline{B}_R and the interaction field from currents in the plasma is \underline{B}_D . Fluctuations in the external field \underline{B}_E induce eddy currents in the moon. The poloidal field associated with these currents opposes the change in the external field. This poloidal induction mode dominates magnetization, toroidal, and diamagnetic modes when the moon is in the solar wind. However, in the limit of low-frequency driving field fluctuations, the poloidal induction vanishes. Therefore in the analysis one hour averaged data are used in which the residual poloidal fields are $\sim 10\%$ of the external field.

Furthermore, since the induced fields \underline{B}_p have dipolar symmetry about the direction of the external field change, and not about the remanent field, poloidal contributions will tend to reduce the correlation in the data without biasing the analysis.

Appendix B: Theory for Lunar Permeability and Iron Abundance Analysis

Consider a radially symmetric two-layer permeable sphere in an initially uniform magnetic field \underline{H}_0 . In the absence of current $\underline{H} = -\nabla\Phi$ and since $\underline{B} = \mu\underline{H}$, at any point $\nabla \cdot \underline{H} = 0$. Therefore Φ satisfies Laplace's equation consistent with the continuity of the normal components of \underline{B} and tangential components of \underline{H} at the spherical boundaries. The potential must be

$$\Phi = \begin{cases} -H_0 r \cos \theta + \sum_{n=1}^{\infty} \frac{\alpha_n}{r^{n+1}} P_n(\cos \theta) & r > R_1 \\ \sum_{n=1}^{\infty} \left(\beta_n r^n + \gamma_n \frac{1}{r^{n+1}} \right) P_n(\cos \theta) & R_2 < r < R_1 \\ \sum_{n=1}^{\infty} \delta_n r^n P_n(\cos \theta) & r < R_2 \end{cases}$$

with R_1 and μ_1 the outer radius and permeability, and R_2 and μ_2 the inner radius and permeability. Using Jackson's (1962) notation conventions we match the boundary conditions

$$\begin{aligned} \frac{\partial \Phi}{\partial \theta}(R_1) &= \frac{\partial \Phi}{\partial \theta}(R_1) & \frac{\partial \Phi}{\partial \theta}(R_1) &= \frac{\partial \Phi}{\partial \theta}(R_1) \\ \frac{\partial \Phi}{\partial r}(R_1) &= \mu_1 \frac{\partial \Phi}{\partial r}(R_1) & \mu_1 \frac{\partial \Phi}{\partial r}(R_1) &= \mu_1 \frac{\partial \Phi}{\partial r}(R_1) \end{aligned}$$

All but the $i = 1$ coefficients vanish leaving the four simultaneous equations

$$\begin{aligned} \alpha - R_1 \beta - \gamma &= R_1 H_0 \\ 2\alpha + \mu_1 R_1 \beta - 2\mu_1 \gamma &= -R_1 H_0 \\ R_2 \beta + \gamma - R_2 \delta &= 0 \\ \mu_1 R_2 \beta - 2\mu_1 \gamma - \mu_2 R_2 \delta &= 0 \end{aligned}$$

We are interested in α , the induced dipole moment, which is given by

$$F = \frac{\alpha}{H_0 R_1} = \frac{(2\eta + 1)(\mu_1 - 1) - \lambda^2(\eta - 1)(2\mu_1 + 1)}{(2\eta + 1)(\mu_1 + 2) - 2\lambda^2(\eta - 1)(\mu_1 - 1)}$$

REPRODUCIBILITY OF THE
ORIGINAL PAGE IS POOR

where $\eta = \mu_1/\mu_2$ and $\lambda = R_2/R_1$. The resulting dipolar field in an (r, θ, ϕ) spherical coordinate system is

$$\mathbf{B}_d = \frac{\mu_0}{R_1^3} (2 \cos \theta \hat{r} + \sin \theta \hat{\theta})$$

We rotate the coordinate system about the r (or ALSEP x) axis so that θ and ϕ correspond to the ALSEP y and z axes; then

$$\mathbf{B}_d = F(2H_x \hat{x} - H_y \hat{y} - H_z \hat{z})$$

The total field at the surface is the sum of the uniform external field \mathbf{H} and the dipole field \mathbf{B}_d :

$$\mathbf{B} = H_x(1+2F)\hat{x} + H_y(1-F)\hat{y} + H_z(1-F)\hat{z}$$

Limits imposed on F in this expression from the analysis of Explorer and Apollo magnetic data can be used to calculate the lunar iron abundance using suitable lunar compositional and thermal models. Two of the models are described, including magnetic and other geophysical constraints. In both cases the lunar interior is modeled by a sphere of homogeneous composition. Free iron of multidomain noninteracting grains is assumed to be uniformly distributed throughout a paramagnetic mineral. The paramagnetic component in one case is olivine $[y\text{Fe}_2\text{SiO}_4 \cdot (1-y)\text{Mg}_2\text{SiO}_4]$ and in the other case is orthopyroxene $[y\text{FeSiO}_3 \cdot (1-y)\text{MgSiO}_3]$. The free iron is ferromagnetic in the regions where the temperature T is less than the iron Curie temperature T_c , and it is paramagnetic where $T > T_c$. Therefore, each model is a two layer permeable sphere. We consider the magnetic contributions from both free and combined iron in both the shell and core of the model with $\mu_{1,2} = 1 + 4\pi K_{1,2}$ where

$$\begin{aligned} K_1 &= K_p(y, T_1) + K_f(q) \\ K_2 &= K_p(y, T_2) + K_f(q) \end{aligned}$$

and K_p is the paramagnetic susceptibility of the olivine or orthopyroxene, y is the mole fraction of ferrosilicate in the mineral, T_1 is the uniform temperature

of the shell, T_2 is the temperature of the core, K_f is the apparent ferromagnetic susceptibility of free iron in emu/cm^3 , K'_f is the apparent paramagnetic susceptibility of free iron ($T > T_c$), and q is the mass fraction of free iron in the moon.

The measured susceptibility of the free iron K_f is an apparent value which differs from the intrinsic susceptibility of iron K because of self-demagnetization of the iron grains and the fraction of iron in the moon. The apparent and intrinsic susceptibility of the free iron are related (see Nagata, 1961) by

$$K_f = \frac{q\rho}{\rho_f} \frac{K}{1 + NK}$$

where ρ is the lunar density (assumed uniform throughout the moon), and ρ_f is the density of iron. An analogous expression relates K'_f , the apparent paramagnetic susceptibility and K' , intrinsic paramagnetic susceptibility of free iron ($T > T_c$).

Nagata et al. (1957) found the susceptibility of olivine to be 2.4×10^{-2} emu/mole at room temperature. Using this expression, the Curie law temperature dependence, and the following empirical equation for olivine density (Dana, 1966)

$$\rho_r(y) = 0.94y + 3.26 \text{ g/cm}^3,$$

we obtain for olivine

$$K_r = 0.14 \frac{y}{T} \frac{46y + 158}{63y + 141} \text{ emu/cm}^3.$$

Similarly Akimoto et al. (1958) give the susceptibility for pyroxenes:

1.1×10^{-2} emu/mole. From Deer et al. (1962) we obtain the following empirical expression for pyroxene density:

$$\rho_r(y) = 0.71y + 3.15 \text{ g/cm}^3.$$

Again, combining the expressions from Akimoto et al. and Deer et al. with the Curie law temperature dependence, we obtain for pyroxene

$$K_r = 0.095 \frac{y}{T} \frac{24y + 108}{32y + 100} \text{ emu/cm}^3.$$

The lunar moment of inertia is approximately that of a sphere of uniform density (Ringwood and Essene, 1970). Choosing a uniform density for our lunar model we can write

$$\frac{I}{M^2} = \frac{q}{\rho} + \frac{1-q}{\rho_0(y)}$$

The free iron abundance q can be determined as a function of μ for the olivine or orthopyroxene/ free iron model by simultaneously solving the above equations and the solutions are presented graphically by Dyal et al. (1975). The fractional lunar mass due to both chemically combined and uncombined iron is constrained by q and the lunar density. For the orthopyroxene/free iron model

$$Q = q + \frac{56y}{32y + 100} (1 - q)$$

and for the olivine/free iron model

$$Q = q + \frac{112y}{64y + 140} (1 - q).$$

Model parameters used in the calculations are:

uniform density of moon

$$\rho = 3.34 \text{ g/cm}^3$$

density of free iron

$$\rho_F = 7.85 \text{ g/cm}^3$$

demagnetization factor of iron grains

$$N = 3.5 \text{ (Nagata, 1961)}$$

initial intrinsic ferromagnetic susceptibility of iron

$$K = 12 \text{ emu/cm}^3 \text{ (Bozorth, 1951)}$$

intrinsic paramagnetic susceptibility of iron

$$K' = 2.2 \times 10^{-4} \text{ emu/cm}^3$$

(Tebble and Craik, 1969)

thermal models

$$T_1 = 900^\circ\text{K}, T_2 = 1700^\circ\text{K},$$

$$\lambda = 0.98, 0.96, 0.94, 0.92$$

$$T_1 = 800^\circ\text{K}, T_2 = 1600^\circ\text{K},$$

$$\lambda = 0.88, 0.84$$

$$T_1 = 700^\circ\text{K}, T_2 = 1400^\circ\text{K},$$

$$\lambda = 0.80$$

$$T_1 = 600^\circ\text{K}, T_2 = 1000^\circ\text{K}$$

$$\lambda = 0.70$$

REPRODUCIBILITY OF THE
ORIGINAL PAGE IS POOR

Appendix C: Theory For Lunar Electrical Conductivity

Analysis

We assume that plasma effects are negligible in the lobe regions of the geomagnetic tail, and that the response of the moon can be represented as that of a radially symmetric conducting sphere in a vacuum. To describe the response of the sphere to an arbitrary input field we define the magnetic vector potential \underline{A} such that $\nabla \times \underline{A} = \underline{B}$ and $\nabla \cdot \underline{A} = 0$. We seek the response to an input $\Delta \underline{B}_E b(t)$, where $b(t)=0$ for $t < 0$ and $b(t)$ approaches unity as $t \rightarrow \infty$. The direction of $\Delta \underline{B}_E$ is taken to be the axis of a spherical coordinate system (r, θ, ϕ) . If the conductivity is spherically symmetric, the transient magnetic field response has no ϕ component, and hence $\underline{A} = A \hat{e}_\phi$ and $\partial/\partial\phi = 0$. Under these conditions (and neglecting displacement currents) the laws of Faraday, Ampere, and Ohm combine to yield a diffusion equation (Dyal et al., 1972) for the magnetic potential (in MKS units):

$$\nabla^2 A(r, \theta; t) = \mu \sigma(r) \frac{\partial A}{\partial t}(r, \theta; t)$$

From the work of Parkin et al. (1974) we know that $\mu \approx \mu_0$. Then, for $t > 0$, the magnetic field must be continuous at the surface, so that \underline{A} and $\partial \underline{A}/\partial r$ are always continuous at $r = R_m$, the radius of the sphere. We also have the boundary condition $\underline{A}(0, t) = 0$ and the initial condition $\underline{A}(r, \theta, \phi) = 0$ inside the moon. Outside the moon, where $\sigma = 0$,

$$A = \Delta B_E \left(\frac{r}{2} \right) b(t) \sin \theta + \frac{\Delta B_E}{r^2} f(t) \sin \theta$$

The first term on the right is a uniform magnetic field modulated by $b(t)$; the second term in the (as yet unknown) external transient response, which must vanish as r and $t \rightarrow \infty$. Note that at $r = R_m$, where R_m is normalized to unity,

and
$$A = \Delta B_E \sin \theta \left(\frac{b(t)}{2} + f(t) \right)$$

$$\frac{\partial A}{\partial r} = \Delta B_E \sin \theta \left(\frac{b(t)}{2} - 2f(t) \right)$$

Therefore, at $r = R_m = 1$,

$$\frac{\partial A}{\partial r} = -2A + \frac{3}{2}(\Delta B_E \sin \theta b(t))$$

Since the magnetic field is continuous at $r = R_m$, this is a boundary condition for the interior problem. Letting $G(r,t) = A/\Delta B_E \sin \theta$ and $\bar{G}(r,s)$ be the Laplace transform of G , the first equation becomes

$$\frac{1}{r} \left(\frac{\partial^2}{\partial r^2} (r\bar{G}) - \frac{2}{r} \bar{G} \right) = s\mu_0\sigma(r)\bar{G}$$

for the interior. The boundary conditions are

$$\frac{\partial \bar{G}}{\partial r} = -2\bar{G} + \frac{3}{2}\bar{b}(s)$$

at $r = R_m$ and

$$\bar{G} = 0$$

at $r = 0$.

The governing equations are linear so the response of a given input function can be obtained by superposition of solutions of convenient input functions. In practice succession ramp functions $b_i(t)$ are chosen such that their sum approximates the external field measured by Explorer 35. For each $b_i(t)$ and given conductivity $\sigma(r)$ the above equations are numerically integrated to obtain $\bar{G}_i(r,s)$ for $0 \leq r \leq R_m$. Then $\bar{G}_i(r,s)$ is numerically inverse Laplace transformed to find the transient response $f_i(t)$ to $b_i(t)$. The $f_i(t)$ are then superimposed to yield the response $F(t)$ to the input function measured by Explorer 35. This time series response is compared to actual lunar response measured by the Apollo magnetometer and the conductivity profile is iteratively adjusted until the difference between calculated and measured response is minimized.

REFERENCES

- Akimoto, S., K. Horai, and T. Boku, Magnetic susceptibility of orthopyroxene, J. Geomag. Geoelect., 10, 7-11, 1958.
- Alfvén, H. and L. Lindberg, Magnetization of celestial bodies with special application to the primeval earth and moon, The Moon, 10, 323-335, 1974.
- Anderson, K. A., R. P. Lin, R. E. McGuire, J. E. McCoy, C. T. Russell, and P. T. Coleman, Jr., Linear magnetization feature associated with Rima Sirsalis, Earth Planet. Sci. Lett., 34, 141-151, 1977.
- Backus, G. E. and J. F. Gilbert, Numerical applications of a formalism for geophysical inverse problems, Geophys. J. Roy. Astron. Soc., 13, 247-276, 1967.
- Backus, G. E. and J. F. Gilbert, Uniqueness in the inversion of inaccurate gross earth data, Phil. Trans. Roy. Soc. A266, 123-192, 1970.
- Barnes, A., P. Cassen, J. D. Mihalov, and A. Eviator, Permanent lunar surface magnetism and its deflection of the solar wind, Science, 171, 716-718, 1971.
- Behannon, K. W., Intrinsic magnetic properties of the lunar body, J. Geophys. Res., 73, 7257-7268, 1968.
- Bozorth, R. M., Ferromagnetism, D. Van Nostrand, 1951.
- Cisowski, S., M. Fuller, M. E. Rose, and P. J. Wasilewski, Magnetic effects of experimental shocking of lunar soil, in Proc. Lunar Sci. Conf. 3rd, Geochim. Cosmochim. Acta, 3, edited by E. A. King, Jr., 3003-3017, 1973.
- Cisowski, S. M., M. Fuller, Ming Wu Yee, M. F. Rose, and P. J. Wasilewski, Magnetic effects of shock and their implications for magnetism of lunar samples, in Proc. Lunar Sci. Conf. 6th. Geochim. Cosmochim. Acta, 3, edited by R. B. Merrill, 3123-3141, 1975.
- Cisowski, S. M., J. R. Dunn, M. Fuller, Ming Wu Yee, M. F. Rose, and P. J. Wasilewski, Magnetic effects of shock and their implication for lunar magnetism (II), in Proc. Lunar Si. Conf. 7th, Geochim. Cosmochin. Acta, 3, edited by R. B. Merrill, 3299-3320, 1976.
- Cisowski, S. M., C. Hale, and M. Fuller, On the intensity of ancient lunar fields, in Proc. Lunar Sci. Conf. 8th. Geochim. Cosmochim. Acta, 1, edited by R. B. Merrill, 725-750, 1977.
- Colburn, D. S., R. G. Currie, J. D. Mihalov, and C. P. Sonett, Diamagnetic solar-wind cavity discovered behind the moon, Science, 158, 1040-1042, 1967.
- Coleman, P. J., Jr., G. Schubert, C. T. Russell, and L. R. Sharp, The particles and fields subsatellite magnetometer experiment, in NASA Apollo 15 Prelim. Sci. Rep., SP-289, 22-1 to 22-9, 1972a.
- Coleman, P. J., Jr., B. R. Lichtenstein, C. T. Russell, G. Schubert, and L. R. Sharp, Magnetic fields near the moon, in Proc. Lunar Sci. Conf. 3rd, 2271-2286, 1972b.

- Daily, W. D. and P. Dyal, Magnetometer data errors and lunar induction studies, J. Geophys. Res., in press, 1979a.
- Daily, W. D. and P. Dyal, Theories for the origin of lunar magnetism, Phys. Earth Planet. Int., in press, 1979b.
- Dana, E. S., Textbook of mineralogy, 4th Edition by W.E. Ford, John Wiley & Sons, 1966.
- Deer, W. A., R. A. Howie, and J. Zussman, Rock-forming minerals, John Wiley Co., 1962.
- Dolginov, Sh. Sh., E. G. Eroshenko, L. N. Zhuzgov, and N. V. Pushkov, Measurements of the magnetic field in the vicinity of the moon by the artificial satellite Luna 10, Akad. Nauk USSR, Doklady, 1966.
- Dolginov, Sh. Sh., E. G. Eroshenko, V. A. Sharova, T. A. Vnuchkova, L. L. Vanyan, B. A. Okul'sky, and A. T. Bazilevsky, Study of magnetic field, rock magnetization and lunar electrical conductivity in the Bay Lemonnier, The Moon, 15, 3-14, 1976.
- Dolginov, Sh. Sh., E. G. Eroshenko, L. N. Zhuzgov, V. A. Sharova, G. A. Vnuchkov, B. A. Okul'sky, and A. T. Bazilevsky, Magnetic field in Lemonnier Bay according to data of Lunokhod 2, NASA SP-370, 433-441, 1977.
- Duba, A., and E. A. Ringwood, Electrical conductivity, internal temperatures and thermal evolution of the moon, The Moon, 7, 356-376, 1973.
- Duba, A., E. C. Heard, and R. N. Schock, The lunar temperature profile, Earth Planet. Sci. Lett., 15, 301-304, 1972.
- Dyal, P., and C. W. Parkin, Electrical conductivity and temperature of the lunar interior from magnetic transient-response measurements, J. Geophys. Res., 76, 5947-5969, 1971a.
- Dyal, P., and C. W. Parkin, The Apollo 12 magnetometer experiment: internal lunar properties from transient and steady magnetic field measurements, in Proc. Lunar Sci. Conf. 2nd, 2391-2413, 1971b.
- Dyal, P., and D. I. Gordon, Lunar surface magnetometers, IEEE Transactions on Magnetism, MAG-9, No. 3, 226-231, 1973.
- Dyal, P., and W. D. Daily, Electrical conductivity anomalies associated with circular lunar maria, in Proc. Lunar Sci. Conf. 10th, submitted, 1979.
- Dyal, P., C. W. Parkin, and C. P. Sonett, Apollo 12 magnetometer: measurement of a steady magnetic field on the surface of the moon, Science, 169, 762-764, 1970a.
- Dyal, P., C. W. Parkin, C. P. Sonett, and D. S. Colburn, Electrical conductivity and temperature of the lunar interior from magnetic transient-response measurements, NASA TMX-62,012, 1970b.

- Dyal, P., C. W. Parkin, and P. Cassen, Surface magnetometer experiments: internal lunar properties and lunar field interactions with the solar plasma, in Proc. Lunar Sci. Conf. 3rd, 2287-2307, 1972.
- Dyal, P., C. W. Parkin, and W. D. Daily, Surface magnetometer experiments: internal lunar properties, in Proc. Lunar Sci. Conf. 4th, 2229-2945, 1973.
- Dyal, P., C. W. Parkin, and W. D. Daily, Lunar electrical conductivity, permeability, and temperature from Apollo magnetometer experiments, Conference of Cosmochemistry of the Moon and Planets, Moscow, USSR, 1974.
- Dyal, P., C. W. Parkin, and W. D. Daily, Lunar electrical conductivity and magnetic permeability, in Proc. Lunar Sci. Conf. 6th, 2909-2926, 1975.
- Dyal, P., C. W. Parkin, and W. D. Daily, Structure of the lunar interior from magnetic field measurements, in Proc. Lunar Sci. Conf. 7th, 3077-3095, 1976.
- Dyal, P., C. W. Parkin, and W. D. Daily, Global lunar crust: electrical conductivity and thermoelectric origin of remanent magnetism, in Proc. Lunar Sci. Conf. 8th, 767-783, 1977.
- Dyal, P., W. D. Daily, and L. L. Vanyan, Crustal evolution inferred from Apollo magnetic measurements, in Proc. Lunar Sci. Conf. 9th., 231-248, 1978.
- England, A. W., G. Simmons, and D. Strangway, Electrical conductivity of the Moon, J. Geophys. Res., 73, 3219-3226, 1968.
- Fricker, P. E., R. T. Reynolds, and A. L. Summers, On the thermal history of the moon, J. Geophys. Res., 72, 2649-2663, 1967.
- Fuller, M., Lunar magnetism, Rev. Geophys. Space Phys., 12, 23-70, 1974.
- Goins, N. R., A. M. Dainty, and M. N. Toksöz, The structure of the lunar interior as determined from seismic data (abstract) in Lunar Science VIII, 354-356, The Lunar Science Institute, Houston, 1977.
- Green, D. H., A. E. Ringwood, N. G. Ware, W. O. Hibberson, A. Major, and E. Kiss, Experimental petrology and petrogenesis of Apollo 12 basalts, in Proc. Lunar Sci. Conf. 2nd, 601-615, 1971.
- Hanks, T. C., and D. L. Anderson, Origin, Evolution and present thermal state of the moon, Phys. Earth Planet. Interiors, 5, 409-425, 1972.
- Hargraves, R. B., and W. E. Perkins, Investigations of the effect of shock on natural remanent magnetization, J. Geophys. Res., 74, 2576-2589, 1969.
- Hide, R., Comments on the moon's magnetism, The Moon, 1, 39, 1972.
- Hobbs, B. A., The inversion problem of the moon's electrical conductivity, Earth Planet. Sci. Letters, 17, 380-384, 1973.
- Hood, L. L., and D. E. Wilhelms, Some evidence on the sources of lunar crustal magnetic anomalies, submitted to Science, 1978.
- Hood, L., C. T. Russell, and P. J. Coleman, Jr., Evidence for a non-random magnetization of the moon, Geophys. Res. Lett., 5, 305-308, 1978.

- Hood, L. L., P. J. Coleman, Jr., and D. E. Wilhelms, The moon: sources of the crustal magnetic anomalies, Science, 204, 53-57, 1979.
- Horning, B. L., and G. Schubert, Lunar electromagnetic scattering: propagation at arbitrary angles to the cavity axis, J. Geophys. Res., 80, 4215-4229, 1975.
- Jackson, J. D., Classical electrodynamics, John Wiley and Sons, New York, 162-164, 1962.
- King, J. H., and N. F. Ness, Lunar magnetic permeability studies and magnetometer sensitivity, Geophys. Res. Lett., 4, 129-132, 1977.
- Kuckes, A. F., Lunar electrical conductivity profile, Nature, 232, 249-251, 1971.
- Kuckes, A. F., W. D. Daily, P. Dyal, and C. W. Parkin, Temperature profile of the lunar interior (abstract), Trans. American Geophys. Union (EOS) 55, 331, 1974.
- Levy, E. H., and C. P. Sonett, Meteorite magnetism and early solar system fields, Conf. on Protostars and Planets, Tucson, in press, 1978.
- Lin, R. P., A search for impact crater-associated surface magnetic fields in mare regions (abstract), Lunar and Planetary Science IX, 651-653, Lunar and Planetary Institute, Houston, 1978.
- Lin, R. P., High spatial resolution measurements of surface magnetic fields on the lunar frontside., in Proc. Lunar and Planet. Sci. Conf. 10th, submitted, 1979.
- Lin, R. P., R. E. McGuire, H. C. Howe, and K. A. Anderson, Mapping of lunar surface remanent magnetic fields by electron scattering, in Proc. Lunar Sci. Conf. 6th, 2971-2973, 1975.
- Mihalov, J. D., D. S. Colburn, J. H. Binsack, and M. D. Moutsoulas, Possible fossil lunar magnetism inferred from satellite data, Science, 171, 892-895, 1971.
- Murthy, V. R., and S. K. Banerjee, Lunar evolution: How well do we know it now?, The Moon, 7, 149-171, 1973.
- Nagata, T., Rock magnetism, Maruzen Co. Ltd., 1961.
- Nagata, T., T. Yukutake, and S. Uyeda, On magnetic susceptibility of olivines, J. Geomag. Geoelect., 9, 51-56, 1957.
- Nagata, T., Y. Ishikawa, H. Kinoshita, M. Kono, Y. Syono, and R. M. Fisher, Magnetic properties and natural remanent magnetization of lunar materials, in Proc. of the Apollo 11 Lunar Sci. Conf., 2325-2340, 1970.
- Nagata, T., R. M. Fisher, F. C. Schwerer, M. D. Fuller, and J. R. Dunn, Magnetic properties and remanent magnetization of Apollo 12 lunar materials and Apollo 11 lunar microbreccia, in Proc. Lunar Sci. Conf. 2nd., 2461-2476, 1971.
- Nagata, T., R. M. Fisher, and F. C. Schwerer, Lunar rock magnetism, The Moon, 4, 160-186, 1972.

- Ness, N. F., K. W. Behannon, C. S. Searce, and S. C. Santarano, Early results from the magnetic field experiment on Lunar Explorer 35, J. Geophys. Res., 72, 5769-5778, 1967.
- Olhoeft, G. R., A. L. Frisillo, D. W. Strangway, and H. Sharpe, Electrical properties of lunar solid samples (abstract) in Lunar Sci. 1V, 575-577, Lunar Science Institute, Houston, 1973.
- Parker, R. L., The inverse problem of electrical conductivity in the mantle, Geophys. J. Roy. Astron. Soc., 22, 121-138, 1970.
- Parkin, C. W., P. Dyal, and W. D. Daily, Iron abundance in the moon from magnetometer measurements., in Proc. Lunar Sci. Conf. 4th, 2947-2961, 1973.
- Parkin, C. W., W. D. Daily, and P. Dyal, Iron abundance and magnetic permeability of the moon, in Proc. Lunar Sci. Conf. 5th, 2761-2778, 1974.
- Pearce, G. W., D. W. Strangway, and E. E. Larson, Magnetism of two Apollo 12 igneous rocks, in Proc. Lunar Sci. Conf. 2nd, 2451-2460, 1971.
- Pearce, G. W., D. W. Strangway, and W. A. Gose, Remanent magnetization of the lunar surface, in Proc. Lunar Sci. Conf. 3rd, 2449-2464, 1972.
- Pearce, G. W., W. A. Gose, and D. W. Strangway, Magnetic studies on Apollo 15 and 16 lunar samples, in Proc. Lunar Sci. Conf. 4th, 3045-3076, 1973.
- Petrova, G. N., The difference between types of magnetization as a basis of study of the magnetic stability of rocks, (Dissert.), Earth Physics Inst., 1963.
- Phillips, R. J., The lunar conductivity profile and the nonuniqueness of electromagnetic data inversion, Icarus, 17, 88-103, 1972.
- Reisz, A. C., D. L. Paul, and T. R. Madden, Lunar electrical conductivity, Nature, 238, 144-147, 1972.
- Reynolds, R. T., and A. L. Summers, Calculations on the composition of the terrestrial planets, J. Geophys. Res., 74, 2494-2511, 1969.
- Rikitake, T., Electromagnetism and the earth's interior, Elsevier, Amsterdam, 1966.
- Ringwood, A. E., and E. Essene, Petrogenesis of lunar basalts and the internal constitution and origin of the moon, Science, 167, 607-610, 1970.
- Runcorn, S. K., An ancient lunar magnetic dipole field, Nature, 253, 701-703, 1975.
- Runcorn, S. K., Inferences concerning the early thermal history of the moon, In Proc. Lunar Sci. Conf., 7th. Geochim. Cosmochim. Acta, 3, edited by R. B. Merrill, 3321-3328, 1976.
- Runcorn, S. K., Early melting of the moon, in Proc. Lunar Sci. Conf. 8th, Geochim. Cosmochim. Acta, 1, edited by R. B. Merrill, 463-469, 1977.
- Runcorn, S. K., On the possible existence of superheavy elements in the primeval moon, Earth and Planet. Sci. Lett., 39, 193-198, 1978a.

- Runcorn, S. K., The ancient lunar dynamo (abstract), Conf. on Origins of Planet. Mag., 81-83, Lunar and Planetary Institute, Houston, 1978b.
- Runcorn, S. K., and H. C. Urey, A new theory of lunar magnetism, Science, 180, 636-638, 1973.
- Runcorn, S. K., D. W. Collinson, W. O'Reilly, A. Stephenson, M. H. Batley, A. J. Manson, and P. W. Readman, Magnetic properties of Apollo 12 Lunar Samples, in Proc. Roy. Soc. London, Ser. A 325, 157-174, 1971.
- Russell, C. T., P. J. Coleman, Jr., B. R. Lichenstein, G. Schubert, and L. R. Sharp, Subsatellite measurements of the lunar magnetic field, in Proc. Lunar Sci. Conf. 4th, 2833-2845, 1973.
- Russell, C. T., P. J. Coleman, Jr., B. R. Lichtenstein, and G. Schubert, The permanent and induced magnetic dipole moment of the moon, in Proc. Lunar Sci. Conf. 5th, 2747-2760, 1974.
- Russell, C. T., H. Weiss, P. J. Coleman, Jr., L. A. Sodeblom, D. E. Stuart Alexander, and D. E. Wilhelms, Geologic-magnetic correlations on the moon: Apollo subsatellite results, in Proc. Lunar Sci. Conf. 8th Geochim. Cosmochim. Acta, 1, edited by R. B. Merrill, 1171-1185, 1977.
- Schubert, G., and K. Schwartz, A theory for the interpretation of lunar surface magnetometer data, The Moon, 1, 106-117, 1969.
- Schubert G., B. F. Smith, C. P. Sonett, D. S. Colburn, and K. Schwartz, The night side electromagnetic response of the moon, J. Geophys. Res., 78, 3638-3696, 1973.
- Schubert, G., B. F. Smith, C. P. Sonett, D. S. Colburn, and K. Schwartz, Polarized magnetic field fluctuations at the Apollo 15 site: possible regional influence on lunar induction, Science, 183, 1194-1197, 1974.
- Schwartz, K., and G. Schubert, Time-dependent lunar electric and magnetic fields induced by a spatially varying interplanetary magnetic field, J. Geophys. Res., 74, 4777-4780, 1969.
- Schwartz, K., and G. Schubert, Lunar electromagnetic scattering I. propagation parallel to the diamagnetic cavity axis., J. Geophys. Res., 78, 6496-6506, 1973.
- Schwerer, F. C., G. P. Huffman, R. M. Fisher, and T. Nagata, D.C. electrical conductivity of lunar surface rocks, The Moon, 4, 187-189, 1972.
- Shapiro, V. A., and N. I. Alova, Characteristics of the dynamic remanent magnetization of ferromagnetic rocks at temperatures from 0 to 600 °C. Izv., Earth Physics, 11, 95-98, 1970.
- Sill, W. R., Lunar conductivity models from the Apollo 12 magnetometer experiment, The Moon, 4, 3-17, 1972.
- Sill, W. R. and J. L. Blank, Method for estimating the electrical conductivity of the lunar interior, J. Geophys. Res., 75, 201-210, 1970.

- Sonett, C. P., and D. S. Colburn, Establishment of a lunar unipolar generator and associated shock and wake by the solar wind, Nature, 216, 340-343, 1967.
- Sonett, C. P., and J. D. Mihalov, Lunar fossil magnetism and perturbations of the solar wind, J. Geophys. Res., 77, 588-603, 1972.
- Sonett, C. P., D. S. Colburn, R. G. Currie, and J. D. Mihalov, The Geomagnetic tail: topology, reconnection and interaction with the moon, in Physics of the Magnetosphere, edited by R. L. Carovillano, J. F. McClay, and H. R. Radoski, 461-484, D. Reidel, Dordrecht, Holland, 1967.
- Sonett, C. P., D. S. Colburn, and K. Schwartz, Electrical heating of meteorite parent bodies and planets by dynamo induction from premain sequence, T Tauri solar wind, Nature, 219, 924-926, 1968.
- Sonett, C. P., C. Schubert, B. F. Smith, K. Schwartz, and D. S. Colburn, Lunar electrical conductivity from Apollo 12 magnetometer measurements: compositional and thermal inferences, in Proc. Lunar Sci. Conf. 2nd, 2415-2431, 1971a.
- Sonett, C. P., D. S. Colburn, P. Dyal, C. W. Parkin, B. F. Smith, G. Schubert, and K. Schwartz, Lunar electrical conductivity profile, Nature, 230, 359-362, 1971b.
- Sonett, C. P., B. F. Smith, D. S. Colburn, G. Schubert, and K. Schwartz, The induced magnetic field of the moon: conductivity profiles and inferred temperature, in Proc. Lunar Sci. Conf. 3rd, 2309-2336, 1972.
- Sonett, C. P., B. F. Smith, D. S. Colburn, and K. Schwartz, Polarized electromagnetic response of the moon, in Proc. Lunar Sci. Conf. 5th, 3073-3089, 1974.
- Spreiter, J. R., M. C. Marsh, and A. L. Summers, Hydromagnetic aspects of solar wind flow past the moon, Comic Electrodynamics, 1, 5-50, 1970.
- Srnka, L. J., Spontaneous magnetic field generation in hypervelocity impact, in Proc. Lunar Sci. Conf. 8th, 785-792, 1977.
- Srnka, L. J., and M. H. Mendenhall, Theory of global thermoremanent magnetization of planetary lithospheres in dipole fields, submitted to J. Geophys. Res., 1978.
- Stephenson, A., The residual permanent magnetic dipole moment of the moon, The Moon, 15, 67-81, 1976.
- Strangway, D. W., History of the earth's magnetic field, McGraw Hill, New York, 168, 1970.
- Strangway, D. W., The record of magnetic fields in the early solar system, The Moon and Planets, 18, 273-279, 1978.
- Strangway, D. W., E. E. Larson, and G. W. Pearce, Magnetic studies of lunar samples - breccia and fines, in Proc. Apollo 11 Lunar Sci. Conf., 2435-2451, 1970.
- Strangway, D. W., G. W. Pearce, W. A. Gose, and R. W. Timme, Remanent magnetization of lunar samples, Earth Planet. Sci. Lett., 13, 42-52, 1971.

- Strangway, D. W., W. A. Gose, G. W. Pearce, and R. K. McConnell, Lunar magnetic anomalies and the Cayley formation, Nature, 246, 112-115, 1973a.
- Strangway, D. W., W. A. Gose, G. W. Pearce, and J. G. Carnes, Magnetism and the early history of the moon, in Proc. of the 18th Annual Conf. on Magnetism and Magnetic Materials, J. Applied Phys., 1178, 1973b.
- Tabole, R. S., and D. J. Craik, Magnetic materials, Wiley-Interscience, 107, 1969.
- Toksöz, M. N., S. C. Solomon, J. W. Minear, and D. H. Johnston, Thermal evolution of the moon, The Moon, 4, 331-355, 1972.
- Urey, H. C., The origin of the moon, in The Moon, edited by Z. Kopal and Z. K. Mikhailov, 133-148, Academic Press, New York, 1962.
- Urey, H. C., and G. J. F. MacDonald, Origin and history of the moon, in Physics and Astronomy of the Moon, edited by Z. Kopal, 213-289, 1971.
- Urey, H. C., K. Marti, J. W. Hawkins, and M. K. Liv, Model history of the lunar surface, in Proc. Lunar Sci. Conf. 2nd, 987-998, 1971.
- Vanyan, L. L., The interaction of the solar wind with lunar magnetic anomalies, The Moon, 16, 321-324, 1977.
- Vanyan, L. L., T. A. Vnuchkova, I. V. Yegorov, A. T. Basilevsky, E. G. Eroshenko, E. B. Fainberg, P. Dyal, and W. D. Daily, Electrical conductivity anomaly beneath Mare Serenitatis detected by Lunokhod 2 and Apollo 16 magnetometers, The Moon and Planets, in press, 1979.
- Wanke, H., H. Baddenhausen, G. Driebus, M. Quijano-Rico, M. Palme, B. Spettel, and F. Teschke, Multielement analysis of Apollo 16 samples and about the composition of the whole moon (abstract), in Lunar Science IV, 761-763, The Lunar Science Institute, Houston, 1973.
- Wasilewski, P., Magnetic remanence mechanisms in FeNiCo alloys and the magnetization of lunar rocks and soils (abstract), in Lunar Science IV, 770, The Lunar Science Institute, Houston, 1972.
- Wasilewski, P. J., Shock remagnetization associated with meteorite impact at planetary surfaces, The Moon, 6, 264-291, 1973.
- Wasilewski, P. J., Magnetic properties of FeNi alloys--microstructure and remanent magnetization mechanisms (abstract), in Conf. on Origins of Planetary Magnetism 119-120, Lunar and Planetary Institute, Houston, 1978a.
- Wasilewski, P. J., Shock induced effects in fine particle iron (abstract), in Conf. on Origins of Planetary Magnetism, 121-122, Lunar and Planetary Institute, Houston, 1978b.
- Weeks, R. A., Magnetic phases in lunar material and their electron magnetic resonance spectra: Apollo 14, in Proc. Lunar Sci. Conf. 3rd, 2503-2517, 1972.
- Weiss, H., L. L. Hood, and P. J. Coleman, Jr., Extended analysis of the cratered shell model of the moon's permanent magnetic field, in Proc. Lunar Sci. Conf. 8th, Geochim. Cosmochim. Acta, 1, 757-766, 1977.

Wiskerchen, M. J., and G. P. Sonett, A lunar metal core?, in Proc. Lunar Sci. Conf. 8th, Geochim. Cosmochim. Acta, 1, 515-535, 1977.

Wood, J. A., J. S. Dickey, Jr., U. B. Marvin, and B. J. Powell, Lunar anorthosites and geophysical model of the moon, in Proc. Apollo 11 Lunar Sci. Conf., 965-988., 1970.

Zussman, J., The mineralogy, petrology, and geochemistry of lunar samples-a review, The Moon, 5, 422-435, 1972.

Zhuzgov, L. N., Sh. Sh. Dolginov, and E. G. Eroshenko, Kosmicheskie Issledovaniya, Vol. 4, No. 6, 880-899, November-December, 1966.

Table 1

Characteristic	Explorer 35 ARC	Explorer 35 GSFC	Luna 10	Luna 22	Apollo 15,16 Subsatellite	Apollo 12,15,16 LSM	Apollo 14,16 LPM	Lunokhod
Orbital period	11.5 hrs.	11.5 hrs	3.9 hrs	3.2 hrs	2 hrs	---	---	---
Distance	9390 km	9390 km	1015 km	1409 km	100 km	---	---	---
Altitude	2570 km	2570 km	350 km	200 km	100 km	---	---	---
Range	0 to $\pm 200\gamma$	0 to ± 64	0 to $\pm 450\gamma$	---	0 to $\pm 100\gamma$	0 to $\pm 400\gamma$	0 to $\pm 256\gamma$	0 to ± 5
Resolution	$\pm 0.6\gamma$	$\pm 0.25\gamma$	$\pm 0.1\gamma$	---	$\pm 0.2\gamma$	$\pm 0.1\gamma$	$\pm 1.0\gamma$	---
Frequency response	dc to 0.05Hz	dc to 5Hz	dc to 0.008Hz	dc to 0.8Hz	dc to 0.5Hz	dc to 3Hz	dc to 0.05Hz	dc to 0.
Sensors	Fluxgate	Fluxgate	Ferrosonde	Ferrosonde	Fluxgate	Fluxgate	Fluxgate	Ferrosone
Reference	Sonett et al. (1967)	Ness et al. (1967)	Zhuzgoc et al. (1966)	---	Coleman et al. (1972a)	Dyal & Gordon (1973)	Dyal & Gordon (1973)	Dolginov et al. (1973)

REPRODUCIBILITY OF THE
ORIGINAL PAGE IS POOR

TABLE 2. Summary of Lunar Surface Remanent Magnetic Field Measurements

		Magnetic Field Components, γ		
Site	Field Magnitude, γ	Up	East	North
Apollo 16; 8.9°S, 15.5°E				
Alsep site	235 \pm 4	-186 \pm 4	-48 \pm 3	+135 \pm 3
Site 2	189 \pm 5	-189 \pm 5	+3 \pm 6	+10 \pm 3
Site 5	112 \pm 5	+104 \pm 5	-5 \pm 4	-40 \pm 3
Site 13	327 \pm 7	-159 \pm 6	-190 \pm 6	-214 \pm 6
LRV final site	113 \pm 4	-66 \pm 4	-76 \pm 4	+52 \pm 2
Apollo 15; 26.1°N, 3.7°E				
Alsep site	3.4 \pm 2.9	+3.3 \pm 1.5	+0.9 \pm 2.0	-0.2 \pm 1.5
Apollo 14; 3.7°S, 17.5°W				
Site A	103 \pm 5	-93 \pm 4	+38 \pm 5	-24 \pm 5
Site C'	43 \pm 6	-15 \pm 4	-36 \pm 5	-19 \pm 8
Apollo 12; 3.2°S, 23.4°W				
Alsep site	38 \pm 2	-25.8 \pm 1.0	+11.9 \pm 0.9	+25.8 \pm 0.4

Data in this table are from Dyal et al. [1973].

FIGURE CAPTIONS

- Figure 1. Schematic representation of the remanent field-solar wind interaction. Magnetic fields near the lunar surface are produced by natural magnetic remanence in the crust. The neutral solar plasma impinges on the lunar surface with little change in its flow due to interaction with these local fields. The orthogonal coordinate system used in the analysis is also shown.
- Figure 2. The remanent magnetic field change tangential to the surface at Apollo 12, 15, and 16 landing sites plotted as a function of the solar wind plasma density measured at the lunar surface. The averaged data for each site are compared to 3 different models of the lunar remanent magnetic field. For the Apollo 12 models a small scale field of 33 gammas is superimposed on a 4.6 gamma 100 km scale field. The Apollo 15 models are a 4 gamma field of scale 5, 50, and 100 km. The Apollo 16 models are a small scale 146 gamma field superimposed on a 100 km scale, 1 gamma field.
- Figure 3. Magnetization induction in the moon. When the moon is immersed in a uniform external field \underline{H} (in this case the steady geomagnetic tail field), a dipolar magnetization field \underline{M} is induced in permeable material in the lunar interior, with the dipole axis of \underline{M} aligned along the direction of \underline{H} . The total field near the moon, schematically represented here, is the sum of external and induced fields. The magnetic permeabilities of the two layers are μ_1 and μ_2 , and for regions outside the moon, $\mu = \mu_0 = 1$ (free space). \underline{H} is measured by the lunar orbiting Explorer 35, whereas \underline{B} is measured by an Apollo lunar surface magnetometer. Measurements of \underline{B} and \underline{H} allow construction of a B-H hysteresis curve for the sphere, from which permeability and iron abundance can be calculated.

Figure 4. Hysteresis curve for the moon from Parkin et al. (1974). Data points are 2703 simultaneous two-minute averages of radial components of the external geomagnetic field data H measured by the lunar orbiting Explorer 35 Ames magnetometer and total magnetic induction B measured by the Apollo 12 lunar surface magnetometer. Data points are selected from four lunations of measurements made when the moon is immersed in the uniform geomagnetic tail field, far from the neutral sheet in the tail. In this low-external-field regime (~ 10 gammas or 10^{-4} Oe), the hysteresis curve is linear and is fitted by a least-squares line of slope 1.008 ± 0.004 . This slope corresponds to a whole-moon magnetic permeability of 1.012 ± 0.006 . The least-squares line intersects the origin exactly in this figure because the vertical-axis intercept (the radial or x-component of the remanent field at the Apollo 12 site) was subtracted out after the least-squares fit was made.

Figure 5. Global eddy current induction. Eddy currents and corresponding poloidal magnetic fields are induced by response to time-dependent fluctuations in the external field. The lunar orbiting Explorer 35 magnetometer measures the external field change and the surface Apollo magnetometer measures the lunar poloidal field response. The induced field experiences greatly reduced plasma effects in deep-lobe regions of the tail far from the neutral sheet. The poloidal field can be considered to be an unconfined (vacuum) dipole field for analytical purposes.

Figure 6. Lunar radial response to solar event. Lunar response is shown for a large field change measured in the geomagnetic tail by the orbiting Explorer 35 magnetometer (external field). The lunar radial (ALSEP-x) components are plotted. The calculated lunar response is based on the conductivity profile of Figure 7.

Figure 7. Electrical conductivity profile of the moon. The solid line is a preferred profile which best fits the data shown in Figure 6. The set of profiles which fit the data within the error criteria discussed in the text are bounded by the shaded region.

Figure 8. Lunar temperature profiles calculated from thermal history models and electrical conductivity analyses. (1) Urey (1962). (2) Fricker et al. (1967). (3) Hanks and Anderson (1972). (4) Toksöz and Solomon (1973). (5) Temperature profile calculated from the conductivity profile shown in Figure 7 and laboratory data for olivine from Duba et al. (1972).

REMANENT FIELD SOLAR WIND INTERACTION

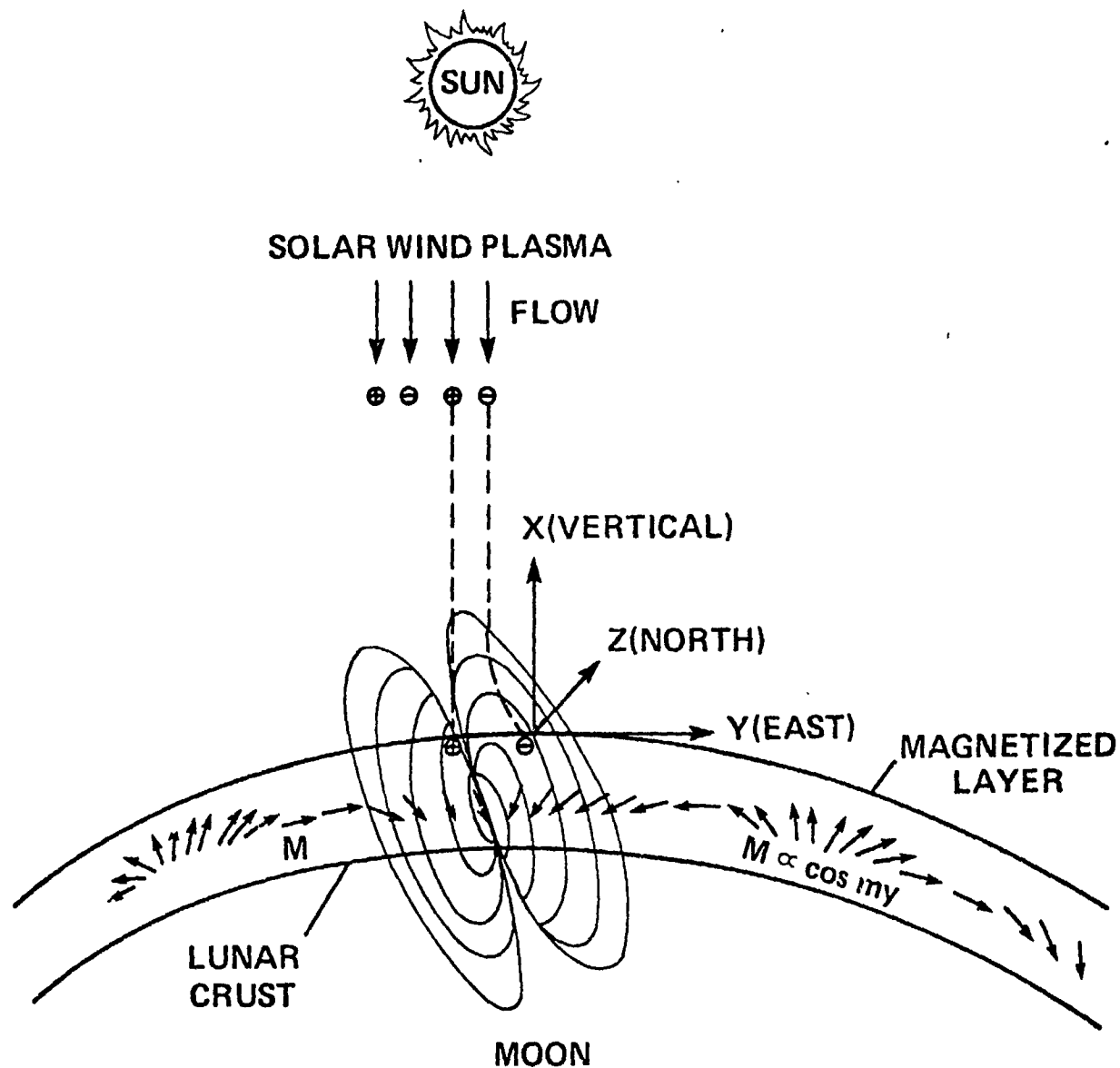
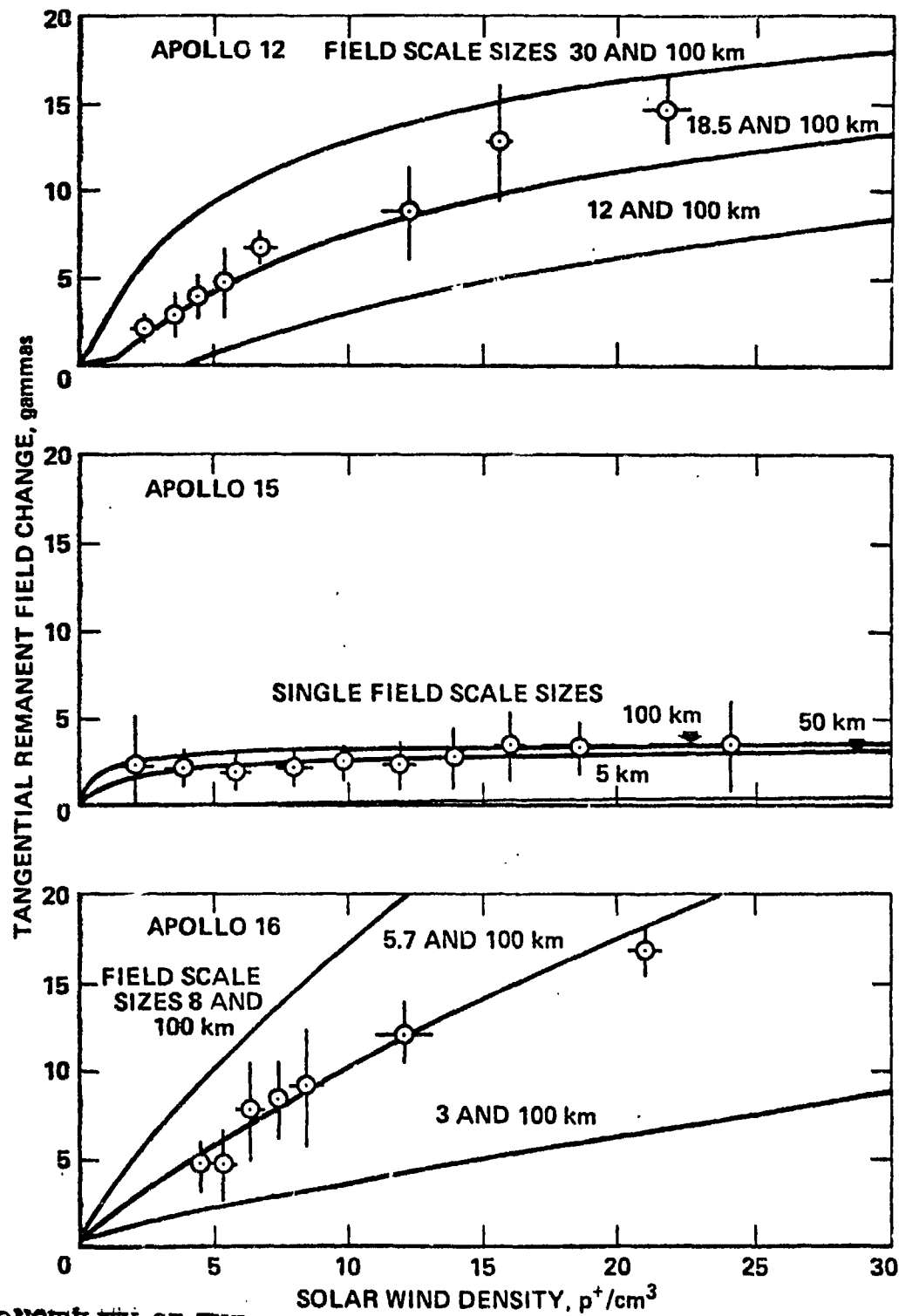


Figure 1

REPRODUCIBILITY OF THE
ORIGINAL PAGE IS POOR



REPRODUCIBILITY OF THE
ORIGINAL PAGE IS POOR

Figure 2

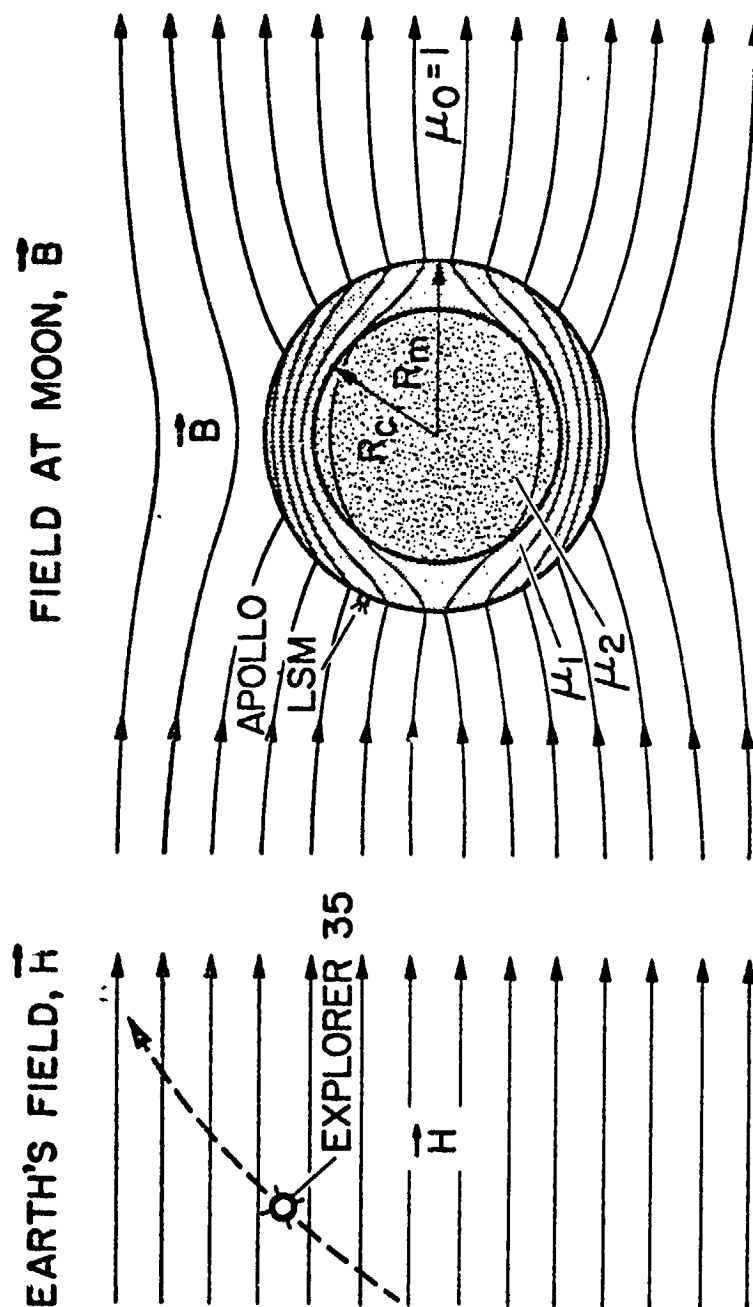


Figure 3

REPRODUCIBILITY OF THE
ORIGINAL PAGE IS POOR

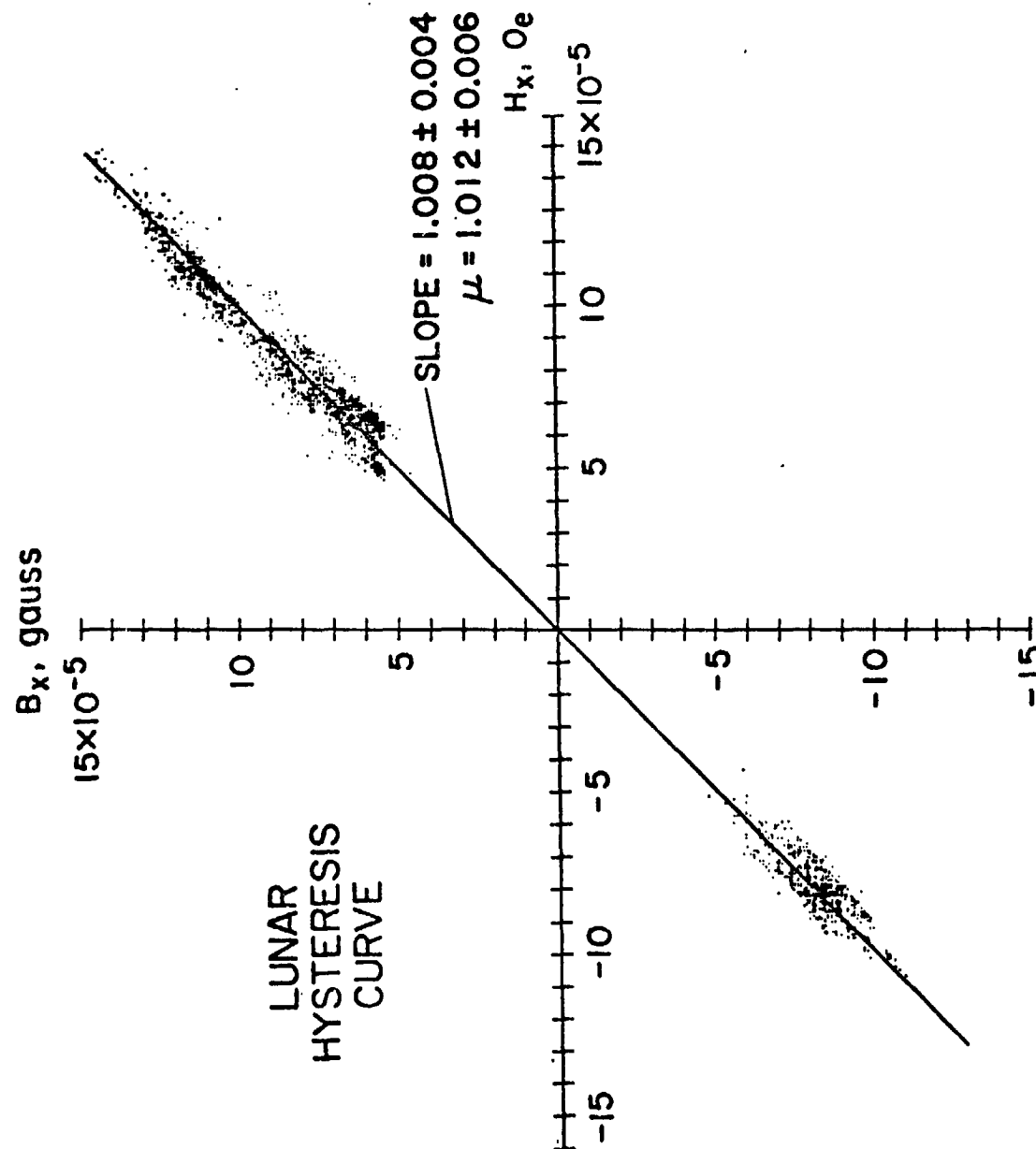


Figure 4.

REPRODUCIBILITY OF THE
ORIGINAL PAGE IS POOR

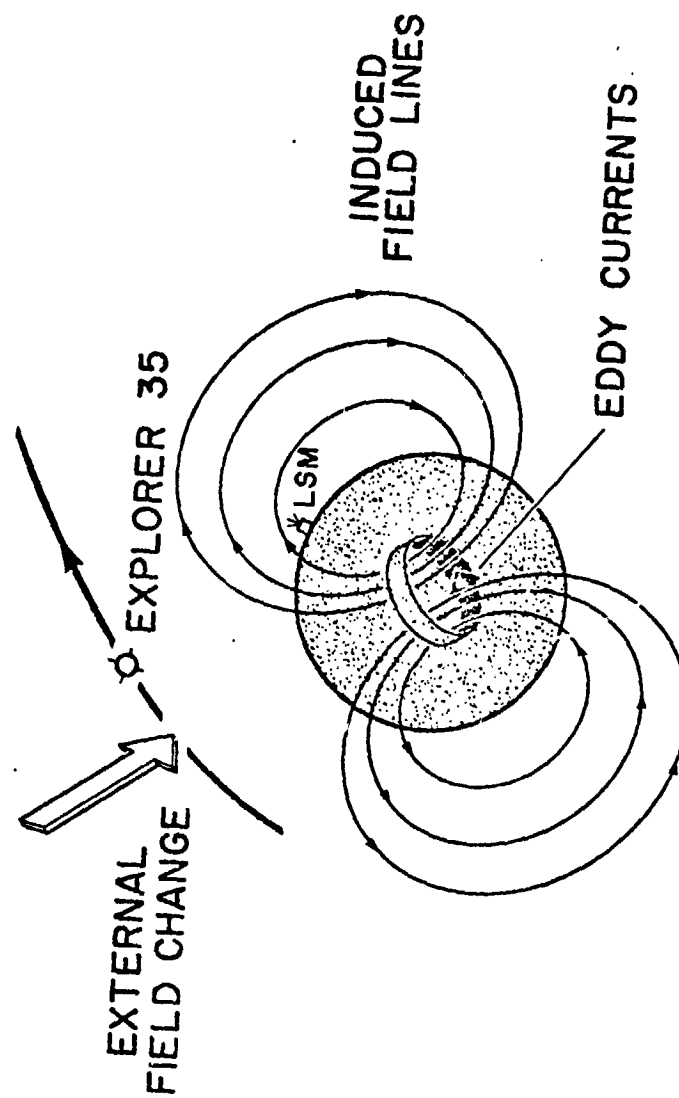
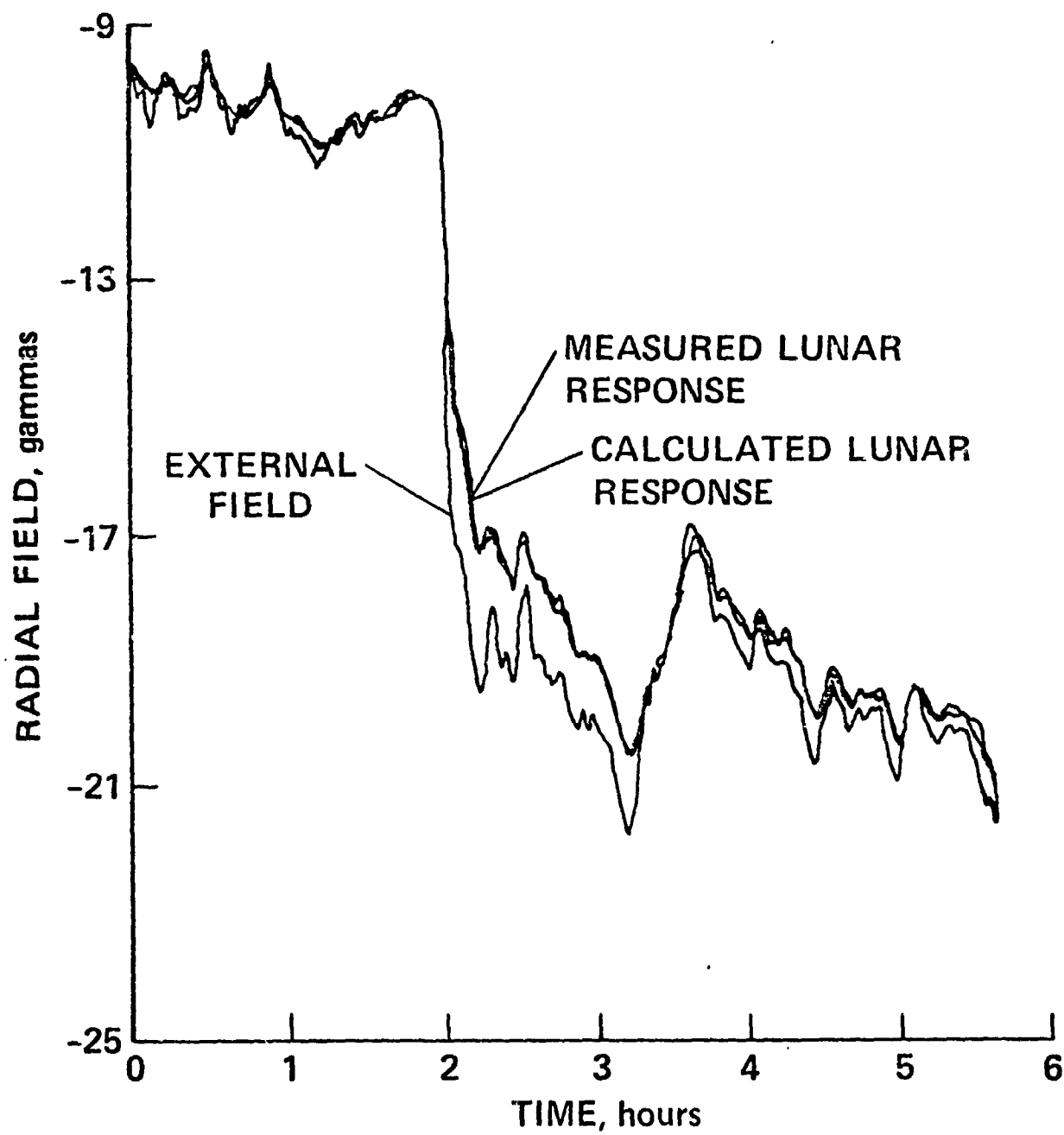


Figure 5

REPRODUCIBILITY OF THE
ORIGINAL PAGE IS POOR



REPRODUCIBILITY OF THE
ORIGINAL PAGE IS POOR

Figure 6

LUNAR ELECTRICAL CONDUCTIVITY

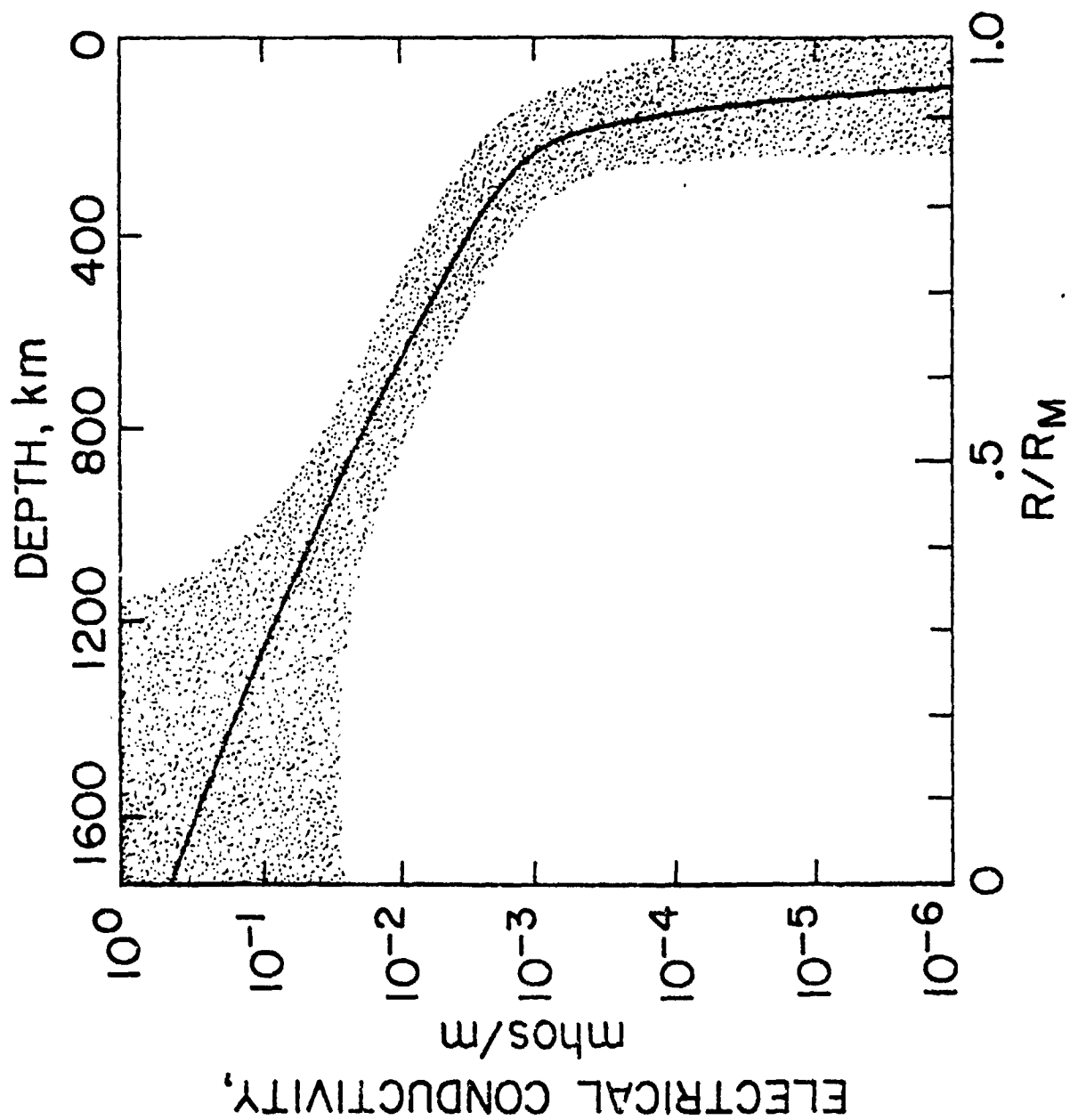


Figure 7

REPRODUCIBILITY OF THE
ORIGINAL PAGE IS POOR

REPRODUCIBILITY OF THE
ORIGINAL PAGE IS POOR

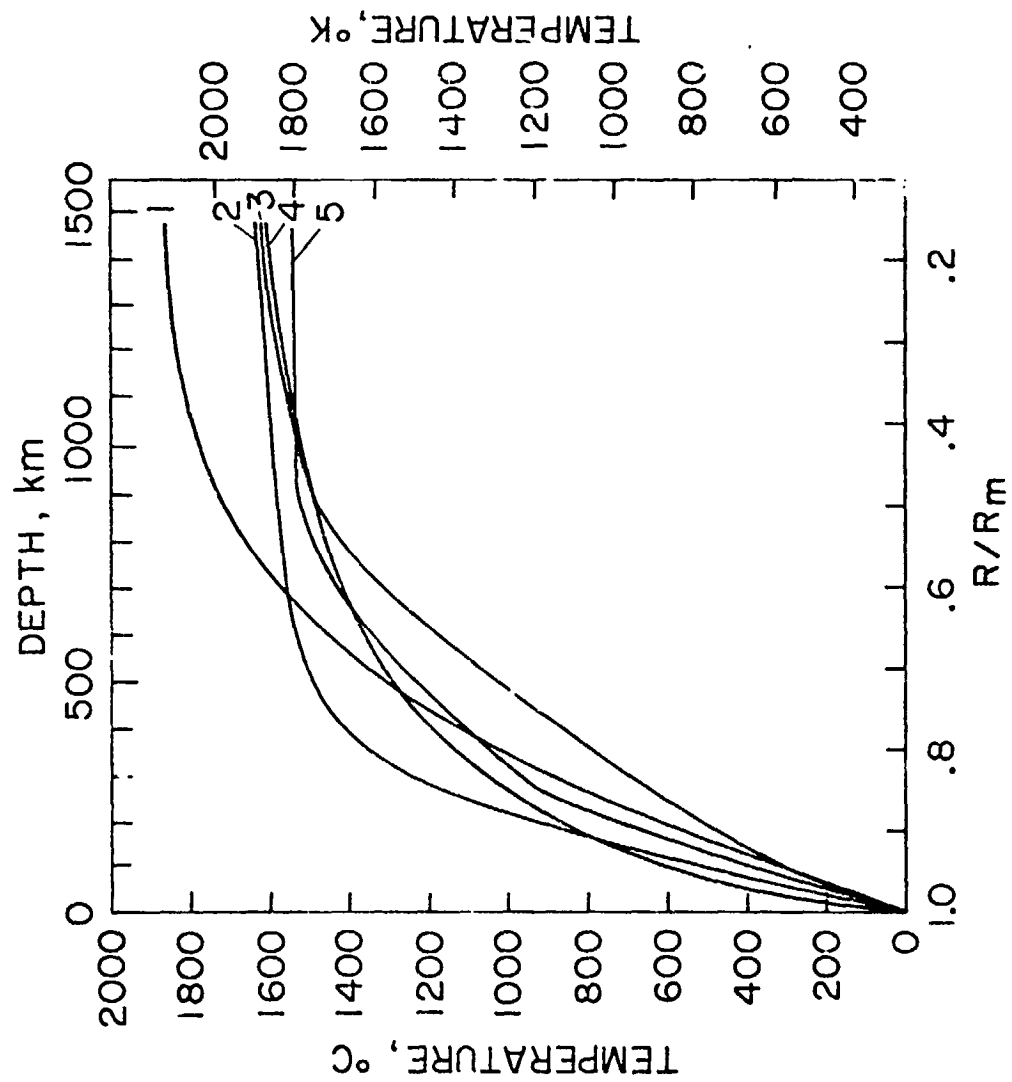


Figure 8

APPENDIX E

MARE SERENITATIS CONDUCTIVITY ANOMALY
DETECTED BY APOLLO 16 AND LUNOKHOD 2 MAGNETOMETERS

MARE SERENITATIS CONDUCTIVITY ANOMALY DETECTED BY APOLLO 16 AND
LUNOKHOD 2 MAGNETOMETERS

P. Dyal, NASA-Ames Research Center, Moffett Field, CA 94035

L. L. Vanyan, U.S.S.R. Academy of Sciences, Moscow, U.S.S.R.

W. D. Daily, Eyring Research Institute, Provo, UT 84601

Analysis of simultaneous Lunokhod 2 and Apollo 16 magnetometer data has revealed the presence of an anisotropy in magnetic field fluctuations near Mare Serenitatis which indicates the presence of anomalous electrical conductivity beneath the Serenitatis basin (Vanyan *et al.*, 1979) similar to that discovered beneath Mare Imbrium (Schubert *et al.*, 1974; Sonett *et al.*, 1974). Lunokhod 2 magnetometer is located at the eastern margin of Mare Serenitatis within Bay Le Monnier, and at this location the horizontal magnetic field fluctuations between 6.7×10^{-3} and 0.2 Hz have a strong linear polarization which is aligned with the mare center in the northwest-southeast direction (Dolginov *et al.*, 1976). Simultaneous Apollo 16 data measured in the Descartes Highlands 1100 km from the center of Serenitatis does not show any polarization in the horizontal field fluctuations. One explanation for the observed field anisotropy at Lunokhod 2 is a region beneath Serenitatis of either anomalously low or high electrical conductivity. We have chosen to model the mantle conductivity distribution in the area by a dielectric layer of conductivity less than 10^{-6} mhos/m and thickness 150 km overlaying a base of conductivity 10^{-3} mhos/m. Beneath Maria Serenitatis and Imbrium the dielectric layer is thicker than beneath the surrounding highlands by an additional 150 km as shown by the contours of constant dielectric thickness in Figure 1. The dielectric thickness was adjusted until the anisotropy observed at Lunokhod 2 matched the anisotropy calculated from the model. Although this model is not unique and an anomalously high electrical conductivity beneath Serenitatis could produce the same magnetic polarization, we believe the model depicted in Figure 1 is consistent with current knowledge of basin formation and evolution. In fact, we propose that during the process of mare volcanism large quantities of heat associated with the magma were brought from 200-300 km depth to the surface where the heat was dissipated by radiation. Mantle regions beneath the highlands were cooled by the less efficient process of conduction. In addition to the intrinsic thermal energy, the magma extruded into the maria were enriched in the radioactive heat sources potassium, uranium, and thorium, leaving the sub maria regions depleted in these heat sources. The net effect is a proposed enhancement of thermal cooling rates beneath Maria Serenitatis and Imbrium with an associated depression in the electrical conductivity relative to the surrounding highlands. This model relating electrical conductivity anomalies and mare volcanism predicts depressed electrical conductivity beneath all circular lunar maria with the magnitude of the anomaly directly related to the volume of erupted magma.

A thorough analysis has been completed of errors in lunar magnetic data obtained by Apollo 12, 15, and 16 surface and the Explorer 35 Ames and Goddard orbiting magnetometers (Daily and Dyal, 1979). The effects of magnetic data errors on electrical conductivity studies of the moon using Apollo 12 and Explorer 35 data are summarized in Figure 2. In this figure the envelopes for the conductivity profile of Dyal *et al.* (1976) are shown for several values of instrumental errors in the simultaneous field measurements. The shaded envelope defines the profile nonuniqueness for conductivity analyses using data with a 2% relative instrumental error (0.2 gamma error in a 10 gamma step transient). The measured lunar magnetic permeability of 1.012 ± 0.006

SERENITATIS CONDUCTIVITY ANOMALY

Dyal, P. et al.

reported by Parkin et al. (1974) has been revised to 1.012 ± 0.011 to reflect uncertainties in magnetometer gains as determined by our study of Apollo 12 and Explorer 35 instrumental errors. This wider confidence interval allows model dependent lunar free iron abundance (see Parkin et al., 1974) to vary from 0 to 5.8 wt. % with a total iron abundance of 3.5 to 13.9 wt. %.

References

- Daily W.D. and Dyal P. (1978) Magnetometer data errors and lunar induction studies, submitted to J. Geophys. Res.
- Dyal P., Parkin C.W., and Daily W.D. (1976) Structure of the lunar interior from magnetic field measurements, Proc. Lunar Sci. Conf. 7th, 3077-3095.
- Dolginov Sh.Sh., Yeroshenko Ye.G., Sharova V.A., Vnuchkova T.A., Vanyan L.L., Okulesaky B.A., and Basilevsky A.T. (1976) Study of magnetic field, rock magnetism, and lunar electrical conductivity in the Bay Le Monnier, The Moon, 15, 3-14.
- Parkin C.W., Daily W.D., and Dyal P. (1974) Iron abundance and magnetic permeability of the moon, Proc. Lunar Sci. Conf. 5th, 3, 2761-2778.
- Schubert G., Smith B.F., Sonett C.P., Colburn D.S., and Schwartz K. (1974) Polarized magnetic fluctuations at the Apollo 15 site: Possible regional influence on lunar induction, Science, 183, 1194-1197.
- Sonett C.P., Smith B.F., Schubert G., Colburn D.S., and Schwartz K. (1974) Polarized electromagnetic response of the moon, Proc. Lunar Sci. Conf. 5th, 3, 3049-3058, Pergamon Press, New York.
- Vanyan L.L., Vnuchkova T.A., Egorov I.V., Basilevsky A.T., Eroshenko E.G., Fainberg E.B., Dyal P., and Daily W.D. (1979) Electrical conductivity anomaly beneath Mare Serenitatis detected by Lunokhod 2 and Apollo 16 magnetometers, submitted to The Moon and The Planets.

SERENITATIS
CONDUCTIVITY ANOMALY

Figure 1: SERENITATIS AND IMBRIUM
ELECTRICAL CONDUCTIVITY ANOMALIES

Dyal, P. et al.

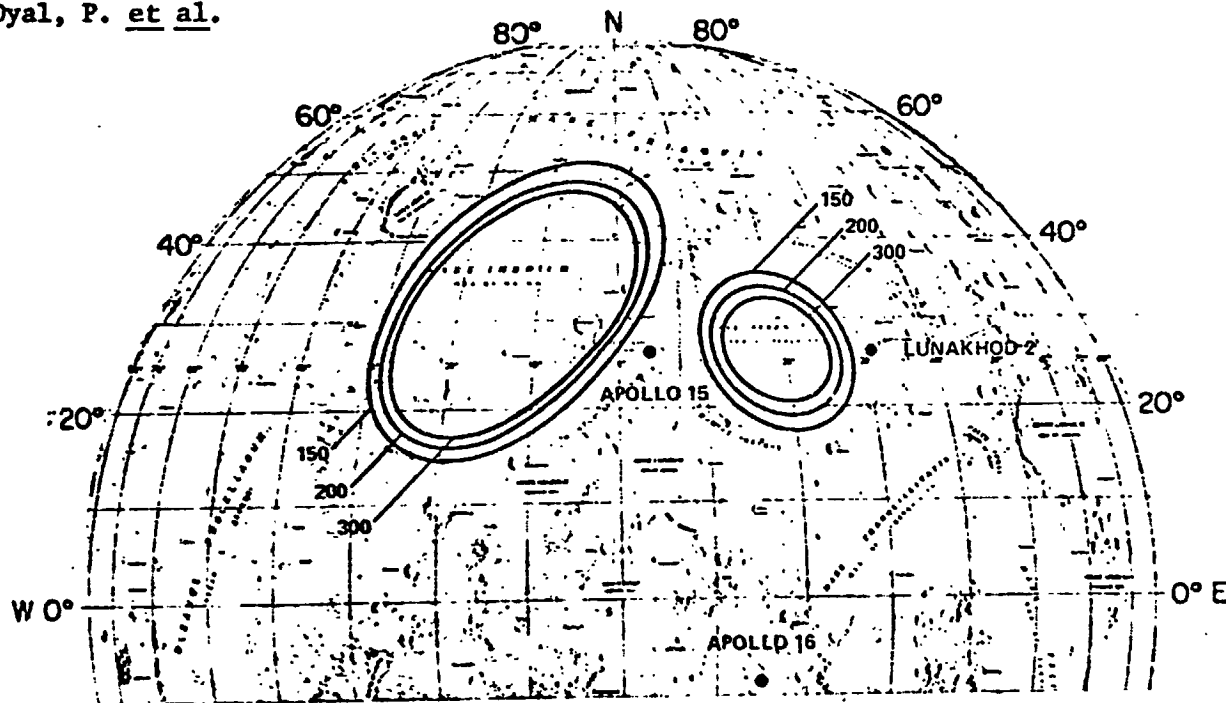
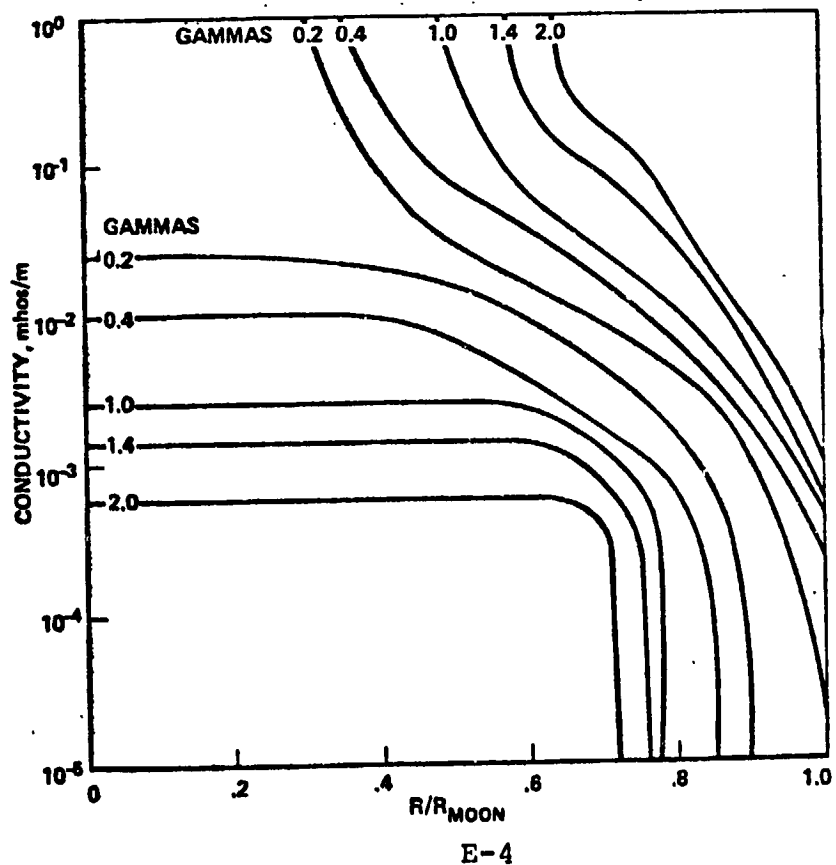


Figure 2: FIELD MEASUREMENT
ACCURACY AND CONDUCTIVITY
PROFILE LIMITS



REPRODUCIBILITY OF THE
ORIGINAL PAGE IS POOR

APPENDIX F

LUNAR PROPERTIES FROM MAGNETOMETER DATA:
EFFECTS OF DATA ERRORS

LUNAR PROPERTIES FROM MAGNETOMETER DATA:
EFFECTS OF DATA ERRORS

W. Daily (Eyring Research Institute, Provo, UT
84601)

P. Dyal (NASA-Ames Research Center, Moffett
Field, CA 94035)

Previously published electrical conductivity profiles and magnetic permeability estimates of the moon have been evaluated in light of recent analysis of errors in magnetometer data used to study these lunar interior properties. The relative gains and offsets of the Apollo 12 and Explorer 35 Ames and Goddard magnetometers are found to agree within 2% and 0.5 gamma respectively during the first 4 lunations of Apollo 12 operation. From the fifth through the eighth Apollo 12 lunation, the two Explorer magnetometer gains and offsets differ by as much as 60% and 1 gamma respectively. During these last four lunations the gains and offsets of all three magnetometers show this increased relative error. Effects of these data errors on electrical conductivity are estimated by determining the envelope of conductivity profiles produced by intentional introduction of errors into the analysis to simulate the measured range of uncertainty in the data. Adjustment of previously published bulk lunar magnetic permeability results, to account for magnetometer gain uncertainties, yields a revised lunar permeability estimate of 1.012 ± 0.011 . We conclude that careful selection of magnetic data used in any study of the moon is the best procedure for minimizing the effects of these errors.